Development and implementation of conceptual density-functional theory for solid-state

Thesis
submitted to the
University of Chile
in partial fulfilment of the requirements
for the degree of
Master of Science in Physics
Faculty of Sciences

by

Nicolás F. Barrera Pavez

July 12, 2024

Thesis Advisors: **Prof. Carlos Cárdenas Valencia**
Dr. Tatiana Gómez Cano

Examination Committee:
Dr. Mercedes Alonso G.
Prof. Fernando Mendizábal E.
Dr. Francisco Muñoz S.

FACULTY OF SCIENCES
UNIVERSIDAD DE CHILE

FINAL REPORT
MASTER'S THESIS

It is informed to the Graduate School of the Faculty of Sciences that the Master's thesis presented by the candidate

Nicolás F. Barrera Pavez

has been approved by the Examination Committee of the Thesis as a partial requirement for the degree of Master of Science in Physics, in the Public Defense taken on August 29, 2024.

Thesis Advisors

Prof. Carlos Cárdenas V. _____

Dr. Tatiana Gómez C. _____

Examination Committee

Dr. Mercedes Alonso G. _____

Prof. Fernando Mendizábal E. _____

Dr. Francisco Muñoz S. _____
(President)

To my grandmothers, Eliana and Aída.

BIOGRAPHY

I was born on September 14, 1996 in Santiago. I studied at the Liceo José Victorino Lastarria, was there where I realised that I had great skills in chemistry and a big interest in quantum numbers, orbitals, spin, and so on. Nevertheless, the way to chemistry (physical chemistry in fact) was a little difficult. I started studying engineering and then chemistry at PUC. However, the happiness and enthusiasm for science really came to me in the Faculty of Science or *las palmeras*.

In 2021, I joined to the Theoretical Chemical Physics group as an undergraduate student and I done my Bachelor's thesis in Chemistry under the supervision of Profs. Patricio Fuentealba and Carlos Cárdenas. With the aim of continues my studies I enrolled into the Master in Physics program at Universidad de Chile. Of course, for a chemist, this was quite a challenge. However, I have always felt the support of Carlos, Francisco and Patricio and that has been very important to me.

During the second year of my master's, I started working on my thesis project, a collaboration between my research group at Universidad de Chile, Dr. Tatiana Gómez at Universidad Autónoma de Chile and Prof. Mònica Calatayud at Sorbonne Université, Paris. For this reason, at the beginning of 2024, I did a four-month long research internship at Laboratoire de Chimie Théorique (LCT) of Sorbonne Université, specifically in the *pôle de modélisation des systèmes complexes* under the supervision of Prof. Calatayud, where I could learn from her both expertise and knowledge and from the experience of working with high-level professors and students from all over the world.

ACKNOWLEDGEMENTS

This work was financed by ANID through the National Master Degree Scholarship No. 22220676, FONDECYT through project No. 122036, Center for the Development of Nanosciences and Nanotechnology, CEDENNA AFB 220001, the Physics Department of the Faculty of Sciences at Universidad de Chile, and Theoretical Chemistry Laboratory of Sorbonne Université. Additionally, this research was partially supported by the supercomputing infrastructure of the NLHPC (ECM-02).

I want to thank everyone who contributed to this thesis, both with knowledge, advice, and kind support. First of all, I extend my deepest gratitude to my advisor, Carlos, also known as *Charly*. I remember my first meetings with him, a very busy person who wanted to do everything as soon as possible. So, I preferred to ask Patricio my questions because Carlos intimidated me a little. However, this relationship changed over time (I think I became more than just a photo on his screen). During the development of this thesis, Carlos was there at every moment, even during difficult times for him. I really appreciate this a lot. He has been there with his knowledge, experience, and dedication, helping and guiding me with immense patience, which has been of immeasurable importance throughout this work. Thank you for giving me the opportunity to be your student, for the chance to work with other people, and for getting to know you beyond your role as an advisor.

My heartfelt thanks go to my internship supervisor, Prof. Mònica Calatayud, for her guidance and support during the four months of my internship in her group. Mònica is one in a million; she made my internship a wonderful experience (or as she would say, *súper guay*) for both my scientific career and personal life.

I would also like to thank Dr. Tatiana Gómez for providing us with the chemical and technological importance of the systems studied and for her support during the development of this thesis.

I am deeply grateful to Prof. Patricio Fuentealba for the opportunity to join the Theoretical Chemical Physics Group and for all the knowledge he has imparted to me over the years. Without his initial support, I might not be in science today.

I extend my appreciation to everyone in the Department of Physics at the Universidad de Chile, especially the Theoretical Chemical Physics group students: Javiera, Loreto, Edgar, Wilver, Ignacio, and Andrea. Special thanks to my office mates, Javiera Cabezas (or *jcabezas*) and Loreto Portales (or *lolo*), whose friendship filled my master's degree with laughter and many wonderful moments. *Son las mejores y las quiero mucho!* I also want to extend my gratitude to the unofficial student of our office, Ítalo (*isalas*).

I am also grateful to the LCT crew, especially Marina, Mary, and Jessica, for their friendship and for making my internship more enjoyable. My words about LCT would not be complete without mentioning my "Chilean" friends: Andrea, Trinidad, and Diego. I really appreciate your support and advice. Also, of course, the dances and beers. You have been an example to me of how to do things right.

Back in Chile, I want to thank to Rocío - *Guuti*, Marjorie - *Maggi* and Javiera - *jcabezas*, my besties. I really feel lucky to have them in my life. They are the best and are my safe place to express myself and share my emotions and thoughts. *Las quiero muchísimo!*

Last but not least, I want to thank my family, especially my aunts Inés and Margarita, for always being there for me, supporting me in this career that sometimes seems eternal and consumes a large part of my time. To my parents (M. Teresa and Manuel), without whom I could hardly be in this position. To my sister (Liz) and my nephews (Augusto and Raimundo) for supporting me and brightening my days with their company (even with my little patience), thank you.

RESUMEN

La interacción de especies químicas, cómo los enlaces se crean y rompen para dar pie a nuevas especies, es un fenómeno esencialmente cuántico y un problema fundamental de la física química. Por esta razón el poseer un marco teórico simple que permita dilucidar, comprender y predecir este fenómeno resulta esencial. La Teoría del Funcional de la Densidad provee una estructura matemática y física que ha permitido la construcción de este marco, que ha sido denominado Teoría del Funcional de la Densidad Conceptual o Teoría del Funcional de la Densidad Química. De ella emergen funciones de respuesta físicas y químicas que dan cuenta de las pertubaciones generadas en el proceso de interacción. Una de las más importantes es la denominada función de Fukui y su potencial electrostático.

A pesar de que la Teoría del Funcional de la Densidad Conceptual ha sido ampliamente usada para estudiar la reactividad de sistemas finitos (átomos, molécula, etc), su uso en sistemas extendidos o periódicos es escaso debido a problemas técnicos y formales. Uno de ellos es la necesidad de incorporar un fondo de carga homogéneo en el cálculo de la estructura electrónica de sistemas cargados con condiciones de borde periódicas, el cual genera un potencial electrostático ficticio en y entre las imágenes de las superceldas.

En esta tesis, estudiamos el efecto de las interacciones espurias del fondo de carga homogéneo en el cálculo e interpretación química de las funciones de Fukui para superficies inorgánicas mediante el uso de distintas metodologías. Junto con lo anterior, utilizamos métodos de corrección para el cálculo del potencial electrostático de la función de Fukui, el denominado potencial de Fukui. Además, demostramos su importancia en el problema de predicción de reacciones químicas, analizando una familia de superficies de titanio: titanio metálico, carburo de titanio y óxido de titanio en sus polimorfos anatasa y rutilo.

ABSTRACT

The interaction of chemical species, how bonds are created and broken to give rise to new species, is an essentially quantum phenomenon and a fundamental problem of chemical physics. For this reason, a simple theoretical framework to elucidate, understand and predict this phenomenon is essential. The Density Functional Theory provides a mathematical and physical structure that has allowed the construction of this framework, which has been called Conceptual Density Functional Theory or Chemical Density Functional Theory. From it emerge physical and chemical response functions that account for the perturbations generated in the interaction process. One of the most important is the so-called Fukui function and its electrostatic potential.

Although the Conceptual Density Functional Theory has been widely used to study the reactivity of finite systems (atoms, molecules, etc.), its use in extended or periodic systems is scarce due to technical and formal problems. One of them is the need to incorporate a homogeneous charge background in the calculation of the electronic structure of charged systems with periodic boundary conditions, which generates a fictitious electrostatic potential in the supercell and between its images.

In this thesis, we study the effect of spurious interactions of the homogeneous charge background on the calculation and chemical interpretation of Fukui functions for inorganic surfaces by using different methodologies. Along with the above, we use correction methods for the calculation of the electrostatic potential of the Fukui function, the so-called Fukui potential. In addition, we demonstrate its importance in the problem of chemical reaction prediction by analyzing a family of titanium surfaces: titanium metal, titanium carbide and titanium oxide in its polymorphs anatase and rutile.

Contents

Acronyms

ACS American Chemical Society.

CBC Compensating background charge.

CDFT Conceptual Density-functional theory.

CPMD Car-Parinello molecular dynamics.

DFA Density-functional approximations.

DFT Density-functional theory.

ECC Exact Coulomb cutoff technique.

FD Finite differences.

FD-ECC Finite differences with Exact Coulomb Cutoff technique.

FD-SCPC Finite differences with the SCPC method.

FFT Fast Fourier transform.

FMO Frontier molecular orbital theory.

GGA Generalized gradient approximation.

HEG Homogeneous electron gas.

HK-theorems Hohenberg-Kohn theorems.

HOMO Highest occupied molecular orbital.

interpolation Interpolation scheme.

LDA Local-density approximation.

LDOS Local density of states.

LUMO Lowest unoccupied molecular orbital.

meta-GGA Meta generalized gradient approximation.

NCPP Norm-conserving pseudopotentials.

ONCVPSP Optimized nonlocal norm-conserving pseudopotentials.

PAW Projector augmented wave.

PBC Born–von Kármán periodic boundary conditions.

PBE Perdew-Burke-Ernzerhof exchange-correlation.

RPA Random phase approximation.

RPED Resonant photoelectron diffraction.

SCPC Self-Consistent Potential Correction.

VASP Vienna Ab initio simulation package.

Introduction

The evolution of the interaction between two chemical systems (i.e., atoms, molecules, clusters, solids, and so on) is one of the key paradigms of chemistry: reactivity. The theory of chemical reactivity , that is to say, the models to understand and predict the way a chemical specie will react it is one of the main subjects of the theoretical chemistry and molecular physics. It is common to classify reactions as being controlled by either electrostatic effects or electron transfer. However, both are borderline cases, as both effects are always present in actual reactions. Thus, a chemical reaction may be viewed as the chemical species' response to a perturbation, which is caused not only by a change in the external potential but also by changes in the number of electrons. The corpus of Density-functional theory (DFT) offers a natural framework to build a chemical reactivity theory because of is able to deal with non-integer number of electrons [1–7]. The construction of this theory, known as Conceptual Density-functional theory (CDFT) [8–11], began with the seminal work of Prof. Parr et al. [12] in 1978 in which they realized that the Lagrange multiplier of the Euler-Lagrange equation of the DFT is no more than the chemical potential of the system, μ, and that its negative gives a non-empirical scale of electronegativity.

CDFT has demonstrated remarkable success in elucidating established principles of chemical reactivity (e.g., hard/soft acid/base principle [13–15] and electronegativity equalization [12, 16, 17]) and also for the development of new principles (e.g., the maximum hardness principle [18–20]). One of the its most successful chemical descriptor is the Fukui function [21–26]. This provides a DFT-based alternative to the standard rationalization of the Fukui's Frontier molecular orbital theory (FMO) [27–30], can be

considered a generalisation of it, since it is based on density rather than orbitals, being able to incorporate correlation effects without obscuring their meaning and interpretation [10].

Although the Fukui function is extremely useful for characterising the reactivity [31, 32], it says nothing about whether these regions are really accessible by the active site of a reagent. On the contrary, the Fukui potential, that is defined as the electrostatic potential due to a distribution equal to the Fukui function, specifies what regions are energetically favorable to the approach of the active site of a reagent that will take or donate electrons from or to the substrate [11, 33].

Both the Fukui function and its electrostatic potential have been extensively used in characterizing the reactivity of atoms, molecules and clusters [34–36]. However, its use in solid-state chemistry/physics is sparse because of its calculation brings theoretical and computational challenges [37, 38].

The *ab initio* calculations of periodic systems frequently employ Born–von Kármán periodic boundary conditions (PBC) and discrete plane-wave basis set [39–41]. This choice allows exploit the translational symmetry of the periodic systems, by performing the simulation in one primitive cell only. Moreover, the Fast Fourier transform (FFT) algorithms [42, 43] allow the calculation of electrostatic equations very efficiently, considerably reducing the computational cost of the calculations. In many cases, like modelling points defects [44, 45] and surface chemistry [46–48], the supercell model is used. In this approximation, the system is treated as fully 3D-periodic one, but the new unit cell is built in such way that some empty space is add in the non-periodical direction to separate the supercell from its periodic images. This method allows to retain the advantages of the plane-wave expansions and PBC. Despite these enormous advantages, the periodic images see each other through the long-range Coulomb interaction, introducing spurious interactions, even if much empty space is add in the non-periodic direction [41, 49, 50].

The situation is further complicated when the supercell has a net charge, as is encountered in the computation of the Fukui function and Fukui potential. This arises from

the fact that the total charge of the infinite system represented by the supercell becomes infinite, resulting in a divergent Coulomb repulsion energy [49, 51]. To avoid the divergence of the Coulomb energy due to the repetition of the supercell, a uniform Compensating background charge (CBC) is always introduced to keep the supercell neutral [52, 53]. The use of the CBC introduces two complications. Firstly, the presence of a uniform charge in the vacuum region is physically unrealistic. Secondly, the screening of the CBC varies depending on its location within regions characterized by different dielectric profiles [52, 54]. This problems must be take in account at the moment of calculating the Fukui function and Fukui potential. Recently, Cardenas et al. [37, 38] has proposed a methodology to, in principle, overcome these drawbacks in the calculation of the solid-state Fukui function.

In this thesis, we will examine the advantages and disadvantages of various methods used to compute Fukui functions, along with schemes to correct the Fukui potential in solid-state chemistry. We will introduce an efficient method for obtaining the latter. Furthermore, we will provide examples illustrating the powerful impact of the Fukui potential on the Chemical Reaction Prediction Problem. As a case study, we will analyze a family of four titanium surface slabs: metallic titanium, titanium carbide, and anatase and rutile TiO_2.

For completeness we have included in chapter 1 a summary of the electronic structure problem and Kohn-Sham method, so that the reader familiar with it could skip that chapter. Likewise the reader familiar with conceptual DFT, could skip chapter 2. Finally, chapter 4 deals with how we calculate the surfaces we study here, so the reader who is not interested in these details may as well skip that chapter.

Hypothesis

Spurious electrostatic interactions in charged systems with periodic boundary conditions can be corrected with electrostatic models. This allows the Fukui potential, and other chemical response functions, in these systems to be calculated. The Fukui potential can be used to get insights on the adsorption energies of chemical species in inorganic surfaces of interest for catalysis.

Objectives

General Objective

The main objective of this master's thesis is to develop and implement chemical response functions in extended systems with periodic boundary conditions.

Specific Objectives

Specifically, we propose the following objectives:

1. Study and elucidate the effect of CBC on Fukui functions.
2. Develop and implement a method to correct the spurious electrostatic interaction between images in the case of the Fukui potential.
3. To develop and apply a model based on chemical response functions to predict the adsorption energy of chemical species on prototypical surfaces for catalysis.

Part I

Theoretical background

Chapter 1

On the electronic problem

Chemistry may be seen, in a restricted sense, as the science that study the formation and rupture of interactions in the matter in the scale of atoms and their higher structures (molecules, clusters, solids, etc). These interactions are intrinsically linked to the electronic structure (to the energy and spatial arrangement of electrons) of components in interaction. As electrons are quantum particles, all chemical phenomena are quantum also. This idea, which is the basis of modern chemistry, was stated in the dawn of quantum mechanics by Prof. Paul A.M. Dirac: "The fundamental laws necessary for the mathematical treatment of a large part of physics and the whole of chemistry are thus completely known, and the difficulty lies only in the fact that application of these laws leads to equations that are too complex to be solved [$\cdots$]" [55]. In this chapter, we will give an overview on how to obtain the electronic structure of a material from the postulates of quantum mechanics. In particular, we will start showing the Schrödinger equation and its form to the many-electron system in Section 1.1. Born-Oppenheimer approximation used to separate the electron and nuclear degrees of freedom is presented in Section 1.2. Then, the main ideas and theorems of density-functional theory will be laid out in Section 1.3. Pseudopotentials will be introduced in Section 1.4. Finally, Bloch's theorem and Kohn-Sham equations in periodic systems will be describe in Section 1.5.

1.1 The Schrödinger equation

In the non-relativistic limit, the evolution of a quantum state is determinate by the Schrödinger equation. Therefore, any problem about electronic structure within that limit is covered by the time-dependent Schrödinger equation in its position representation,

$$i\hbar\frac{\partial}{\partial t}\Phi\big(\{\mathbf{r}_i\},\{\mathbf{R}_I\};t\big)=\hat{H}\Phi\big(\{\mathbf{r}_i\},\{\mathbf{R}_I\};t\big). \tag{1.1}$$

Here, Φ is the wavefunction and $\hat{H}$ is the Hamiltonian operator. In atomic units (a.u.), the Hamiltonian operator for a system composed by M nuclei and N electron is

$$\begin{aligned}\hat{H}&=-\sum_I^M\frac{1}{2M_I}\nabla_I^2-\sum_i^N\frac{1}{2}\nabla_i^2+\sum_{i<j}^N\frac{1}{|\mathbf{r}_i-\mathbf{r}_j|}-\sum_{I,i}^{M,N}\frac{Z_I}{|\mathbf{R}_I-\mathbf{r}_i|}+\sum_{I<J}^M\frac{Z_IZ_J}{|\mathbf{R}_I-\mathbf{R}_J|}\\&=\hat{T}_N\big(\{\mathbf{R}_I\}\big)+\hat{T}_e\big(\{\mathbf{r}_i\}\big)+\hat{V}_{e-e}\big(\{\mathbf{r}_i\}\big)+\hat{V}_{e-n}\big(\{\mathbf{r}_i\},\{\mathbf{R}_I\}\big)+\hat{V}_{n-n}\big(\{\mathbf{R}_I\}\big)\\&=\hat{T}_N\big(\{\mathbf{R}_I\}\big)+\hat{H}_e\big(\{\mathbf{r}_i\},\{\mathbf{R}_I\}\big)\end{aligned} \tag{1.2}$$

for the electronic $\{\mathbf{r}_i\}$ and nuclear $\{\mathbf{R}_I\}$ degrees of freedom. Note that here, M_I y Z_I are the mass and atomic number of the Ith nuclei. The first two terms correspond to kinetic energies of nuclei and electrons, respectively; the third term represents the Coulomb repulsion between electrons; the fourth term corresponds to Coulomb attraction between electrons and nuclei; and the last one is the Coulomb repulsion between nuclei.
In most cases, and for the purposes of this thesis as well, however, the electronic structure is not related to time-dependent interactions. Thus, our problem is actually the time-independent Schrödinger equation

$$\hat{H}\Psi\big(\{\mathbf{r}_i\},\{\mathbf{R}_I\}\big)=E\Psi\big(\{\mathbf{r}_i\},\{\mathbf{R}_I\}\big) \tag{1.3}$$

In the above equation, the Hamiltonian operator corresponds to the given by Eq. 1.2. As we can see, the electrons and nuclei are coupled through the operator $\hat{V}_{e-n}\big(\{\mathbf{r}_i\},\{\mathbf{R}_I\}\big)$. This fact means that the equation is not one of separable variables and it is not possible to despise it because it is so big. Moreover, its $3M+3N$ degrees of freedom make it

practically impossible to solve. Therefore, resorting to approximations becomes imperative.

1.2 Decoupling electrons and nuclei

The vast majority studies of theoretical chemistry and condensed matter physics use approximate solutions to the time-independent non-relativistic Schrödinger equation formulated within the Born-Oppenheimer approximation as a method to deal with the decoupling of electrons and nuclei [56].

The classic picture to justify the Born-Oppenheimer approximation is that electrons move faster than nuclei. that is, electrons "feel" or "see" the instantaneous position of the nuclei. In contrast, nuclei "feel" the average potential of the electronic cloud. Hence, the electronic structure can be studied by considering the nuclei as stationary (referred to as the "clamped nuclei" approximation).

The Born-Oppenheimer approximation implies that Eq. 1.3 is solved in two steps and the total wavefunction may be write as a simple product

$$\Psi\big(\{\mathbf{r}_i\},\{\mathbf{R}_I\}\big) \approx \Psi_e\big(\{\mathbf{r}_i\};\{\mathbf{R}_I\}\big)\Psi_N\big(\{\mathbf{R}_I\}\big) \tag{1.4}$$

where $\Psi_e\big(\{\mathbf{r}_i\};\{\mathbf{R}_I\}\big)$ corresponds to the electronic wavefunction in the field of clamped nuclei and $\Psi_N\big(\{\mathbf{R}_I\}\big)$ is the nuclear wavefunction.

The two steps already mentioned result in two Schrödinger equations. The first one is the electronic Schrödinger equation,

$$\hat{H}_e\Psi_{e,k}\big(\{\mathbf{r}_i\};\{\mathbf{R}_I\}\big) = E_k\big(\{\mathbf{R}_I\}\big)\Psi_{e,k}\big(\{\mathbf{r}_i\};\{\mathbf{R}_I\}\big) \tag{1.5}$$

where the electronic Hamiltonian (including the energy due to nuclear-nuclear repulsion) is

$$\hat{H}_e = \hat{T}_e\big(\{\mathbf{r}_i\}\big) + \hat{V}_{e-e}\big(\{\mathbf{r}_i\}\big) + \hat{V}_{e-n}\big(\{\mathbf{r}_i\},\{\mathbf{R}_I\}\big) + \hat{V}_{n-n}\big(\{\mathbf{R}_I\}\big). \tag{1.6}$$

$E_k(\{\mathbf{R}_I\})$ and $\Psi_{e,k}(\{\mathbf{r}_i\};\{\mathbf{R}_I\})$ are calculated at fixed nuclei position. That is, $\hat{V}_{n-n}(\{\mathbf{R}_I\})$ is a constant and both electronic energy and electronic wavefunction depend parametrically on the nuclei position.

The other one is the nuclear Schrödinger equation,

$$\hat{H}_N \Psi_{N,j}(\{\mathbf{R}_I\}) = E_N(\{\mathbf{R}_I\})\Psi_{N,j}(\{\mathbf{R}_I\}) \tag{1.7}$$

where the nuclear Hamiltonian is

$$\hat{H}_N = \hat{T}_N + E_k(\{\mathbf{R}_I\}) \tag{1.8}$$

Even with the Born-Oppenheimer approximation, the task of solving the Eq. 1.6 remains a challenge. There are two main different ways to solve the electronic Schrödinger equation: wavefunction-based methods and density-functional theory (DFT). Because we use density functional theory methods in this thesis, we will not describe the basic wavefunction methods in this thesis and we will limit ourselves to give an brief introduction to DFT. Detailed descriptions about wavefunction-based methods can be found in great books [57–61].

1.3 Density-functional theory

DFT is nowadays the workhorse for electronic structure calculations in both quantum chemistry and condensed matter physics and is also the basis for the construction of a theory of chemical reactivity. Its fundamentals and physics formalism are supported in existence theorems. The first theorems corresponds to the Hohenberg-Kohn theorems [62] (1964), which essentially state that all that is needed to know the properties of ground- and stationary excited states of a non-relativistic many-particles system is its ground-state electron density, $\rho(\mathbf{r})$. Moreover, the theorems ensure that the exact ground-state density follows a variational principle and it can be therefore calculated

without the necessity of solving the Schrödinger equation.

1.3.1 Hohenberg-Kohn theorems

The Hohenberg-Kohn theorems (HK-theorems) [62] are the most basic of a number of existence theorems which state that stationary many-particle systems can be fully characterized by the ground-state density.

The first theorem states that for a system of N interacting electrons in an external potential $v_{ext}(\mathbf{r})$, there is a one-to-one correspondence, up to a constant, between said external potential, the non-degenerate ground-state wavefunction $|\Psi_0\rangle$ resulting from the solution of the Schrödinger equation and its associated ground-state density ρ,

$$v_{ext}(\mathbf{r}) \underset{\uparrow}{\Longleftrightarrow} |\Psi_0\rangle \underset{\uparrow}{\Longleftrightarrow} \rho(\mathbf{r}) = N \sum_{\sigma_1 \cdots \sigma_N} \int d\mathbf{r}_2 \cdots \mathbf{r}_N \left|(\mathbf{r}_1\sigma_1, \cdots, \mathbf{r}_N\sigma_N)|\Psi_0\rangle\right|^2 \tag{1.9}$$

unique (up to some additive constant in v_{ext})

The proof that $v_{ext}(\mathbf{r})$ and $\rho(\mathbf{r})$ are determine each other uniquely relies on *reductio ad absurdum* method. We assume that two external potentials $v_{ext}(\mathbf{r})$ and $v'_{ext}(\mathbf{r})$ (which differ by more than a constant) that yield the same electron density $\rho(\mathbf{r})$. Thus we have the two Schrödinger equations,

$$\hat{H}|\Psi_0\rangle = \left(\hat{T} + \hat{V}_{ext} + \hat{V}_{ee}\right)|\Psi_0\rangle = E_0|\Psi_0\rangle \tag{1.10}$$

$$\hat{H}'|\Psi'_0\rangle = \left(\hat{T} + \hat{V}'_{ext} + \hat{V}_{ee}\right)|\Psi'_0\rangle = E'_0|\Psi'_0\rangle \tag{1.11}$$

From the Ritz variational principle one obtains,

$$\begin{aligned} E_0 = \langle\Psi_0|\hat{H}|\Psi_0\rangle &< \langle\Psi'_0|\hat{H}|\Psi'_0\rangle \\ E_0 &< \langle\Psi'_0|\hat{H}' + \hat{H} - \hat{H}'|\Psi'_0\rangle \\ E_0 &< E'_0 + \int \rho(\mathbf{r})\left(v_{ext} - v'_{ext}\right) d\mathbf{r} \end{aligned} \tag{1.12}$$

Exchanging the primes one gets,

$$E_0' = \langle \Psi_0' | \hat{H}' | \Psi_0' \rangle < \langle \Psi_0 | \hat{H}' | \Psi_0 \rangle$$
$$E_0' < E_0 + \int \rho(\mathbf{r}) \left(v_{ext}' - v_{ext} \right) d\mathbf{r} \tag{1.13}$$

After addition of Eqs. 1.12 and 1.13, one ends up with a contradiction,

$$E_0 + E_0' < E_0' + E_0 \tag{1.14}$$

Because of this theorem, we can say that any ground-state observable is a density functional. In particular, this is true for the ground-state energy,

$$E_v[\rho(\mathbf{r})] = T[\rho(\mathbf{r})] + V_{ee}[\rho(\mathbf{r})] + \int \rho(\mathbf{r}) v_{ext}(\mathbf{r})\, d\mathbf{r} \tag{1.15}$$
$$E_v[\rho(\mathbf{r})] = F[\rho(\mathbf{r})] + \int \rho(\mathbf{r}) v_{ext}(\mathbf{r})\, d\mathbf{r} \tag{1.16}$$

where $F[\rho(\mathbf{r})]$ is an universal functional in the sense that it is the same form for all systems.

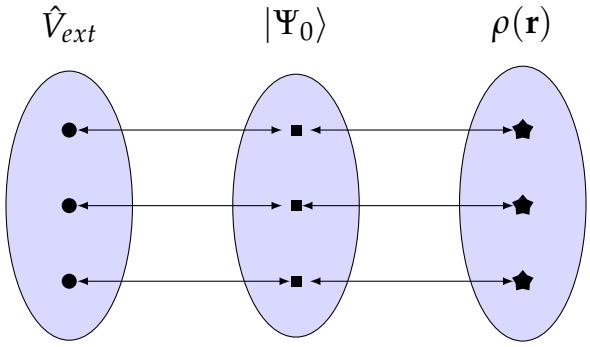

Figure 1.1: One-to-one correspondence, established by the Hohenberg-Kohn, theorems between external potentials $\hat{V}_{ext}$, non-degenerate ground states $|\Psi_0\rangle$ and its associated ground-state densities $\rho(\mathbf{r})$.

The second Hohenberg-Kohn theorem states the existence of a variational principle for

$E_v[\rho]$. This is, for a trial density $\tilde{\rho}(\mathbf{r})$, such that $\tilde{\rho}(\mathbf{r}) \geq 0$ and $\int \tilde{\rho}(\mathbf{r})\, d\mathbf{r} = N$,

$$E_v[\rho] \leq E_v[\tilde{\rho}] \tag{1.17}$$

The proof relies on Ritz variational principle. The first theorem ensures that a electron density $\tilde{\rho}(\mathbf{r})$ determines uniquely its own external potential $\tilde{v}_{ext}$, Hamiltonian $\hat{H}'$ and ground-state $|\tilde{\Psi}\rangle$. Thus, evaluating the energy density functional in this trial density, one obtains

$$E_v[\tilde{\rho}(\mathbf{r})] = F[\tilde{\rho}(\mathbf{r})] + \int v_{ext}(\mathbf{r})\tilde{\rho}(\mathbf{r})\, d\mathbf{r} = \langle \tilde{\Psi}|\hat{H}|\tilde{\Psi}\rangle \tag{1.18}$$

and from the Ritz variational principle the last term satisfies the inequality

$$\langle \tilde{\Psi}|\hat{H}|\tilde{\Psi}\rangle \geq \langle \Psi|\hat{H}|\Psi\rangle = E_v[\rho(\mathbf{r})] = E_0 \tag{1.19}$$

Assuming the existence of variational derivative $\delta E_v[\rho]/\delta\rho$ (its existence requires that the functional $E_v[\rho]$ to be a defined on a sufficiently dense set of densities ρ), the minimum principle (1.17) indicate the possibility to determinate the ground-state density by a variational equation:

$$\frac{\delta}{\delta\rho(\mathbf{r})}\left\{ E_v[\rho(\mathbf{r})] - \mu\left(\int \rho(\mathbf{r})\, d\mathbf{r} - N \right) \right\} = 0 \tag{1.20}$$

which leads to the Euler-Lagrange equation

$$\mu = \frac{\delta E_v[\rho]}{\delta\rho(\mathbf{r})} = v_{ext}(\mathbf{r}) + \frac{\delta F_v[\rho]}{\delta\rho(\mathbf{r})} \tag{1.21}$$

where μ is the Lagrange multiplier that ensures that ρ integrates to N. μ is also the chemical potential of electrons [12].

1.3.2 The constrained search formulation

An important point about the HK-theorems is that both assume that $\rho(\mathbf{r})$ is interacting v-representable; i.e., that the electron density comes from an non-degenerate antisymmetric ground-state wavefunction which is a solution of a Schrödinger equation that has a Hamiltonian with some external potential v_{ext}. This restriction results in a problem because is very difficult to enforce its compliance in the minimization of (1.20). To solve this problem Prof. Mel Levy in 1979 [63] defined the universal functional in a new form

$$F_{LL}[\rho] = \underset{\Psi\to\rho}{min}\langle\Psi|\hat{T}+\hat{V}_{ee}|\Psi\rangle \tag{1.22}$$

in which the density only needs to be N-representable. This variational search is constrained because the space of wavefunctions is limited only to those that gives the density ρ.

We would like to close this section by clarifying that although the HK-theorems has a number of serious restricions such as the assumption of non-degenerate ground states and that only deal with local and time-independent external potentials, the rigorous foundations of density functional theory have been extended to practically all chemical and physical situations of interest, e.g., degenerate ground states, non-local external potentials, relativistic systems, spin-polarised systems, etc [64–67].

1.3.3 The Kohn-Sham scheme

In principle, the HK-theorems allow the determination of the exact ground-state density of a specified many-body system. However, HK-theorems do not give (and it does not exist until this moment) the explicit form of $E_v[\rho(\mathbf{r})]$ (or $F[\rho(\mathbf{r})]$). In 1965, W. Kohn and L. Sham [68] proposed a method in which the direct minimization with respect to density by one based on an orbital picture. The resulting self-consistent equations, known as the Kohn-Sham equations, are in principle exact and have become the cornerstone of the DFT implementations. An overview of its derivation is in order.

As we do not known the exact form of $F[\rho(\mathbf{r})]$, we can not solve the Eq. 1.21. However, we may always ask ourselves in what scenario would be easier to solve it. Let us to consider a system of N non-interacting electrons described by the Hamiltonian,

$$\hat{H} = \hat{T}_s + \hat{V}_s(\mathbf{r}) \tag{1.23}$$

where $\hat{T}_s$ and $\hat{V}_s(\mathbf{r})$ represent the kinetic energy and external potential, respectively. The corresponding ground-state many-body wavefunction, assumed to be non-degenerate, is a Slater determinant,

$$\begin{aligned}\langle \mathbf{r}_1\sigma_1, \cdots, \mathbf{r}_N\sigma_N | \Psi_0 \rangle &= \Psi_0(\mathbf{r}_1\sigma_1, \cdots, \mathbf{r}_N\sigma_N) \\ &= \frac{1}{\sqrt{N}} \det \begin{pmatrix} \phi_1(\mathbf{r}_1\sigma_1) & \cdots & \phi_N(\mathbf{r}_1\sigma_1) \\ \vdots & \ddots & \vdots \\ \phi_1(\mathbf{r}_N\sigma_N) & \cdots & \phi_N(\mathbf{r}_N\sigma_N) \end{pmatrix}\end{aligned} \tag{1.24}$$

which is constructed from the energetically lowest solutions ϕ_i of the single-particle Schrödinger equation,

$$\left[-\frac{\hbar^2}{2m_e}\nabla^2 + v_s(\mathbf{r}) \right] \phi_i(\mathbf{r}_i\sigma_i) = \varepsilon_i \phi_i(\mathbf{r}_i\sigma_i) \tag{1.25}$$

and corresponding the ground-state density $\rho_s(\mathbf{r})$ possesses a unique representation,

$$\rho_s(\mathbf{r}) = \sum_{\sigma=\uparrow,\downarrow} \sum_{i}^{N} |\phi_i(\mathbf{r}_i\sigma_i)|^2 \tag{1.26}$$

Kohn-Sham's great idea is that for any interacting system, there exists a local single-particle potential $v_s(\mathbf{r})$ such that the exact ground-state density $\rho(\mathbf{r})$ of the interacting system equals the ground-state density of the auxiliary non-interacting system,

$$\rho(\mathbf{r}) = \rho_s(\mathbf{r}) \tag{1.27}$$

That is, we are demanding that all interacting v-representable ground-state densities are assumed to be at the same time non-interacting v-representable. As the kinetic energy of the auxiliary system is different from that of the real system, the effective potential must have the potential energy due to interactions among the particles and the difference in the kinetic energy. We may rewrite the universal functional as,

$$F[\rho(\mathbf{r})] = T_s[\rho(\mathbf{r})] + J[\rho(\mathbf{r})] + E_{xc}[\rho(\mathbf{r})] \tag{1.28}$$

where J is Coulomb repulsion and E_{xc} is the exchange-correlation functional, which is defined as

$$E_{xc}[\rho(\mathbf{r})] \equiv T[\rho(\mathbf{r})] - T_s[\rho(\mathbf{r})] + V_{ee}[\rho(\mathbf{r})] - J[\rho(\mathbf{r})] \tag{1.29}$$

So the Euler-Lagrange equation takes the form,

$$\mu = \frac{\delta T_s[\rho]}{\delta \rho(\mathbf{r})} + v_{\mathrm{KS}}(\mathbf{r}) \tag{1.30}$$

where the Kohn-Sham effective potential is given by,

$$\begin{aligned} v_{\mathrm{KS}}(\mathbf{r}) &= v_{ext}(\mathbf{r}) + \frac{\delta J[\rho]}{\delta \rho(\mathbf{r})} + \frac{\delta E_{xc}[\rho]}{\delta \rho(\mathbf{r})} \\ &= v_{ext}(\mathbf{r}) + \int \frac{\rho(\mathbf{r}')}{|\mathbf{r} - \mathbf{r}'|} d\mathbf{r}' + v_{xc}(\mathbf{r}; \rho(\mathbf{r})) \end{aligned} \tag{1.31}$$

with the exchange-correlation potential defined as,

$$v_{xc}(\mathbf{r}) = \frac{\delta E_{xc}[\rho]}{\delta \rho(\mathbf{r})} \tag{1.32}$$

Inserting the Eq. 1.31 into Eq. 1.25 we obtain the celebrated Kohn-Sham equations,

$$\left[-\frac{\hbar^2}{2m_e} \nabla^2 + V_{\mathrm{KS}}(\mathbf{r}) \right] \phi_i(\mathbf{r}) = \epsilon_i \phi_i(\mathbf{r}) \tag{1.33}$$

from which we construct the exact density as

$$\rho(\mathbf{r}) = \sum_{i=1}^{N} |\phi_i(\mathbf{r})|^2 \tag{1.34}$$

and the exact energy is given by

$$E[\rho(\mathbf{r})] = T_s[\rho(\mathbf{r})] + J[\rho(\mathbf{r})] + E_{xc}[\rho(\mathbf{r})] + \int V_{ext}(\mathbf{r})\rho(\mathbf{r})\, d\mathbf{r} \tag{1.35}$$

In principle, this energy corresponds to the real ground state energy for the many body interacting system. Nonetheless, one crucial element remains unknown. The quantum correlations of the many-body system is transferred to the exact exchange correlation energy $E_{xc}[\rho(\mathbf{r})]$, the exact form therof is unknown. Despite this fact, some reasonable approaches can be made that lead to good results.

1.3.4 Density-functional approximations

Approximations to the correlation-exchange functional give life to the so-called Density-functional approximations (DFA) and are the basis for all practical applications of DFT. The "mother" of almost all these approximations is Local-density approximation (LDA), in which the exchange-correlation energy is approximate by,

$$E_{xc}^{LDA} \equiv \int e_{xc}(\rho)\rho(\mathbf{r})\, d\mathbf{r} \tag{1.36}$$

where $e_{xc}(\rho)$ is the exchange-correlation energy per particle of a Homogeneous electron gas (HEG) of density ρ [68]. Physically this means that we treat a real system as if it locally consisted of elements of infinitesimal volume within which the density is homogeneous. As the exchange-correlation functional can be exactly written as

$$E_{xc}[\rho] = E_x[\rho] + E_c[\rho] \tag{1.37}$$

the terms of exchange and correlation can be approximated separately [69]. In the case of the LDA, the exchange of a HEG part was first obtained exactly by P. A. M. Dirac [70]

$$e_x(\rho) = -C_x\rho^{1/3}(\mathbf{r}) \tag{1.38}$$

where $C_x = 3/4\left(3/\pi\right)^{1/3}$. The correlation part have been extensively studied and there are theoretical estimates [71] and very exact analytical fits to quantum Monte Carlo calculations, the best known and most used being the one by Vosko, Wilk and Nussair [72].

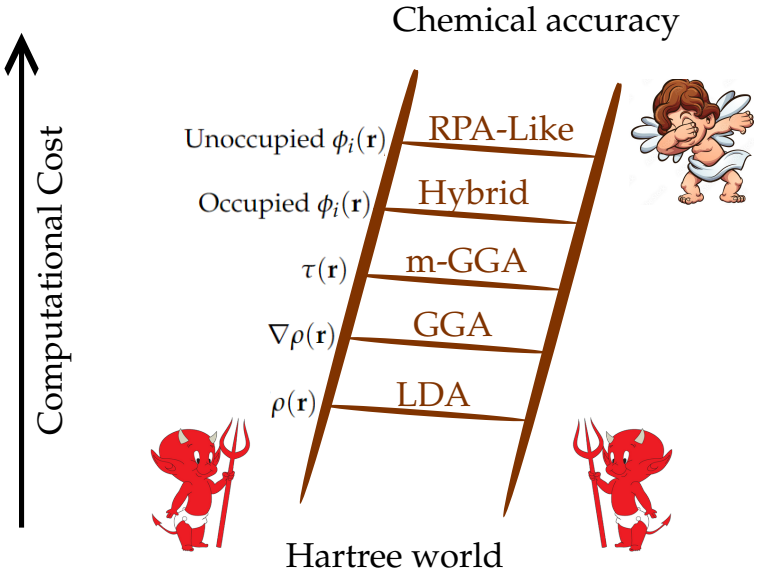

Figure 1.2: Alternative representation of Jacob's ladder of density functional approximations of Prof. Perdew. Each rung represents a family of density functionals based on the same type of approximation.

Another approximations and ways to build the exchange and correlation functionals have been developed, such as: Generalized gradient approximation (GGA), Meta generalized gradient approximation (meta-GGA), hybrid functionals, Random phase approximation (RPA), etc. In 2001, Prof. J.P. Perdew published an analogy between Jacob's ladder (*Genesis* 28:10–19) and the approximations that constitutes the DFA [73]. Fig. 1.2 shows an alternative representation of Jacob's ladder in the DFT context. The idea behind of this analogy is that including exact constraints into approximations beyond the LDA result in more accurate functionals, determining a hierarchy.

Despite the large number of existing functionals (more than two hundred [74]) and studies carried out, one of the weaknesses of DFA persists: it is not possible, in practice, to systematically refine its results, as is possible in wavefunction-based methods. The choice of the functional to use must be an adequate balance between the accuracy of the properties to be studied and the computational cost. Reaching for the heaven is not always the best idea.

1.4 Some ideas about pseudopotentials

Another way to reduce the complexity of determining the electronic structure comes from the clever idea of pseudopotentials. In many problems of molecular and condensed matter physics, the electrons of the system can be divided into two groups: core and valence. Moreover, many properties of atoms or molecules or solids, depended mainly on the electronic distribution of the valence electrons. It results natural to try to reduce the N-electron problem, where N is the total number of electrons, to n-electron problem, where n is the valence electrons number. This reduction means a significant mathematical and computational simplification. This idea was proposed and worked by H. Hellmann (a brilliant man with very bad luck [75]) at the dawn of quantum mechanics. In a series of papers he demonstrated, using the Thomas-Fermi model, that the Pauli exclusion principle for valence electrons can be replaced by a non-classical potential (*Abstossungspotential*), which is now called pseudopotential [76–79].

Currently there are several types of pseudopotentials, each with its own advantages and disadvantages. Of interest for the development of this thesis are Norm-conserving pseudopotentials (NCPP) and Projector augmented wave (PAW). The first ones were introduced by Hamann et al. in 1979 [80] and are built to desirably follow four properties:

1. Real and pseudo valence eigenvalues agree for a chosen "prototype" atomic con-

figuration.

2. Real and pseudo atomic wavefunctions agree beyond a chosen "core radius" r_c.

3. The integrals from 0 to r of the real and pseudo charge densities agree for $r > r_c$, for each valence state (norm conservation),

$$\int_0^{r_c} r^2 |\phi_i^{ps}|^2 \, dr = \int_0^{r_c} r^2 |\phi_i|^2 \, dr \tag{1.39}$$

4. The logarithmic derivatives of the real and pseudo wavefunction and their first energy derivatives agree for $r > r_c$.

On the other hand, PAW method is a general approach to solving the electronic structure problem that retains the full-electron wavefunction of a system. Because the wavefunction changes rapidly near the nucleus of an atom, the integrals are expressed as combinations of smooth functions that extend through space and localized contributions that are evaluated using radial integration over thin spherical regions (muffin-tin spheres) centered at the nuclei.

1.5 Considering the periodicity

In the case of perfect crystalline solids, periodicity is taken into account to reduce the complexity of the calculation. In these systems, the electrons move through a perfectly periodic potential and therefore the Hamiltonian is invariant to the discrete translations that correspond to this periodicity,

$$\hat{H}(\mathbf{r} + \mathbf{T}) = \hat{H}(\mathbf{r}) \tag{1.40}$$

where $\mathbf{T} = n_1\mathbf{a}_1 + n_2\mathbf{a}_2 + n_3\mathbf{a}_3$ are the lattice vectors and $\mathbf{a}_i$ are the primitive lattice vectors. This invariance also holds for any effective single-electron Hamiltonian and potential. Bloch's theorem states that one-electron solution (Bloch states) must have the

following form:

$$\phi_{n,\mathbf{k}}(\mathbf{r}) = e^{i\mathbf{k}\cdot\mathbf{r}} U_{n\mathbf{k}}(\mathbf{r}) \tag{1.41}$$

$$\phi_{n,\mathbf{k}}(\mathbf{r}+\mathbf{T}) = e^{i\mathbf{k}\cdot\mathbf{T}} \phi_{n,\mathbf{k}}(\mathbf{r}) \tag{1.42}$$

where $U_{n\mathbf{k}}(\mathbf{r})$ has the periodicity of the lattice, n is the band index and $\mathbf{k}$ is the wave vector of the electron. The Kohn-Sham equations (Eq. 1.33) can be rewritten as

$$\left[-\frac{\hbar^2}{2m_e}\nabla^2 + V_{\mathrm{KS}}(\mathbf{r}) \right] \phi_{n,\mathbf{k}}(\mathbf{r}) = \epsilon_{n,\mathbf{k}} \phi_{n,\mathbf{k}}(\mathbf{r}) \tag{1.43}$$

Imposition of an appropriate set of periodic boundary conditions (PBC) allows the wave-function $\phi_{n,\mathbf{k}}(\mathbf{r})$ to be expanded as Fourier series,

$$\phi_{n,\mathbf{k}}(\mathbf{r}) = \frac{1}{\sqrt{\Omega}} \sum_{\mathbf{G}} C_{n,\mathbf{k}+\mathbf{G}} e^{i(\mathbf{k}+\mathbf{G})\cdot\mathbf{r}}, \tag{1.44}$$

where $\mathbf{G}$ are the reciprocal lattice vectors.

When attempting to solve Eq. 1.43 for a volume Ω, it is necessary to consider an infinite number of reciprocal lattice vectors $\mathbf{G}$, which is computationally unrealistic. Typically, a cutoff energy, E_{cut}, is introduced so that the $\mathbf{G}$ vectors in the sum of Eq. 1.44 can be truncated according to the condition

$$\frac{1}{2}|\mathbf{k}+\mathbf{G}|^2 < E_{cut} \tag{1.45}$$

The value of E_{cut} should be chosen large enough so to include enough vectors $\mathbf{G}$ to be able to accurately describe the smallest features of wave function $\phi_{n,\mathbf{k}}$

Chapter 2

Chemical and physical response functions

The theory of electronic structure all accounts for the art of skillfully converting information about molecular or crystalline structures into insights about their chemistry, i.e., the reactivity. According to the American Chemical Society (ACS), there are more than 50 million known chemical compounds [81]. These chemical compounds are transformed through chemical reactions. Chemical reactions can be seen as the way in which a chemical species (a many-body system) responds to an external perturbation, which in principle will be given by the change in the external potential and the number of electrons. At the beginning of the reaction this perturbation will be small enough to use perturbation theory of low order. As DFT is able to deal with a non-integer number of particles, offers a natural theoretical framework to build a chemical reactivity theory, CDFT, in which a series of response functions emerge. In this chapter, we briefly review the CDFT. Section 2.1 contains an overview of the fundamental ideas of this theory, while Section 2.2 presents the main response functions and descriptions that emerge and that are of interest to this thesis.

2.1 General consideration

The prediction and description of chemical reactivity essentially involve understanding how and why a chemical species (such as an atom, molecule, surface, etc.) responds to the attack of different types of reactants. The usual reference point is the isolated chemical species, and its response to chemical attack is considered. This description leads to what has been called "inherent chemical reactivity" and it is the essence of CDFT.

One can consider as a starting point for the CDFT that any ground-state property can be sufficiently described by the number of particles, N, and the external potential, $v_{ext}(\mathbf{r})$. In particular, the electronic energy can be rewritten as

$$E = E(N)[v] \equiv E[N, v] \tag{2.1}$$

where we have made explicit the dependence as a function of energy with respect to the number of electrons and as a functional with respect to the external potential. The last identity will be used for simplicity. It is worth noting that this representation is consistent with the Hohenberg-Kohn DFT in the sense that for a given number of electrons, the external potential fixes the electronic density, which determines the energy via Eq. 1.18.

Let us consider in this representation, called canonical ensemble, the scenario in which an attacking agent approaches a chemical species or substrate, causing a change in energy due to the change of both the number of electrons and the external potential. Via Taylor expansion we have that the change in the total energy at $0\,K$ is [82]

$$\begin{aligned}\Delta U = &\int \left[\frac{\delta V_{NN}[\nu]}{\delta \nu(\mathbf{r})}\right] \delta\nu(\mathbf{r})\, d\mathbf{r} + \left(\frac{\partial E}{\partial N}\right)_v \Delta N + \int \left[\frac{\delta E}{\delta v(\mathbf{r})}\right]_N \delta v(\mathbf{r})\, d\mathbf{r} \\ &+ \int \left(\frac{\partial}{\partial N}\left[\frac{\delta E}{\delta v(\mathbf{r})}\right]_N\right)_v \Delta N \delta v(\mathbf{r})\, d\mathbf{r} + \cdots\end{aligned} \tag{2.2}$$

where U denotes the total energy within the Born-Oppenheimer approximation, i.e, U

is the sum of total electronic energy and internuclear repulsion energy. The terms in Eq. 2.2 represent (i) the change in internuclear repulsion energy due to the change in external potential (ii) the change in electronic energy due to electron transfer, (iii) the change in electronic energy due to the change in external potential, (iv) the cross term linking electron transfer to changes in the external potential. Naturally, it is impossible to take into account the complete expansion. Thus, it is necessary to truncate the expansion or, alternatively, to employ the functional-analytic generalization of Taylor's theorem with an accompanying remainder [83]. We are neglecting the second- and higher-order derivatives with respect to the number of electrons because those vanish at 0 K [1, 2]. Higher order response with respect to the external potential could be important. However, polarization effects are commonly neglected in CDFT principally because it is difficult to compute the density polarizability kernel [84] and the interactions that arise from them are short-ranged compared to linear (electrostatic) terms [82]. As such, only the terms that are explicitly shown in Eq. 2.2 can be sufficiently for qualitative and semi-quantitative purposes.

The coefficients in the expansion of Eq. 2.2 can be identified as response functions of the system due to the perturbation, i.e., each response function is a reactivity descriptor. Please note that up to this point, we have assumed differentiability of E with respect both N and $v_{ext}(\mathbf{r})$ (functional). This will be briefly discussed below.

2.1.1 Some insights about the derivative discontinuities of the energy

Some response functions involves derivatives of the energy with respect the number of particles and therefore require that energy to be well defined for fractional particle number and, naturally, to be differentiable with respect the number of particles. Perdew, Levy and Parr extended the DFT to fractional number of electrons (open systems) based on zero-temperature grand canonical ensemble theory [1]. They demonstrated, among other things, that the energy is a series of straight lines interpolating its values at integer number of electrons. That is, the energy for a system with $N + \eta$ particles is given

by

$$E(N+\eta) = (1-\eta)E(N) + \eta E(N+1) \tag{2.3}$$

This relationship between energy and particle number is illustrated in Fig. 2.1. As a consequence of this, the derivative of total energy functional with respect number of electrons is discontinuous at all integer particle numbers. As we will show later, this is a fact of notable importance in the CDFT.

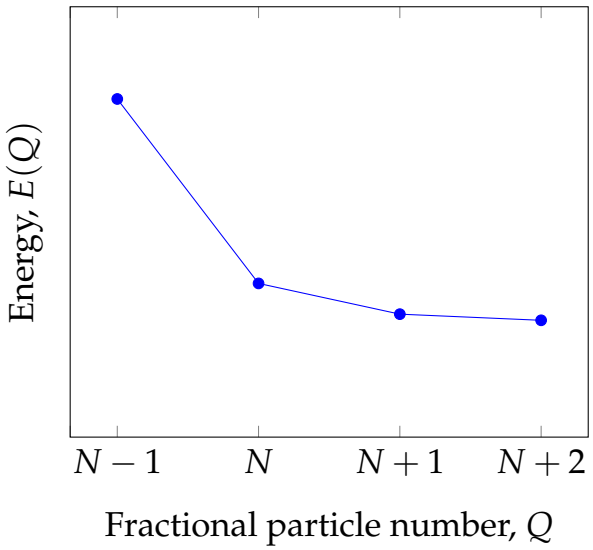

Figure 2.1: Dependence of the total energy, $E(Q)$, on the fractional particle number, Q, under the same external potential, v_{ext}.

2.2 Response functions

One of the main aims of CDFT have been to make sense to the chemical descriptors in Eq. 2.2 through the DFT formalism and both chemical knowledge and language. The response functions that are treated in the development of this thesis are described below. A detailed overview of CDFT can be found in great articles and books [9–11, 85].

2.2.1 Chemical potential and electronegativity

The first response function in Eq. 2.2 corresponds to the electronic chemical potential, μ. As we have previously mentioned, the Lagrange multiplier in the Euler-Lagrange

equation of the DFT, Eq. 1.21, is the chemical potential of the electrons. This can be easily seen by using the chain rule,

$$\mu = \left[\frac{\delta E}{\delta \rho(\mathbf{r})}\right]_v = \left(\frac{\partial E}{\partial N}\right)_v \left[\frac{\delta N}{\delta \rho(\mathbf{r})}\right]_v \tag{2.4}$$

where the second factor in Eq. 2.4 is

$$\left[\frac{\delta N}{\delta \rho(\mathbf{r})}\right]_v = \frac{d}{d\epsilon}\int \left(\rho(\mathbf{r}) + \epsilon\delta(\mathbf{r}-\mathbf{r}')\right) d\mathbf{r}\Big|_{\epsilon=0} = 1 \tag{2.5}$$

As a result one finds

$$\mu = \left(\frac{\partial E}{\partial N}\right)_v \tag{2.6}$$

which was established by Parr et al. in the seminal paper of CDFT [12]. The crucial step in constructing a chemical reactivity theory was to identify the chemical potential as the negative of electronegativity , χ, i.e.

$$\mu = \left(\frac{\partial E}{\partial N}\right)_v = -\chi \tag{2.7}$$

The concept of electronegativity was introduced by Pauling in 1932 as the " atom's tendency to attract electrons within a molecule during the formation of the molecule". Since then, the electronegativity has transformed in a empirical fundamental concept in chemistry and material science. Essentially, it allows to infer important aspects about the interactions between chemical species. Particularly, the distribution of the charge.

The justification of Eq. 2.7 by Parr et al. [12] comes from the work of Iczkowski and Margrave [86] in which they define electronegativity as

$$\chi = -\left(\frac{dE_{vs}}{dQ}\right)_{Q=0} \tag{2.8}$$

where Q was defined as the number of electrons minus the nuclear charge, Z, and E_{vs} denotes the valence state energy, which corresponds essentially to the energy of an atom in a molecule. In contrast, Eq. 2.7 is expressed in terms of the energy of the ground state

of the chemical species, extending the definition of electronegativity to the point where some people consider them to refer to different quantities [87, 88].

2.2.2 Electron density

The second response function in Eq. 2.2 is the electron density,

$$\left[\frac{\delta E}{\delta v_{ext}(\mathbf{r})}\right]_N = \left[\frac{\delta}{\delta v_{ext}(\mathbf{r})}\right]_N \left(F[\rho] + \int \rho(\mathbf{r}) v_{ext}(\mathbf{r})\, d\mathbf{r}\right) = \rho(\mathbf{r}) \tag{2.9}$$

which is a physical observable that represents the average distribution of electrons in a given external potential.

2.2.3 Fukui function

The third response function in Eq. 2.2, which is central in the development of this thesis, was defined by Parr and Yang in 1984 [21] with the name of Fukui Function and is given by

$$\left(\frac{\partial}{\partial N}\left[\frac{\delta E}{\delta v_{ext}(\mathbf{r})}\right]_N\right)_{v_{ext}} = \left(\frac{\partial \rho}{\partial N}\right)_{v_{ext}} \tag{2.10}$$

which locally quantifies the change in electron density with respect to the change in the number of electrons at constant external potential.

Due to the slope of $\rho(\mathbf{r})$ as a function of N has discontinuities at integers numbers of electrons [1], the derivative must be evaluated from above and below [21]. This results in two Fukui functions, one appropriate for describing electrophilic attack, i.e., attacks by electron-poor species

$$f^-(\mathbf{r}) = \left(\frac{\partial \rho(\mathbf{r})}{\partial N}\right)^-_{v(\mathbf{r})} \tag{2.11}$$

and other appropriate for describing nucleophilic attack, that is, attacks by electron-rich species

$$f^+(\mathbf{r}) = \left(\frac{\partial \rho(\mathbf{r})}{\partial N}\right)^+_{v(\mathbf{r})} \tag{2.12}$$

If other effects are ignored, a molecule is prone to donate/accept electrons in those sites where the Fukui function is large [10, 25].

The Fukui function takes its name because it generalizes the Fukui's FMO [27–30] theory, which states that in a reaction electrons are added to the lowest unoccupied molecular orbital (LUMO) and removed from the highest occupied molecular orbital (HOMO). That relation is better seen when the Fukui functions are written in terms of Kohn-Sham (KS) orbitals [22]:

$$f^{-/+}(\mathbf{r}) = \left|\phi_{\text{HOMO/LUMO}}(\mathbf{r})\right|^2 + \sum_{i=1}^{N}\left(\frac{\partial|\phi_i(\mathbf{r})|^2}{\partial N}\right)^{-/+}_{v(\mathbf{r})} \tag{2.13}$$

These expressions comprises two terms: the density of Highest occupied molecular orbital (HOMO) or Lowest unoccupied molecular orbital (LUMO) and a relaxation term. In molecules, the relaxation term is usually small because of the discrete nature of the KS orbitals' spectra [37]. Furthermore, as mentioned earlier, Perdew et al. [1] demonstrated that the density of an open system with $N+\eta$ electrons, where N is an integer, is a linear combination of the densities of the system with the nearest integer numbers of electrons. Thus, the Fukui function for finite system can be calculated in exact way, at least in principle, from finite differences [1, 25]:

$$f^{\pm}(\mathbf{r}) = \pm\big(\rho_{N\pm1}(\mathbf{r}) - \rho_N(\mathbf{r})\big) \tag{2.14}$$

There is another way to compute the Fukui function without the necessity of considering charged systems. It emerges from the relation between the local softness, $s(\mathbf{r})$, Fukui function and Local density of states (LDOS), $g(\mathbf{r}, E)$. The local softness and Fukui function are related through a chain rule,

$$s(\mathbf{r}) = \left(\frac{\rho(\mathbf{r})}{\partial\mu}\right)_{v(\mathbf{r})} = \left(\frac{\partial\rho(\mathbf{r})}{\partial N}\right)_{v(\mathbf{r})}\left(\frac{\partial N}{\partial\mu}\right)_{v(\mathbf{r})} = f(\mathbf{r})S \tag{2.15}$$

Thus Fukui function is the ratio between local softness and global softness, S. As elec-

tron density can be write in terms of LDOS,

$$\rho(\mathbf{r}) = \int^{\mu} g(\mathbf{r}, E) dE \tag{2.16}$$

we can take the derivative with to respect μ (using the Leibniz's rule), obtaining the exact expression for $s(\mathbf{r})$, which was derived first by MH Cohen et al.[89],

$$s(\mathbf{r}) \equiv \left(\frac{\partial \rho(\mathbf{r})}{\partial N} \right)_{v(\mathbf{r})} = g(\mathbf{r}, \mu) + \int^{\mu} \left(\frac{\partial g(\mathbf{r}, E)}{\partial \mu} \right)_{v(\mathbf{r})} dE \tag{2.17}$$

As we can see, the resulting expression is analogous to Eq. 2.13 in the sense that it comprises two terms: a frontier contribution (LDOS at Fermi level) and the relaxation term. In contrast to molecules, the relaxation terms could be not small o negligible because the density of states around the Fermi level is finite, that is to say, the states near to the Fermi level may contribute to the Fukui function [37]. Although Eq. 2.17 is exact, there is not analytic expression or method to compute the relaxation terms. Cárdenas et al. [90] proposed an ansatz to compute the Eq. 2.17 writing the derivative as a limit,

$$s^{\pm}(\mathbf{r}) \approx \pm \lim_{\delta\mu \to 0^+} \frac{1}{\delta\mu} \int_{\mu}^{\mu \pm \delta\mu} g(\mathbf{r}, E) dE \tag{2.18}$$

from where obtaining the Fukui function is straightforward,

$$f^{\pm}(\mathbf{r}) \approx \pm \frac{\lim\limits_{\delta\mu \to 0^+} \int_{\mu}^{\mu \pm \delta\mu} g(\mathbf{r}, E) dE}{\lim\limits_{\delta\mu \to 0^+} \int_{\mu}^{\mu \pm \delta\mu} g(\mathbf{r}, E) dE d\mathbf{r}} \tag{2.19}$$

The advantage of the Eq. 2.18 is that it is easy to compute because the local density of states is implemented in almost all solid-state softwares. However, it does have complexities: i) naturally, the limit cannot taken to 0, i.e., the $s(\mathbf{r})$ value depends on the $\delta\mu$ chosen, ii) it is essentially a "frozen orbital" approximation of the Eq. 2.17 because it does not consider the dependency of $g(\mathbf{r}, E)$ with to respect μ.

Cárdenas et al. [37] has proposed another alternative using finite differences with a frac-

tional number of electrons. The problem of the introduction of the CBC can be partially bypassed in the limit in which δN tends to zero. They proposed that one way to take this limit is to calculate the density of the neutral system, $\rho(\mathbf{r}, N_0)$, and several lightly charged systems, $\rho(\mathbf{r}, N_0 + \delta N), \rho(\mathbf{r}, N_0 + 2\delta N), \cdots$. Then for every point in the real space a linear interpolation of the densities as a function of the number of electrons may be made, the slope of this interpolation, for each point, is the Fukui function because

$$\rho(\mathbf{r}, N) = \rho(\mathbf{r}, N_0) + \left(\frac{\partial \rho(\mathbf{r}, N)}{\partial N}\right)_{v(\mathbf{r})} (N - N_0) + \cdots \tag{2.20}$$

This approximation is valid if the charge of the charged systems is small enough to be within the linear regime of ρ versus N. Although this approach can in principle bypass the problem of introducing the CBC and takes into account the relaxation effects, another problem arises with it. Specifically, there is an issue with the lack of accuracy of approximate functionals to describe the electron density of systems with a fractional number of electrons. It is widely recognized that local density approximation (LDA) functionals, all generalized gradient approximation (GGA) functionals, and most hybrid and corrected long-range functionals fail to correctly predict the piecewise E versus N, obtaining a convex underestimation of E versus N, which results in a delocalization error in the density [7, 91].

Fukui potential

Unlike the Fukui function, its electrostatic potential can shed light on whether those regions in which the system is more prone to accept or donate electrons from/to the reactant are actually accessible to it [11, 33, 92]. This potential is called the Fukui potential and is given by

$$v_f^{\pm}(\mathbf{r}) = \int \frac{f^{\pm}(\mathbf{r}')}{|\mathbf{r}' - \mathbf{r}|} d\mathbf{r}' \tag{2.21}$$

The Fukui potential can be calculate straightforward as a difference of electrostatic potentials

$$v_f^{\pm}(\mathbf{r}) = \pm\big(\Phi_N(\mathbf{r}) - \Phi_{N\pm1}(\mathbf{r})\big) \tag{2.22}$$

Here,

$$\Phi_N(\mathbf{r}) = \sum_{\alpha} \frac{Z_\alpha}{|\mathbf{r}_\alpha - \mathbf{r}|} - \int \frac{\rho_N(\mathbf{r}')}{|\mathbf{r}' - \mathbf{r}|} d\mathbf{r}' \tag{2.23}$$

denotes the electrostatic potential of the system with N electrons due to its electron density and nuclei. Although the calculation via Eq. 2.22 is straightforward, errors are introduced when this equation is used with calculations with PBC and discrete plane-wave basis set in which the charged systems involve the CBC. Details about this problem will be discussed in Chapter 3.

Chapter 3

Electrostatics in Periodic Boundary Conditions

Obtaining the Fukui function and Fukui potential presents technical difficulties for periodic or extended systems. In this chapter, the fundamental ideas and laws of electrostatics are reviewed in Section 3.1 and in the following three sections, three methodologies that have been proposed to overcome these difficulties are presented: Exact Coulomb cutoff technique in Section 3.2, Self-Consistent Potential Correction scheme in Section 3.3 and finally Electrodes' method in Section 3.4.

3.1 Fundamental equations

Electrostatic interaction are described by Maxwell's equations, which relate the electric field, $\mathbf{E}(\mathbf{r})$, and charge density, $\rho(\mathbf{r})$,

$$\nabla \cdot \mathbf{E}(\mathbf{r}) = 4\pi\rho(\mathbf{r}) \tag{3.1}$$

$$\nabla \times \mathbf{E}(\mathbf{r}) = 0 \tag{3.2}$$

Due to the irrotational nature of the electrostatic field, it is frequently more convenient to describe it using the gradient of a scalar potential, i.e., the electrostatic potential, as

$$\mathbf{E}(\mathbf{r}) = -\nabla v(\mathbf{r}) \tag{3.3}$$

Combining Eqs. 3.1 and 3.3, Maxwell's equations are recast into a single second-order differential equation,

$$\nabla^2 v(\mathbf{r}) = -4\pi\rho(\mathbf{r}) \tag{3.4}$$

called Poisson equation.

Once appropriate boundary conditions are established, the above differential equation can be solved exactly. Specifically, within a closed volume of space, specifying either the potential (Dirichlet or open boundary conditions) or the normal component of the field (von Neumann boundary conditions) at the boundary is required to obtain a unique solution to the electrostatic problem.

The Eq. 3.4 can alternatively be rewritten in a general formulation using Green's functions, namely,

$$v(\mathbf{r}) = \int_{\mathscr{B}} G(\mathbf{r} - \mathbf{r}')\rho(\mathbf{r}')\, d\mathbf{r}' \tag{3.5}$$

Here, the integration is carried out across the arbitrary bounded region denoted as $\mathscr{B}$.

For the particular case of an isolated charge density in vacuum, it is customary to impose

homogeneous Dirichlet or von Neumann conditions at infinity, such that

$$v(\mathbf{r}) = \int \frac{\rho(\mathbf{r}')}{|\mathbf{r} - \mathbf{r}'|} d\mathbf{r}' \tag{3.6}$$

On the other hand, when dealing with periodic systems, it is natural to recast the electrostatic equations in reciprocal space, we can rewrite the Eq. 3.6, using the convolution theorem, in the Fourier space as

$$v(\mathbf{G}) = \rho(\mathbf{G}) w(\mathbf{G}) \tag{3.7}$$

where $w(\mathbf{G})$ is the Fourier transform of Coulomb potential

$$w(\mathbf{G}) = \frac{4\pi}{G^2} \tag{3.8}$$

Transforming the Eq. 3.7 back into real space, we obtain, for a unit cell of volume Ω

$$v(\mathbf{r}) = \frac{4\pi}{\Omega} \sum_{\mathbf{G} \neq 0} \frac{\rho(\mathbf{G})}{G^2} e^{i\mathbf{G}\cdot\mathbf{r}} \tag{3.9}$$

Note that the null "wave vector" ($\mathbf{G} = 0$) cannot be included or the potential would diverge. This is not a problem in bulk crystals bulk crystals as $V(\mathbf{G} = 0)$ corresponds to the average value of the potential in the unit cell. Furthermore, this average value can be set to zero ($V(\mathbf{G} = 0) = 0$) by noticing that the overall charge neutrality of the unit cell imposes the average of the sum of the electronic and ionic charge is zero.

Charged systems are more complicated as the Gauss theorem precludes the existence of charge unit cells with PBCs; its electrostatic energy would be infinity. This difficulty is usually circumvent by adding compensating background of charge (CBC, $\langle \rho(\mathbf{r}) \rangle$) that restores neutrality,

$$\rho(\mathbf{r}) \longrightarrow \rho(\mathbf{r}) - \langle \rho(\mathbf{r}) \rangle \tag{3.10}$$

To overcome the complications that arises in charged surfaces, namely, the presence of unphysical uniform charge in the vacuum, a correction of the electrostatic potential is required. The correction methodologies used in this work are detailed below.

3.2 Exact Coulomb cutoff technique

To solve this problem, Rozzi et al. [53] introduced a reciprocal space analytical method to cut off the long range interactions in supercell calculations for systems that are infinite and periodic in one or two dimensions, as a generalization of the technique proposed by Jarvis [49] for finite charged and polar systems. The initial step involves the transformation of Eq. 3.7 into a modified form, given by

$$\tilde{v}(\mathbf{G}) = \tilde{\rho}(\mathbf{G})\tilde{w}(\mathbf{G}) \tag{3.11}$$

ensuring the elimination of all interactions involving the undesired periodic replicas of the system. To do so, it is necessary to: i) define a screening region $\mathscr{D}$, outside of which there is no Coulomb interaction; ii) compute the Fourier transform of the desired effective interaction $\tilde{w}(\mathbf{G})$, such that

$$\tilde{w}(\mathbf{r}) = \begin{cases} \dfrac{1}{r} & \text{if} \quad \mathbf{r} \in \mathscr{D} \\ \\ 0 & \text{if} \quad \mathbf{r} \notin \mathscr{D} \end{cases} \tag{3.12}$$

and iii) modify the density $\rho(\mathbf{r})$ in such a way that the effective density is still 3D-periodic, so that the convolution theorem can be still applied, but densities belonging to undesired images are not close enough to interact through $\tilde{w}(\mathbf{r})$. The step (2) implies that we need to calculate the modified Fourier integral

$$\tilde{w}(\mathbf{G}) = \int \tilde{w}(\mathbf{r}) e^{-i\mathbf{G}\cdot\mathbf{r}} d\mathbf{r} = \int_{\mathscr{D}} w(\mathbf{r}) e^{-i\mathbf{G}\cdot\mathbf{r}} d\mathbf{r} \tag{3.13}$$

where the modified potential $\tilde{w}$ is zero outside the domain $\mathscr{D}$. The results of the integral 3.13 for 2-D periodic systems is the following:

$$\tilde{w}^{2D}(G_{\parallel}, G_z) = \begin{cases} \frac{4\pi}{G^2}\left[1 + e^{-G_{\parallel}R}\left(\frac{|G_z|}{G_{\parallel}}\sin(|G_z|R) - \cos(|G_z|R)\right)\right]; \\ \text{for} \quad G_{\parallel} \neq 0 \\ \\ \frac{4\pi}{G^2}\left[1 - \cos(|G_z|R) - G_z R \sin(|G_z|R)\right]; \\ \quad \text{for} \quad G_{\parallel} \neq 0 \\ \\ -2\pi R^2; \\ \quad \text{for} \quad G_{\parallel} = 0 \quad \text{and} \quad G_z = 0 \end{cases} \tag{3.14}$$

Exact Coulomb cutoff technique (ECC) is implemented in the Octopus code [93–96] to compute the Hartree potential in those system that are periodic in one or two dimensions.

3.3 Self-Consistent Potential Correction scheme

Self-Consistent Potential Correction (SCPC) scheme [97] incorporates a corrective potential (v_{cor}) to the Kohn-Sham equations. During self-consistent iterations, v_{cor} is updated via the following four steps: (i) find the distribution of extra charge within the supercell ($\delta\rho$), (ii) compute its corresponding periodic electrostatic potential (v_{per}), (iii) establish the potential for an identical isolated charge distribution (v_{iso}) utilizing open (Dirichlet) boundary conditions, and lastly, (iv) employing v_{per} and v_{iso} to derive the corrective potential v_{cor}, which is subsequently integrated into the total electrostatic potential.
The extra charge is constructed directly by taking the difference between the electronic density of the charged "defect" system (ρ^{chg}) and that of the reference system (ρ^{ref}) on a real-space grid,

$$\delta\rho(\mathbf{r}) = \rho^{chg}(\mathbf{r}) - \rho^{ref}(\mathbf{r}) \tag{3.15}$$

The corresponding periodic electrostatic potential (v_{per}) is obtained by solving the Poisson equation,

$$\nabla\left[\varepsilon(\mathbf{r})\nabla v_{per}(\mathbf{r})\right] = -4\pi\left[\delta\rho(\mathbf{r}) - \langle\delta\rho\rangle\right] \tag{3.16}$$

where the Dirichlet boundary conditions are determine through the difference between the periodic electrostatic potential of the charged defect system (v_{chg}) and that of the reference system (v_{ref}) on the supercell edges.

A self-consistent process is implemented to incorporate a macroscopic dielectric profile of the material in the Poisson equation of the isolated defect charge,

$$\nabla^2 v_{iso}(\mathbf{r}) = -4\pi\left[\frac{\delta\rho(\mathbf{r})}{\varepsilon(\mathbf{r})} + \rho^{iter}(\mathbf{r})\right] \tag{3.17}$$

$$\rho^{iter}(\mathbf{r}) = \frac{1}{4\pi\varepsilon(\mathbf{r})}\nabla\varepsilon(\mathbf{r})\cdot\nabla v_{iso}(\mathbf{r}) \tag{3.18}$$

Finally, v_{cor} is obtained obtained through the solution of the Poisson equation for the CBC,

$$\nabla\left[\varepsilon(\mathbf{r})\nabla v_{cor}(\mathbf{r})\right] = -4\pi\langle\delta\rho\rangle \tag{3.19}$$

where the difference between v_{iso} and v_{per} is used to determine the Dirichlet boundary conditions at the edges of the supercell.

This scheme is provided by its developers as a patch for VASP on request [98].

3.4 *A posteriori* correction - Electrodes' method

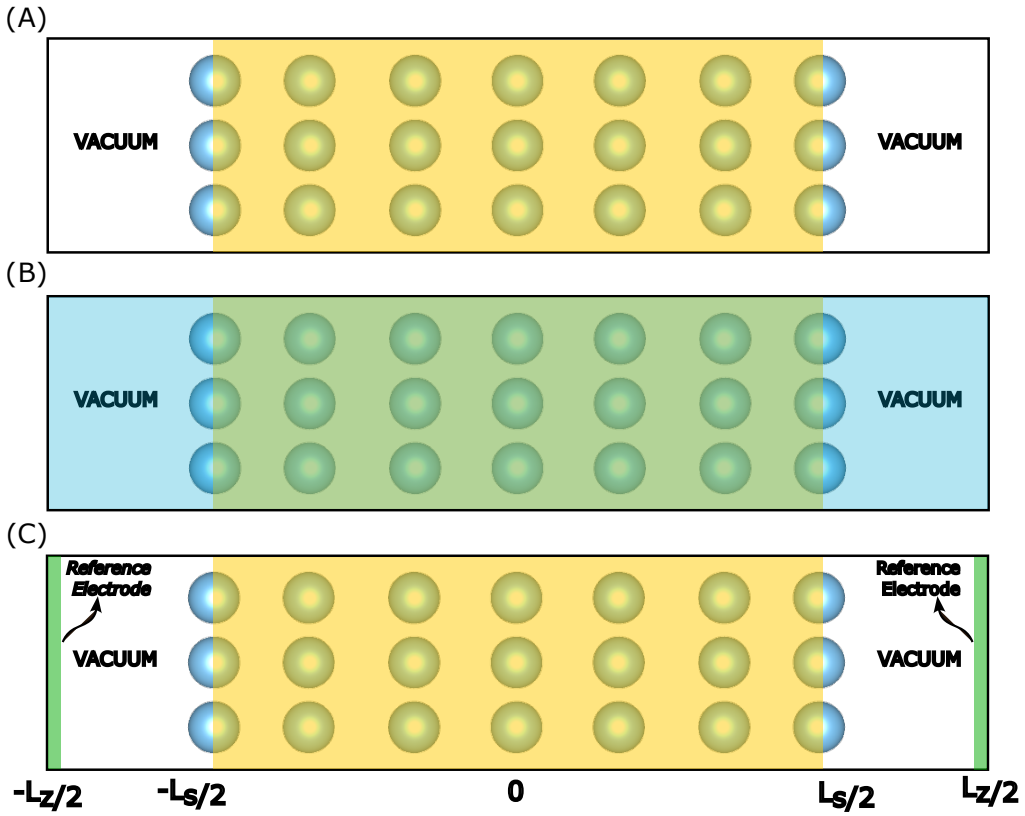

Figure 3.1: Schematic diagram depicting (a) the supercell utilized for computing a symmetric neutral slab with a dielectric constant ε, with vacuum on both sides, (b) the procedure of introducing charge (depicted in yellow) to the slab with a uniform compensating background charge (depicted in sky blue) distributed throughout the supercell, and (c) an auxiliary system featuring reference electrodes at the cell edges. Adaptation of the original illustration by Krishnaswamy et al. [54]

This method was introduced by Krishnaswamy et al. [54] The electrostatic potential from a first principle calculation as a superposition may write as

$$\bar{v}(\mathbf{r}) = v(\mathbf{r}) + v_{CBC}(\mathbf{r}) \tag{3.20}$$

where $\bar{v}(\mathbf{r})$ is the electrostatic potential of the slab including the CBC, $v_{CBC}(\mathbf{r})$ is the electrostatic potential generate by the CBC and $v(\mathbf{r})$ is the real electrostatic potential of the slab. Lozovoi et al.[99] and Komsa and Pasquarello [100] have proposed a simple approximation for $v_{CBC}(\mathbf{r})$. This consists in finding $v_{CBC}(\mathbf{r})$ as the potential of the CBC

screened by the profile of dielectric function of the, $\varepsilon(z)$. Under this approximation, we can readily solve for the electrostatic potential contribution from the CBC, $v_{CBC}(\mathbf{r})$, using the Poisson equation

$$\frac{d}{dz}\left(\varepsilon(z)\frac{d}{dz}v_{CBC}(z)\right) = -\rho_{CBC} = -\frac{q}{\Omega} \tag{3.21}$$

where q is the charge of CBC and Ω is the volume of the supercell. To establish boundary conditions and select a suitable reference potential for comparing systems with different amounts of charge, grounded "reference electrodes" are introduced at cell boundaries. Since the electrodes are grounded, we have the boundary condition $v_{CBC}(\pm L_z/2) = 0$. For simplicity, the dielectric profile is considered as a piecewise function with a constant value ε in the slab and unity in the vacuum. The slab region is assumed to be the one defined by the atomic positions of the outermost surface layers. Moreover, because the position of the ions remains fixed,ε is the electronic part of the static dielectric constant. Solving Poisson's equation gives

$$v_{CBC}(z) = \frac{-q}{2\varepsilon_0\Omega} \times \begin{cases} \left(z^2 - \frac{L_z^2}{4}\right); \\ \text{for} \quad -L_z/2 < z < -L_s/2 \\ \\ \frac{1}{\varepsilon}\left(z^2 - \frac{L_s^2}{4}(\varepsilon - 1) - \varepsilon\frac{L_z^2}{4}\right); \\ \text{for} \quad -L_s/2 < z < L_s/2 \\ \\ \left(z^2 - \frac{L_z^2}{4}\right); \\ \text{for} \quad L_s/2 < z < L_z/2 \end{cases} \tag{3.22}$$

From the result of Eq. 3.22, the free electrostatic potential of the CBC contribution can be obtained by the Eq. 3.20.

Part II

Methods

Chapter 4

Computational methods

4.1 Computational details

The periodic DFT calculations have been performed in the Vienna Ab initio simulation package (VASP) [101–104] Version 6.2.1. PAW method was used to represent the core electron with 2, 4, 4, 6, and 14 valence electrons for Mg, Ti, C, O and Sn, respectively [105, 106]. The generalized gradient approximation (GGA) Perdew-Burke-Ernzerhof exchange-correlation (PBE) was used [107] and the plane-wave basis set was truncated at 700 eV for all systems. For sampling of the reciprocal space, the Monkhorst-Pack scheme [108] was chosen, the set of system-specific **k**-points are shown in Table 4.1. For oxides, the GGA + U approach of Dudarev et al. [109] was used to treat the 3d electrons and 4d electrons of Ti and Sn, respectively. We choose the effective Hubbard on-site Coulomb interaction parameter ($U' = U - J$) to be 4 and 3.5 eV, respectively, according to values proposed in previous works [110–112]. Additionally, the OCTOPUS code version 13 [93–96] was used to carry out all the calculations that include the exact Coulomb cutoff technique [53]. We used optimized Optimized nonlocal norm-conserving pseudopotentials (ONCVPSP) [113, 114] to describe the electron-ion interaction and the PBE functional to describe exchange-correlation effects. We employed a cubic regular mesh for the real-space expansion of the Kohn-Sham equations. The spacing between the grid points is 0.4 a_0 for all systems. The GGA+U approach of Dudarev et al. implemented [115] in OCTOPUS was used at the same way as in VASP calculations.

Table 4.1: Computational parameters employed for bulk and slab models, including energy cutoff, **k**−point grid, smearing and its width.

System	Energy cut off (eV)	**k**−point grid	Smearing	sigma (eV)
hcp Ti	700	$30 \times 30 \times 20$	Methfessel-Paxton order 1	0.05
Ti (0001)	700	$30 \times 30 \times 1$	Methfessel-Paxton order 1	0.05
fcc TiC	700	$13 \times 13 \times 13$	Gaussian	0.1
TiC (001)	700	$13 \times 13 \times 1$	Gaussian	0.1
Rutile TiO_2 bulk	700	$9 \times 9 \times 18$	Gaussian	0.1
Rutile TiO_2 (110)	700	$9 \times 9 \times 1$	Gaussian	0.1
Anatase TiO_2 bulk	700	$15 \times 15 \times 5$	Gaussian	0.1
Anatase TiO_2 (001)	700	$15 \times 15 \times 1$	Gaussian	0.1
fcc Pt	700	$29 \times 29 \times 29$	Methfessel-Paxton order 1	0.05
Pt (111)	700	$29 \times 29 \times 1$	Methfessel-Paxton order 1	0.05
fcc ZrC	700	$17 \times 17 \times 17$	Gaussian	0.1
ZrC (001)	700	$17 \times 17 \times 1$	Gaussian	0.1
fcc MgO	700	$13 \times 13 \times 13$	Gaussian	0.1
MgO (001)	700	$13 \times 13 \times 1$	Gaussian	0.1
Rutile SnO_2 bulk	700	$6 \times 6 \times 12$	Gaussian	0.1
Rutile Reduced SnO_2 (110)	700	$6 \times 6 \times 1$	Gaussian	0.1

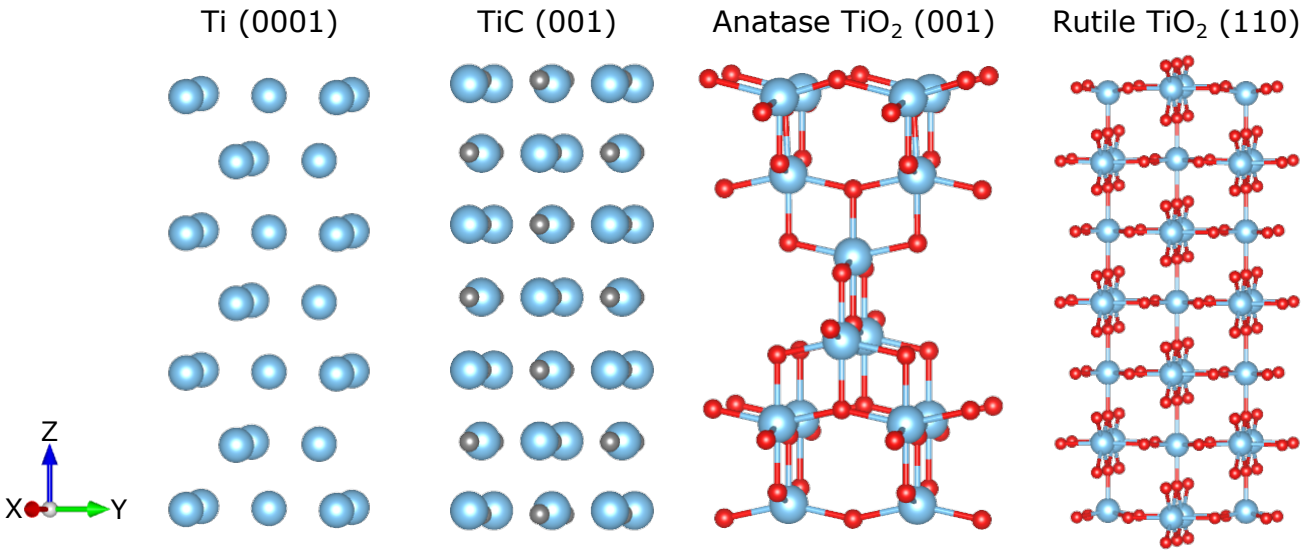

Figure 4.1: Side view of the slab models for Ti (0001), TiC (001), anatase TiO_2 (001), and rutile TiO_2 (110) surfaces. The Ti atoms are shown by blue balls, C atoms by gray balls and O atoms by red balls.

4.2 Bulk and surfaces models

Full optimization of the lattice parameters was performed for each bulk material. The values of the optimized lattice parameters as well as experimental values are reported in Table 4.2, which are in close agreement. Slab models were cut from their corresponding optimized bulk. A vacuum layer of 30 Å (15 Å in each side) in the c (or z) direction, orthogonal to the slab, was employed to prevent interactions between periodic images. Conjugate gradient algorithm was used for geometry optimization of the slab models, with a force threshold for the ionic relaxation of 0.01 eV/Å. The symmetry of the slab models and number of layers are shown in Figs. 4.3 and 4.4. The four titanium surfaces Ti (0001), TiC (001), anatase TiO_2 (001), and rutile TiO_2 (110) are depicted in Figure 4.1. On the surfaces, the coordination number of titanium atoms vary from 5 to 7: Ti (0001) has only Ti_{5c}, TiC (001) has solely Ti_{7c}, anatase TiO_2 (001) has only Ti_{5c}, and rutile TiO_2 (110) has Ti_{5c} and Ti_{6c}. Regarding oxygen atoms in oxides, both anatase TiO_2 (001) and rutile TiO_2 (110) have O_{2c}, and rutile O_{3c}.

Table 4.2: Cell parameters (a and c) of the materials studied and their respective experimental values.

System	Parameter (Å)	This work	Experimental
hcp Ti	a	2.923	2.951[116]
	c	4.625	4.684[116]
fcc TiC	a	4.383	4.327[117]
Anatase TiO_2	a	3.899	3.784[118]
	c	9.913	9.515[118]
Rutile TiO_2	a	4.737	4.593[118]
	c	3.048	2.958[118]
fcc Pt	a	4.016	3.924[119]
fcc ZrC	a	4.754	4.680[120]
fcc MgO	a	4.289	4.210[121]
Rutile SnO_2	a	4.784	4.737[122]
	c	3.217	3.186[122]

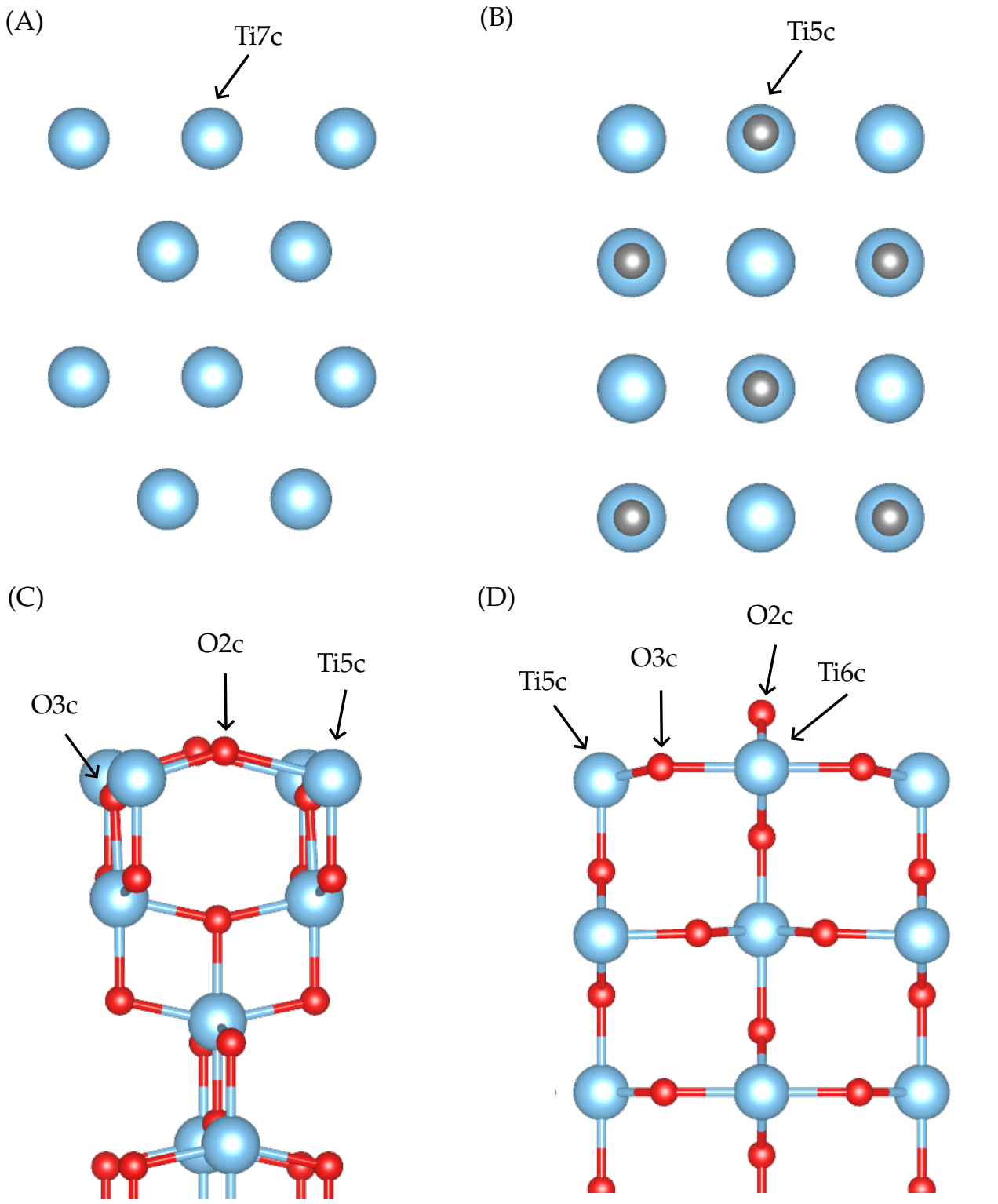

Figure 4.2: Structures and coordination of surface atoms of (A) Ti (0001), (B) TiC (001), (C) anatase TiO_2 (001), and (D) rutile TiO_2 (110) panels. Ti atoms are shown by blue balls, C atoms by gray balls and O atoms by red balls.

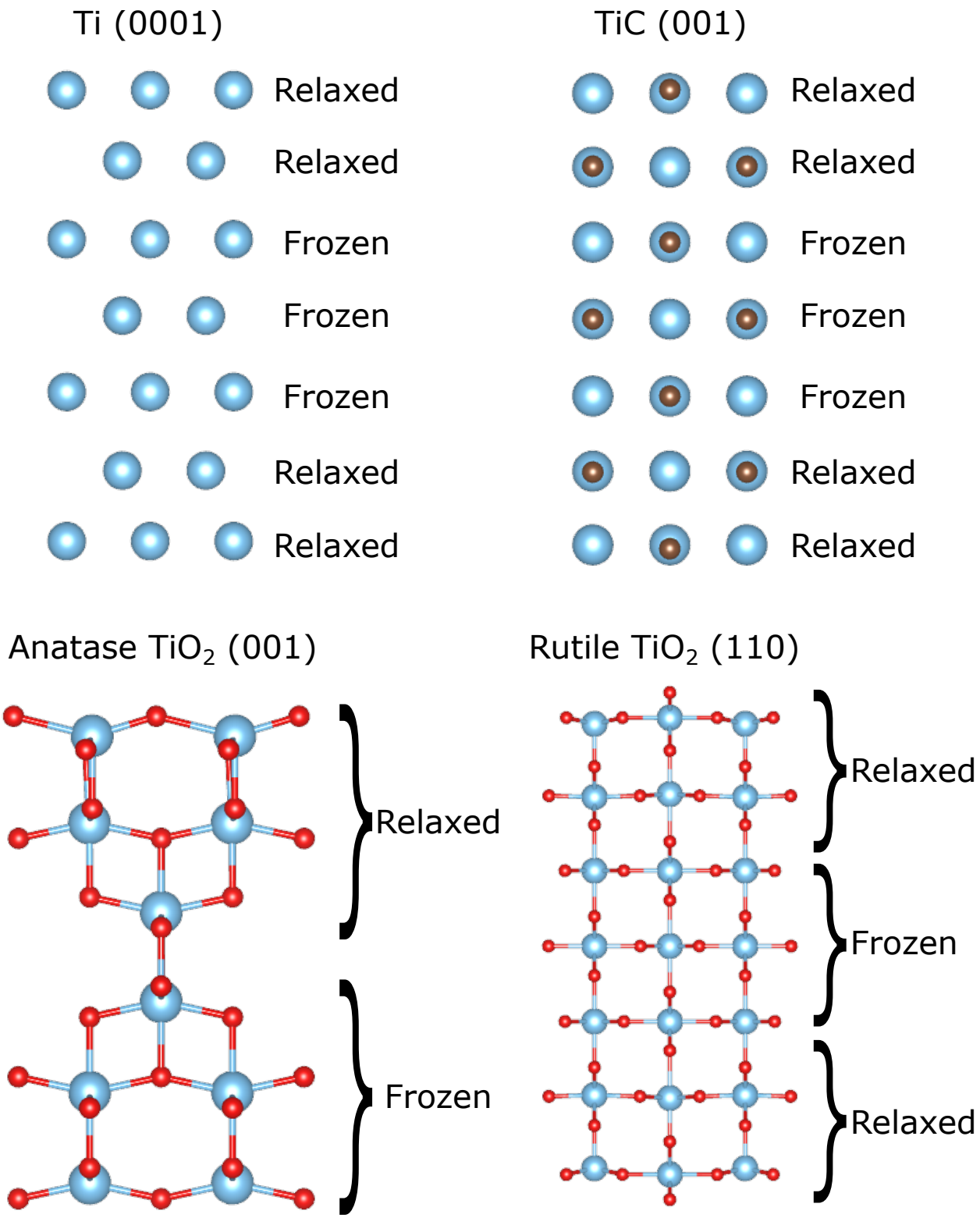

Figure 4.3: Slab models used in this work to study the titanium surfaces: Ti (0001), TiC (001), anatase TiO_2 (001), and rutile TiO_2 (110).

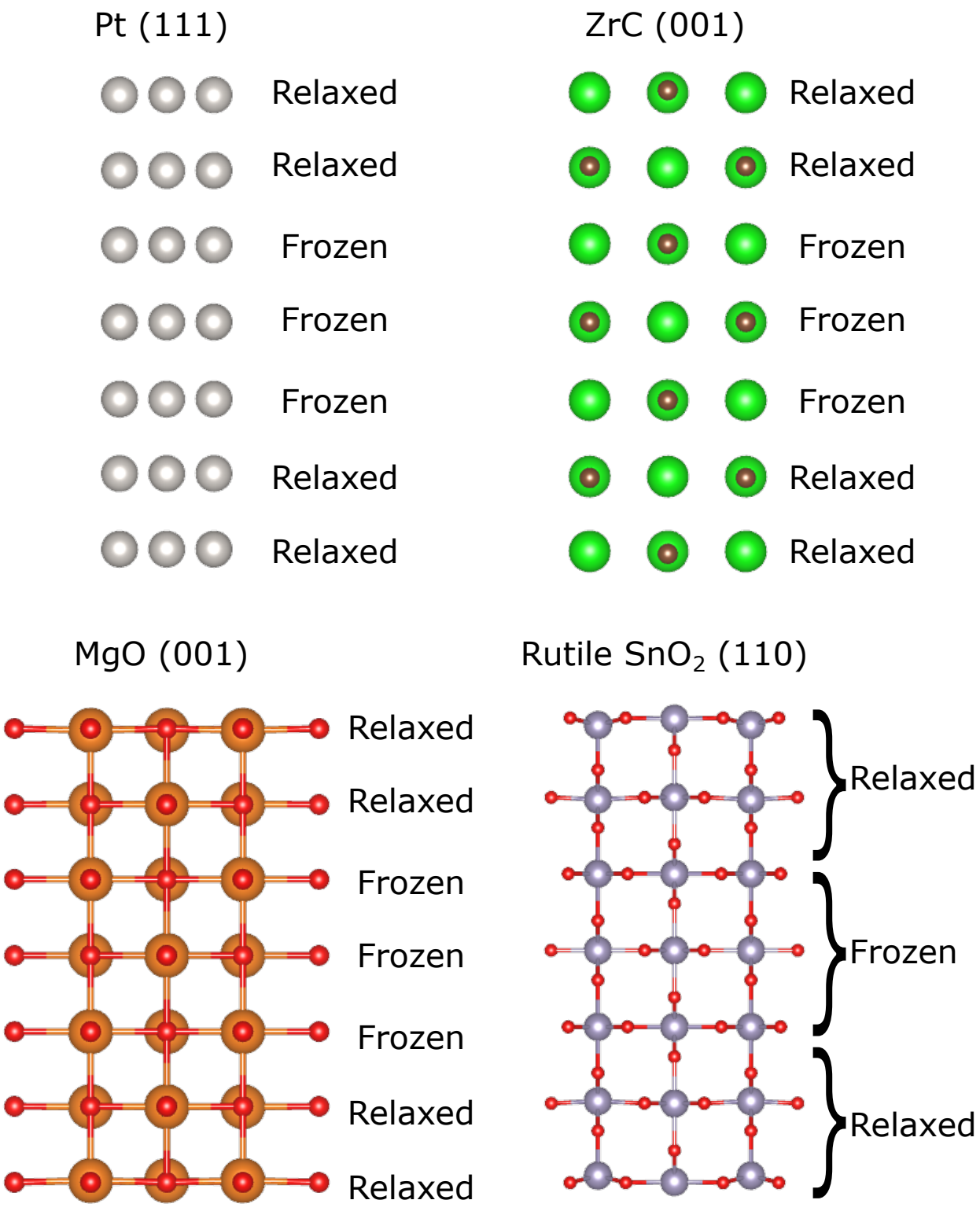

Figure 4.4: Slab models used for Pt (111), ZrC (001), Mg (001), and rutile SnO_2 (110) surfaces.

Part III

Results

Chapter 5

Fukui Functions

In this chapter, we present the results obtained for the calculation of both electrophilic, $f^-(r)$, and nucleophilic, $f^+(r)$, Fukui function for four surfaces of materials containing titanium: Ti (0001), TiC (001), anatase TiO_2 (001), and rutile TiO_2 (110). Additionally, in the Appendixes A and B, we provide results for four other inorganic surfaces: Pt (111), ZrC (001), Mg (001), and rutile SnO_2 (110). We used five different methodologies: i) **Finite differences (FD)** with $\Delta N = \pm 1$ from VASP calculations, i.e., considering the CBC; ii) **Finite differences with the SCPC method (FD-SCPC)**; iii) **Interpolation scheme (interpolation)** with $\delta N = \pm 0.05, \pm 0.10, \pm 0.15$ electrons; iv) **LDOS** with $\delta\mu$ energy from Fermi level; and **Finite differences with Exact Coulomb Cutoff technique (FD-ECC)** from Octopus calculations.

To visualize the differences between the Fukui functions $f^{\pm}(\mathbf{r})$ from different methodologies, we calculated their planar averages. For this, the supercell is split in a homogeneous grid of points, and for all points in a plane parallel to the slab (z), the average is computed (see Fig. 5.1). To have a better understanding of the Fukui distribution around each atom, we also calculated its condensed version. Specifically, we used the method called topological analysis of the Fukui function [34, 123, 124]. Briefly, this consists of finding attractors and basins of the Fukui gradient field and integrating it over each of the basins. Then, the integral in a given basin is assigned to the atom closest to the attractor in that basin. Numerical integrations were performed using Bader, a

code developed by Henkelman's group [125]. Finally, we also use contour maps, when necessary, to visualize the relaxation effects on the difference surfaces.

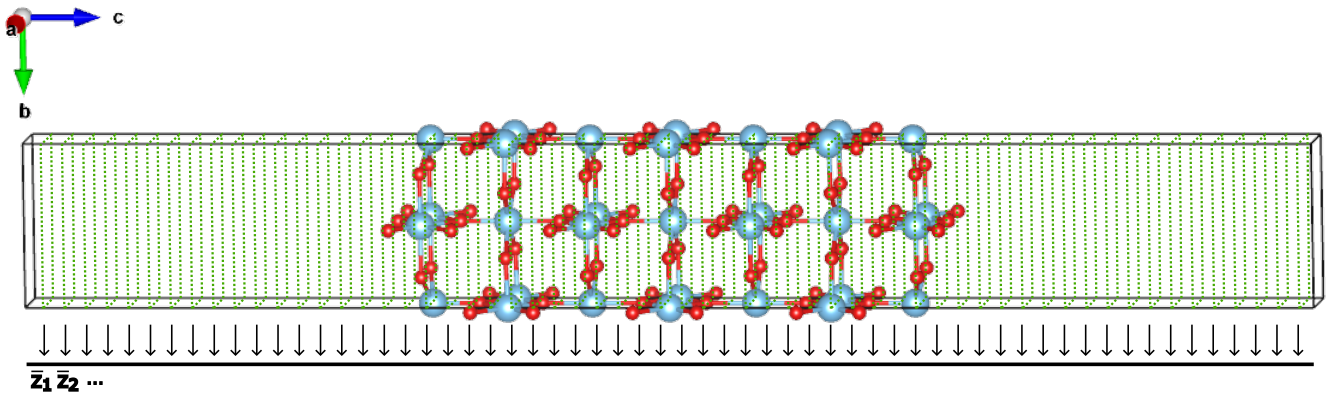

Figure 5.1: Schematic representation of the calculation of planar averages.

The chapter is organized as follows. In section 5.1 we discuss the results on the electrophilic Fukui Function, $f^-(\mathbf{r})$ and in section 5.2, we do it for the nucleophilic Fukui function, $f^+(\mathbf{r})$. Each section is further divided into metal surfaces and titanium oxides.

5.1 Electrophilic Fukui Function, $f^-(\mathbf{r})$

As previously mentioned, the electrophilic Fukui function, $f^-(\mathbf{r})$, is larger in those regions where the chemical species is prone to lose electrons. In a chemical process this usually occurs as a donation of electrons to an electrophile. The planar averages for all titanium surfaces and methodologies used are shown in Fig. 5.2 for $f^-(\mathbf{r})$. For clarity, the whole vacuum of the supercell is not shown. Deep into the vacuum the Fukui function is zero, except a pathological case. In most cases the planar averages is largest in the region between the plane of the outermost atoms of the surface (indicated by a red dashed line) and a plane where the electron density has decayed to $\rho = 10^{-4} a_0^{-3}$ (indicated by a black dashed line). This is, in principle, the expected behaviour as atoms in the surface are normally more reactive than those in the bulk because its lower coordination raises the electronic surface levels close to the Fermi level. Despite this common

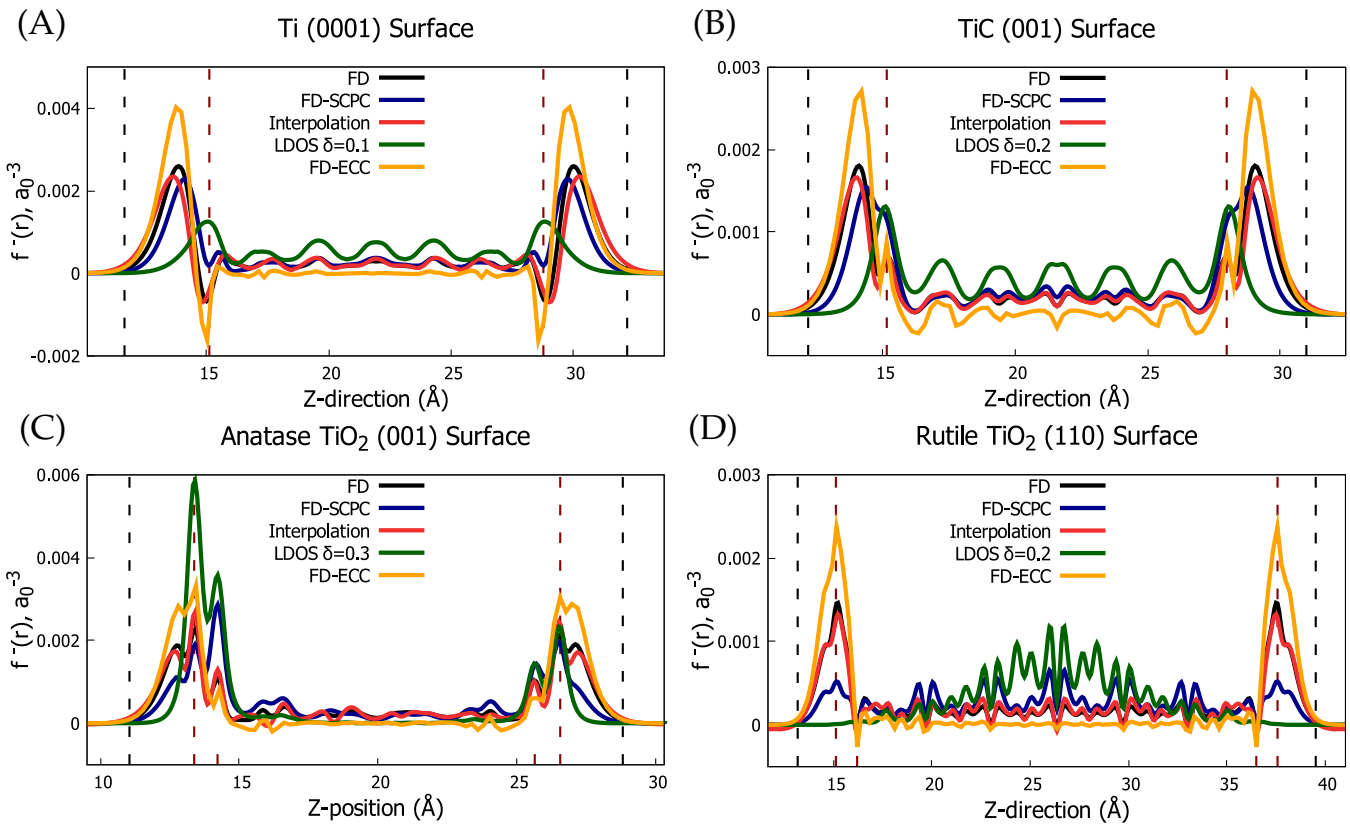

Figure 5.2: Planar average of Fukui functions, $f^-(\mathbf{r})$, for the titanium surfaces: (A) Ti (0001), (B) TiC (001), (C) anatase TiO_2 (001), and (D) rutile TiO_2 (110). The black dashed lines represent the position where the planar average electron density is equal to $\rho = 10^{-4} a_0^{-3}$ and the red dashed lines represent the position of the surface atoms.

feature, there are clear differences.

5.1.1 Metallic surfaces: Ti (0001) and TiC (001)

The planar average of $f^-(\mathbf{r})$ computed with LDOS in Ti(0001) and TiC (001) have their maximum at the surface sites and a non-negligible amount of Fukui function extends to the center of slab, which is the region of the slab representative of the bulk environment. Fukui functions from all other methods penetrate less the bulk and their maxima extend slightly beyond the nuclear position towards the vacuum region. This difference is clearly seen in the contour maps shown in Figs. 5.3 and 5.4 of the $f^-(\mathbf{r})$ of Ti (0001) and TiC (001), respectively. Note that the contours of the Fukui function that includes self-consistent corrections of the potential (panel B) look middle-way between

LDOS and finite differences and interpolation. This suggests that the relaxations effects (not present in LDOS) increases the Fukui function toward the vacuum but the fictitious electric field of the CBC exaggerates this trend in this metallic surfaces. It is also worth mentioning that the planar averages of $f^-(\mathrm{r})$ of Ti (0001) from FD, interpolation, and FD-ECC show significant negative peaks located in the first atomic planes (0001) of the surface. Negative values of the Fukui functions are also observed in planar molecules and it has been associated with orbital relaxation effects and nodal surface of the frontier orbitals [126–128].

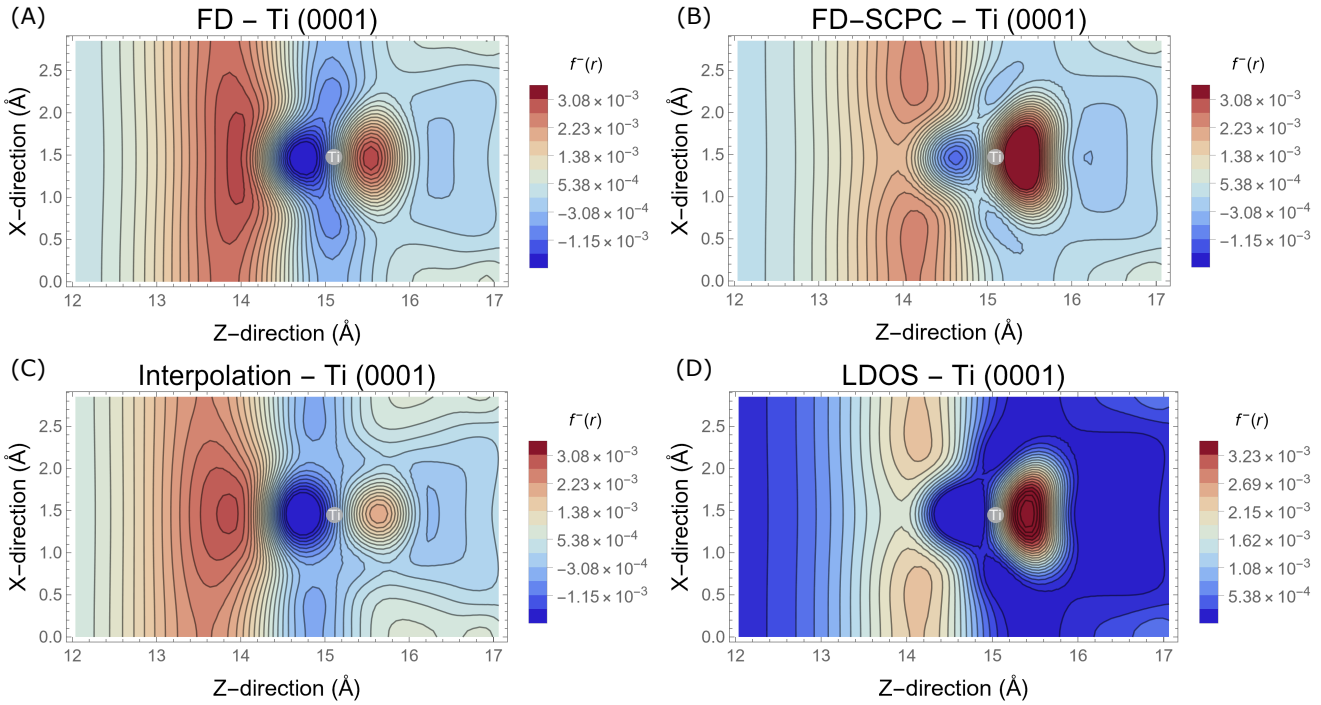

Figure 5.3: Contour maps in the X-Z plane ($y = 2.53$ Å) for the $f^-(\mathbf{r})$ Fukui functions of Ti (0001) with: finite difference (panel A), finite difference with self-consistent corrections of the potential, SCPC, (panel B), Interpolation (panel C), and from LDOS (panel D).

Regarding the topological analysis, condensed Fukui functions of Ti (0001) are presented in Table A.1 in the Appendix A. One can see that condensed values of Fukui function, f_k^-, depend on the methodology but the ratio between the values of different sites does depend much on the method. One is usually interested in relative values of f_k^- as this reveals the relative reactivity of atoms, and in this case all methods are consistent. Note that superficial atoms, Ti13 and Ti14 on one side of the slab and Ti7 and Ti10 on the

other, have the largest values of the condensed Fukui function. On the other hand, the condensed Fukui functions of TiC (001) agree very well among all methods, with the exception of LDOS, for which the values of f_k^- are more evenly distributed on all atoms, showing no clear preferential reactivity between C and Ti (see Table A.2 in the Appendix A). As for the other methods, the atoms more prone to donate electrons are surface carbons (C9, C10, C13 and C14). This agrees with studies that show that atomic species tend to adsorb on carbon atoms [129, 130].

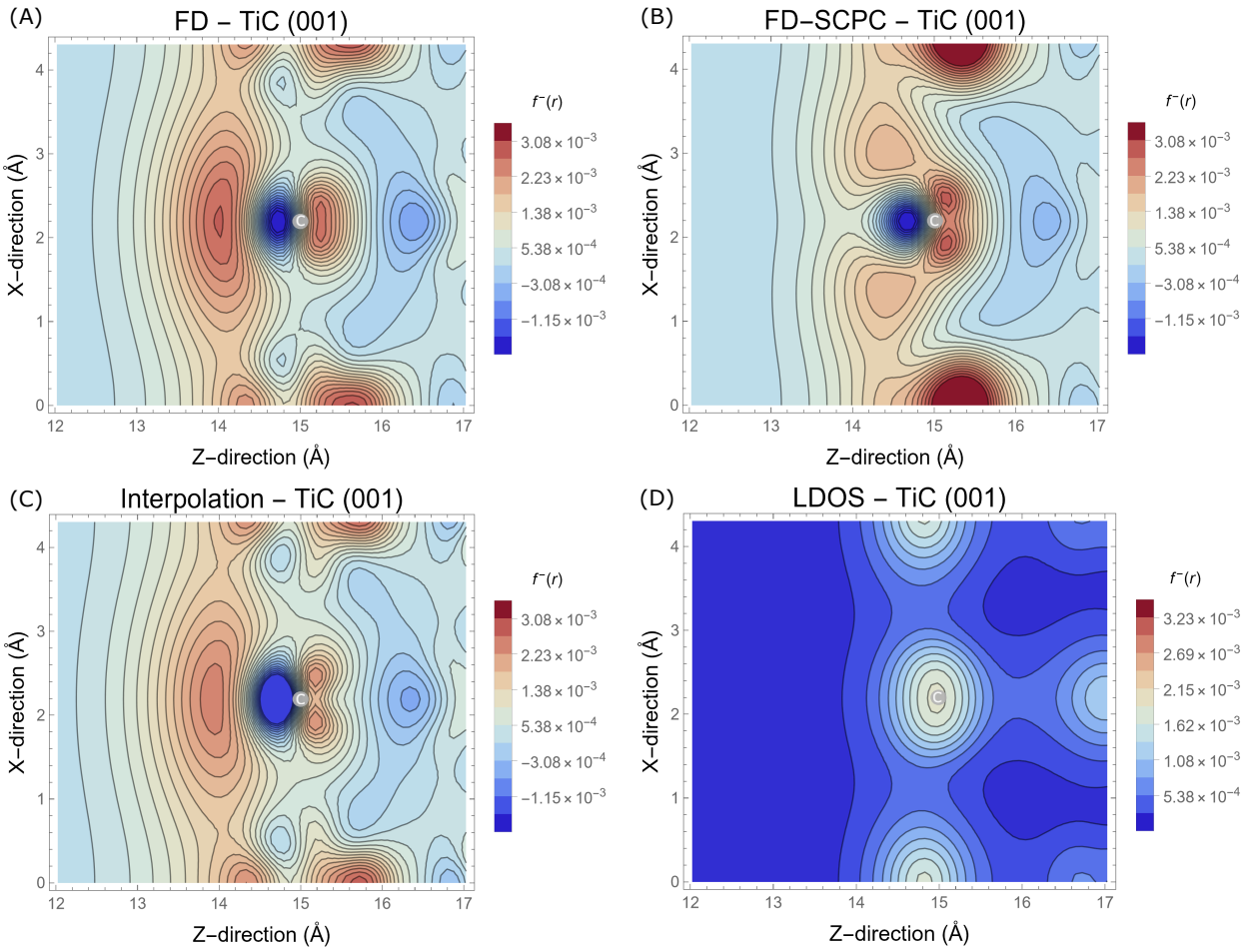

Figure 5.4: Contour maps in the X-Z plane ($y = 0$ Å) for the $f^-(\mathbf{r})$ Fukui functions of TiC (001) with: finite difference (panel A), finite difference with self-consistent corrections of the potential, SCPC, (panel B), Interpolation (panel C), and from LDOS (panel D).

5.1.2 Titanium oxide surfaces: anatase TiO_2 (001) and rutile TiO_2 (110)

Anatase TiO_2 (001) is a peculiar case. It present asymmetry with respect to z direction (i.e. lacks xy mirror planes or inversion center) and its optimized structure has an slight surface reconstruction. The $Ti_{5c} - O_{2c} - Ti_{5c}$ bonds at the surface have different lengths, one of them is shortened to 1.84 Å, while the other is lengthened to 2.21 Å (from the original 1.99 Å); a finding previously reported [131, 132]. This asymmetry causes the appearance of a dipole moment, which could impose additional difficulties since the vacuum in the aperiodic direction is not enough to screen the dipole interaction. To counteract this situation, dipole corrections were introduced to the neutral supercell, resulting a dipole moment of $\mu = 0.15$ D. These structural and charge distribution asymmetries are clearly observed in the profiles of the planar averages of the $f^-(\mathbf{r})$ (see Fig. 5.2 panel C). In this case the planar averages of $f^-(\mathbf{r})$ with all methodologies have the same trend, with the peaks occurring in the same places. The main differences between methodologies is the degree of localization of the Fukui function in the surface, where LDOS and FD-SCPC decay faster toward the vacuum.
In the case of rutile TiO_2 (110), large differences between different methodologies are observed (see Fig. 5.2 panel D and Fig. 5.5). While FD, interpolation and FD-ECC are qualitatively in agreement and strongly localised on the surface of the slab, the profiles of LDOS and FD-SCPC are more delocalised across the slab, to the point that $f^-(\mathbf{r})$ from LDOS is much larger in the bulk region than on the surface.

The condensed Fukui functions f_k^- for anatase TiO_2 (001) are shown in Table A.3 in the Appendix A. In this case, good agreement is observed between the five methodologies, since the largest values are found in the O_{2c}, as we expected because of their low coordination number and relatively electron-rich nature, which make its easy to loose electrons. A similar behavior is observed in the case of rutile TiO_2 (110) (see Table A.4 in the Appendix A) except for LDOS, which predict that oxygen atoms in the bulk could be more reactive than in the surface, which contradicts the chemistry of this surface [133, 134]. What this shows is the importance that the relaxation effects could have to account

for the correct reactivity of some surfaces.

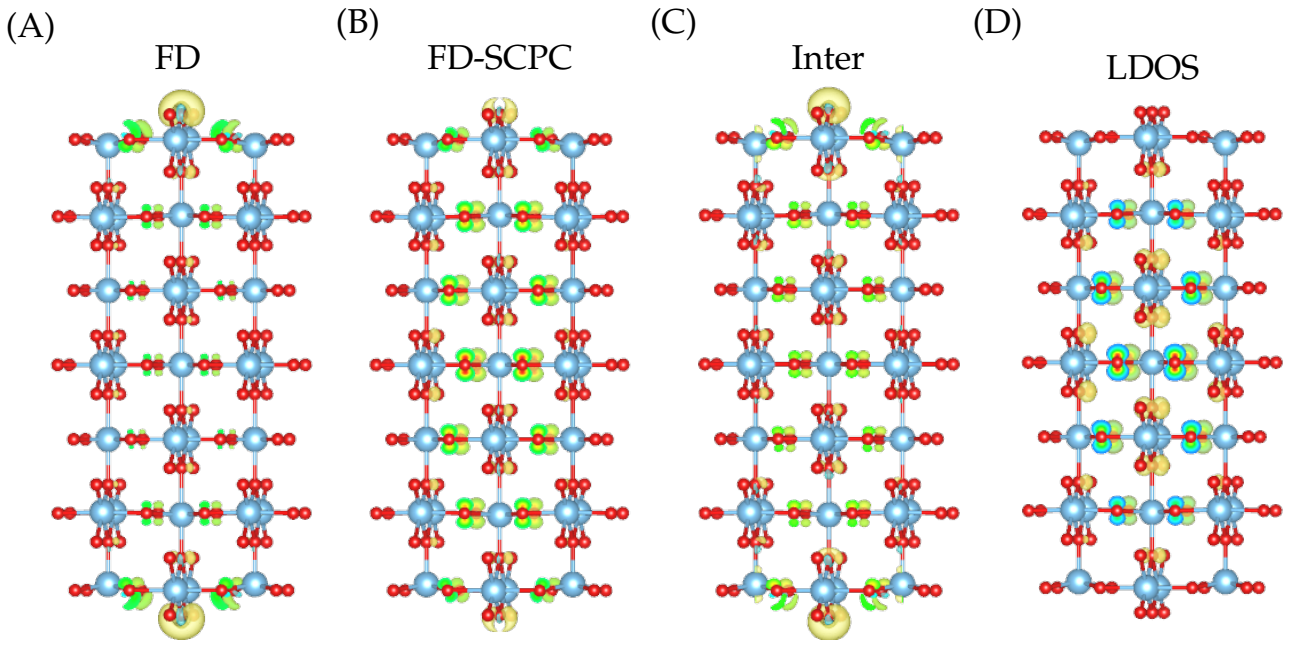

Figure 5.5: Isosurfaces ($\pm$ 0.0025 au) of electrophilic Fukui functions $f^-(\mathbf{r})$ for the rutile TiO_2 (110) surface: A) Finite differences (FD), B) Finite differences with the SCPC method (FD-SCPC), C) Interpolation scheme (Inter), and D) Local density of states (LDOS).

5.2 Nucleophilic Fukui function, $f^+(\mathbf{r})$

The planar averages for Fukui functions $f^+(\mathbf{r})$ are shown in Fig. 5.6. The FD-ECC results are presented only with $N + 0.05$ electrons because we could not obtain converged calculations for the vertical anions with $N + 1$ electrons. Unlike the case of $f^-(\mathbf{r})$, an asymptotic decay into the vacuum is not observed with all schemes. Namely, $f^+(\mathbf{r})$ with FD shows broad peaks in the vacuum region, which represent $\sim 40\%$ of the function itself. This evidences the appearance of ghost states in vertical anions, i.e., nonphysical states in the vacuum. This behavior is sufficiently inadequate to warrant the rejection of the FD ($N + 1$) calculation method for inorganic surfaces. The other three schemes that incorporate relaxation effects–FD-SCPC, FD-ECC, interpolation–and LDOS manage to overcome this serious difficulty.

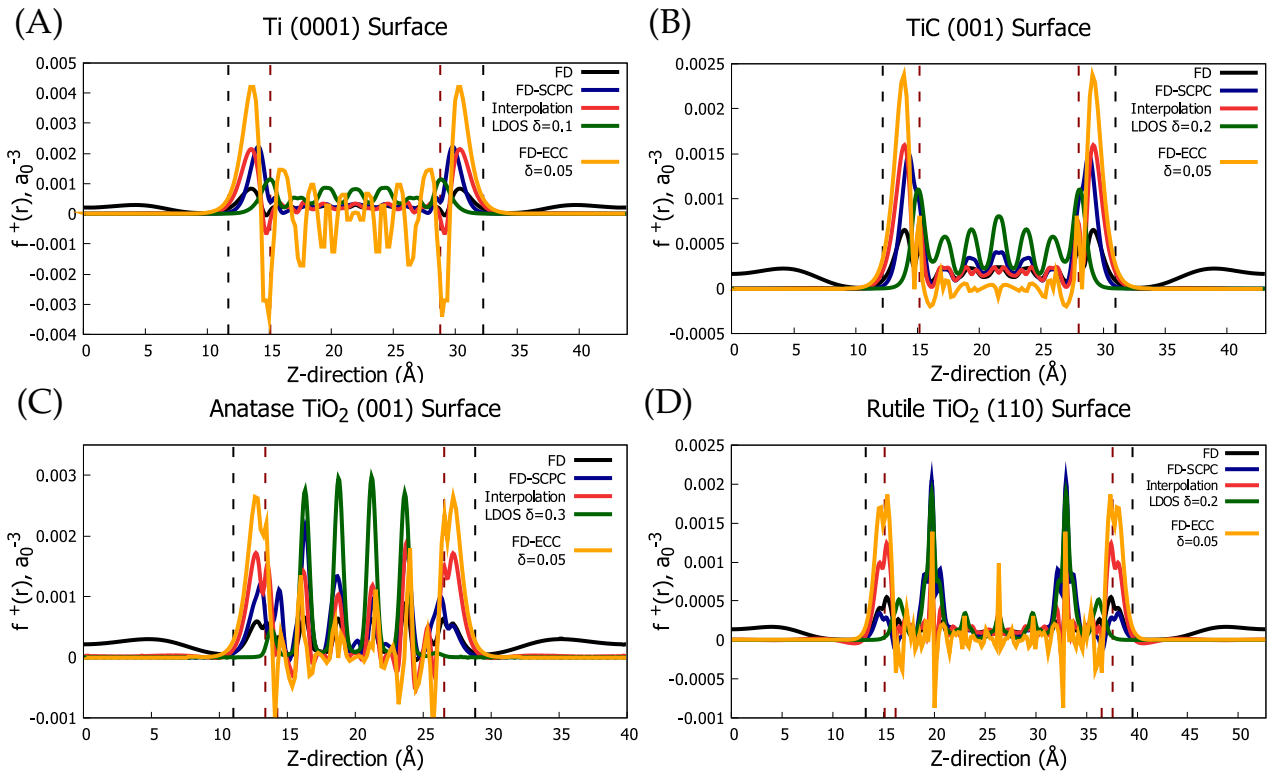

Figure 5.6: Planar average of Fukui functions, $f^+(\mathbf{r})$, for the titanium surfaces: (A) Ti (0001), (B) TiC (001), (C) anatase TiO_2 (001), and (D) rutile TiO_2 (110). The black dashed lines represent the position where the planar average electron density is equal to $\rho = 10^{-4}\, a_0^{-3}$ and the red dashed lines represent the position of the surface atoms.

5.2.1 Metallic surfaces: Ti (0001) and TiC (001)

Most methods predict that $f^+(\mathbf{r})$ in Ti (0001) and TiC (001) is larger in the surface and it rapidly decreases toward inner layers of the slabs (see Fig. 5.6 panels A and B). However, LDOS and FD-ECC are exceptions for different reasons. The Fukui functions from LDOS strongly oscillates along all layers of the slabs. This is a manifestation of the importance of properly accounting for the relaxation effects in gapless-metallic systems; which are largely polarizable. On the other hand, $f^+(\mathbf{r})$ of Ti (0001) computed with FD-ECC not only oscillates but in the inner layers is more negative than positive. Although negative values of the Fukui are not ruled out, the evidence in molecules shows that the regions of negative values are marginal compared to the positive values [83, 127, 128]. We can think of two possible explanations for this behavior. One is that the number of atomic layers (seven) of the slab is not sufficient to represent the surface states with this

method, and the other, which we are inclined to believe, is that the method is more numerically unstable when the system has excess electrons. In fact, as mentioned above, in spite of our many efforts, it was only possible to obtain converged results for all systems when ΔN is at most 0.05 e.

The comparison of planar averages of all methods with LDOS allows us to establish that the major effect of the relaxation in Ti(0001) and TiC(001) is to attenuate the oscillations of $f^+(\mathbf{r})$ in the inner layers and to shift the maximum towards the vacuum, in the same way that happens with $f^-(\mathbf{r})$. Contour maps show the same trend for the case of $f^-(\mathbf{r})$, essentially indicating an exaggerated increase of the Fukui function in the surface calculated with FD and interpolation compared to those that include self-consistent corrections of the potential (panel B in both figures). These maps are displayed in Figs. 5.7 and 5.8 for Ti(0001) and TiC(001), respectively.

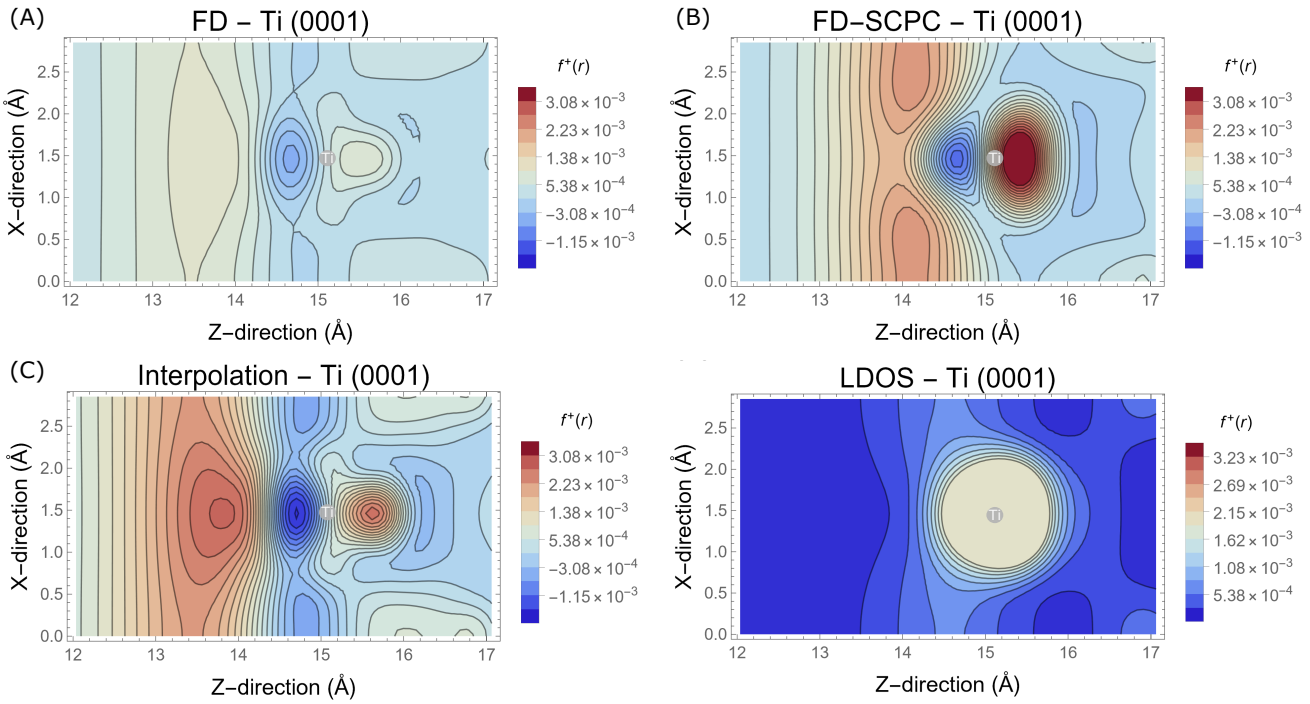

Figure 5.7: Contour maps in the X-Z plane ($y = 2.53$ Å) for the $f^+(\mathbf{r})$ Fukui functions of Ti (0001) with: finite difference (panel A), finite difference with self-consistent corrections of the potential, SCPC, (panel B), Interpolation (panel C), and from LDOS (panel D).

Condensed Fukui functions, f_k^+, for Ti(0001) and TiC(001) are reported in Tables A.9 and A.10, respectively. The most likely sites to accept electrons in Ti(0001) are the surface

titanium atoms (Ti13, Ti14, Ti7, and Ti10). In contrast, for TiC (001), the surface carbon atoms (C9,C10, C13, and C14) are more prone to capture electrons, with the exception of the LDOS, which presents its highest condensed values on the superficial titanium atoms (Ti9, Ti10,Ti13, and Ti14). Thus, the inclusion of relaxation effects in these systems is not only important in the direction perpendicular to the surface but also in the plane. Their non-inclusion may lead to an incorrect prediction of the atomic environment ready to receive electrons.

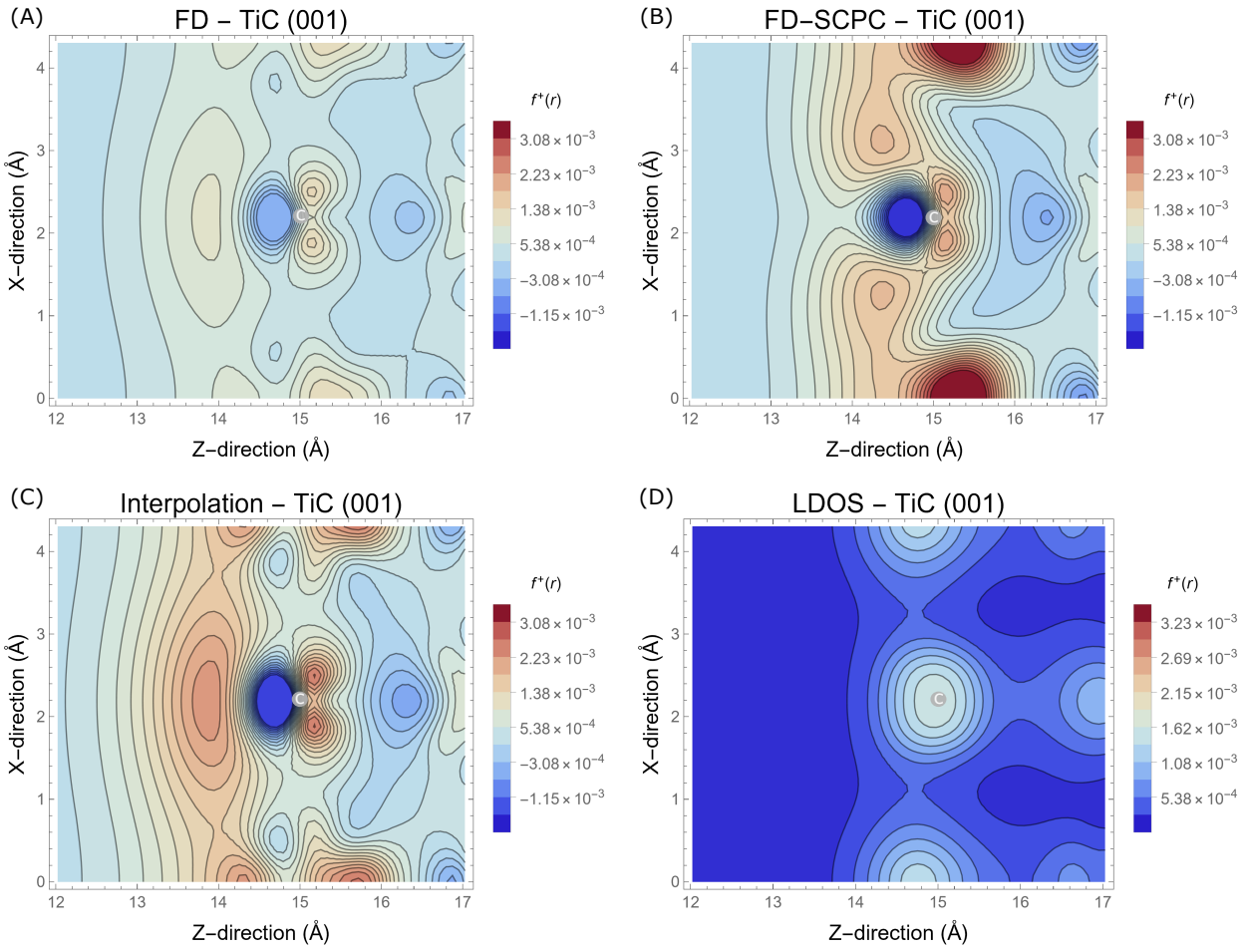

Figure 5.8: Contour maps in the X-Z plane ($y = 0$ Å) for the $f^{+}(\mathbf{r})$ Fukui functions of TiC (001) with: finite difference (panel A), finite difference with self-consistent corrections of the potential, SCPC, (panel B), Interpolation (panel C), and from LDOS (panel D).

5.2.2 Titanium oxide surfaces: anatase TiO_2 (001) and rutile TiO_2 (110)

Planar averages of $f^+(\mathbf{r})$ of anatase TiO_2 (001) are characterized by peaks not only in the surface but also in the bulk region (see Fig. 5.6 panel C). Although inclusion of relaxation decreases the amplitude of the Fukui in the center of the slab, it remains substantial, to varying extents, in all the schemes. Strikingly, the method that includes self-consistent potential corrections, FD-SCPC, has its largest values not in the surface but in the first sub-superficial layer of titanium ($z \approx 16$ Å), while the other methods–FD, interpolation, and FD-ECC $\delta = 0.05$– have their largest peak in the surface. We will see below that there is experimental and computational evidence that electrons tend to accumulate several layers beneath the surface.

Table A.11 summarizes values of the condensed Fukui functions f_k^+ for anatase TiO_2 (001). Surface oxygen atoms O_{2c} (O9 and O10) have the largest values of f_k^+ according to methods FD, interpolation and FD-ECC. Contrary, LDOS has them in the titanium atoms of the inner layers (Ti1,Ti4, Ti2,Ti3) and it is almost null in the atoms of the surface(T6, O10, O5). It is noteworthy that FD-SCPC has its largest value in the titanium atoms of the first inner layer (Ti3, Ti2) followed by superficial titanium (Ti6, Ti5). One would be tempted to anticipate that the electron-greedy sites must be on the surface and not in inner layers, however, in this case there is evidence to suggest that this is not the case. For instance, Selcuk et al. [135] used Car-Parinello molecular dynamics (CPMD) and 'effective screening method' to show that the excess of electrons in anatase TiO_2 (001) surface (which is induced by the adsorption of a hydrogen atom on the bridging oxygen) strongly avoids the surface, forming a quasi-two-dimensional state in a inner (001) plane in the Ti atoms. Furthermore, they found that the excess of charge moves quickly from layer to layer (see Fig. 5.9 panel B). With averages over time, they showed that the most visited sites are the subsurface titanium atoms, followed by the most inner sites, which explains the poor activity of this surface for reduction reactions. This precisely the behavior predicted by the Fukui functions $f^+(\mathbf{r})$ calculated with the FD-SCPC (see Fig. 5.9 panel A).

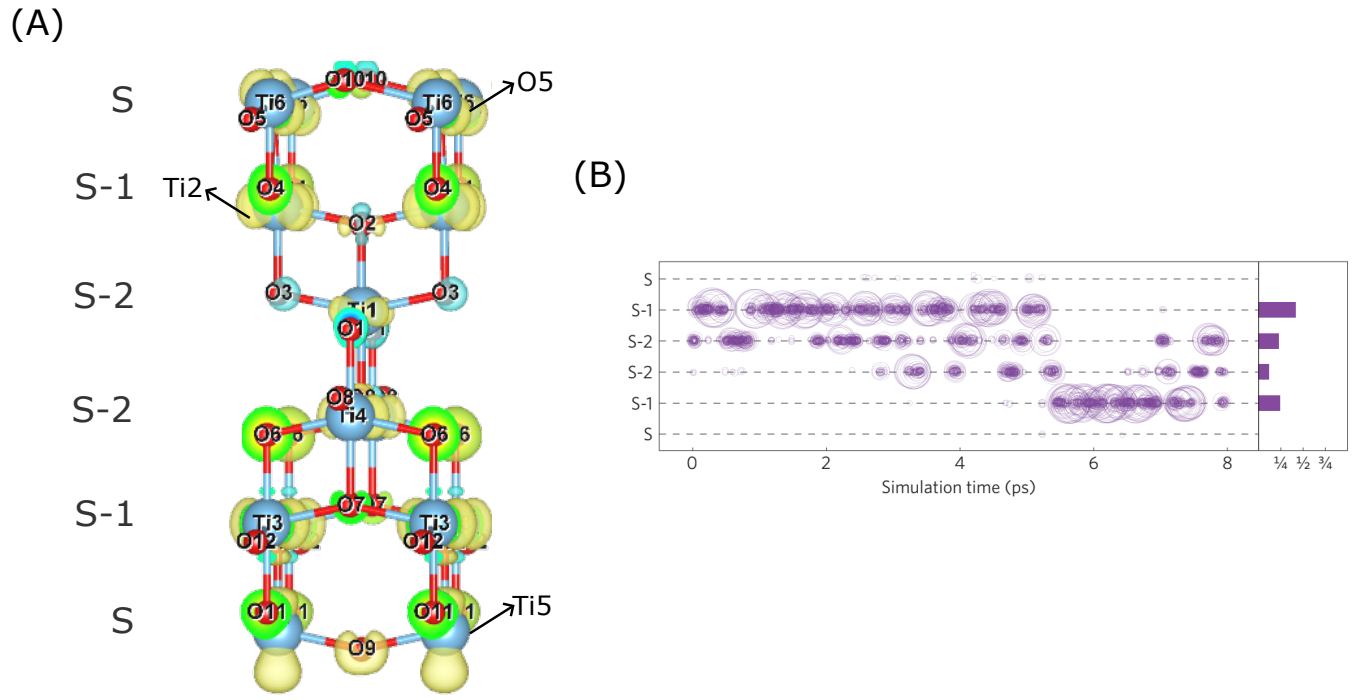

Figure 5.9: Excess charge on the anatase TiO_2 (001) surface. Panel A shows the isosurface ($\pm$ 0.0025 au) of nucleophilic Fukui functions $f^+(\mathbf{r})$ calculated using the FD-SCPC methodology. Panel B displays the localization of excess charge in the direction perpendicular to the surface during a CPMD simulation carried out by Selcuk et al. [135], along with the corresponding distribution. The labels S, S-1 and S-2 indicate the surface layer and the subsequent layers below the surface.

The planar averages of $f^+(\mathbf{r})$ for rutile TiO_2 (110) show are also peculiar (see Fig. 5.6 panel D). Although in all methods the Fukui amplitude is large both on the surface and in the first inner layer of Ti atoms ($z \approx 20$), only for LDOS and FD-SCPC it is larger in the inner layer. Likewise, the condensed Fukui results largest in the bicoordinated oxygen atoms O_{2c}, when computed with FD, FD-ECC, and interpolation , while for FD-SCPC and LDOS it is largest in the subsurface Ti atoms (Ti7 and Ti10 in Table A.12 in the Appendix A). Let's contrast our results with the work by Krüger et al. [136], in which they studied the distribution of excess electrons in a reduced surface of rutile TiO_2 (110) through the adsorption of Na atoms. Using Resonant photoelectron diffraction (RPED), they found that the excess of negative charge, coming from the adsorbed Na, locates mainly in the subsurface Ti atoms (see Fig. 5.10). Namely, 44% of the excess charge

is located in the subsurface titanium Ti_{6c}/Ti7. This behavior is partially recovered or rather predicted only by the $f^+(\mathbf{r})$ calculated with FD-SCPC and LDOS.

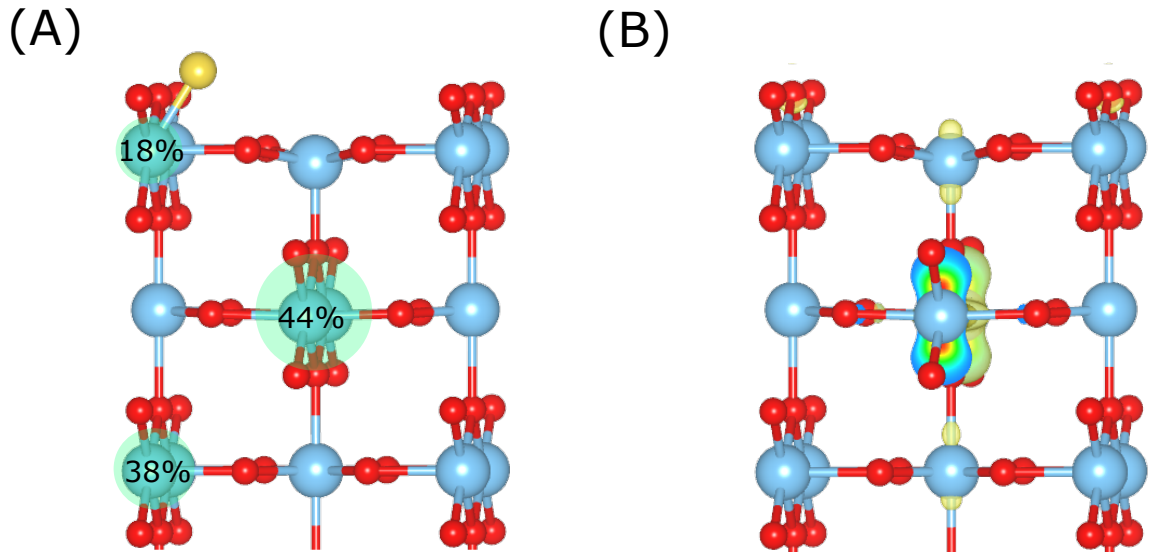

Figure 5.10: Excess charge on the rutile TiO_2 (110) surface. Panel A shows a schematic representation of the excess charge location and the relative weights, measured through RPED by Kruger et al. [136] Panel B displays the isosurface ($\pm$ 0.0025 au) of nucleophilic Fukui functions $f^+(\mathbf{r})$ calculated using the FD-SCPC methodology.

Chapter 6

Fukui Potentials

As previously mentioned, the Fukui potential corresponds to the electrostatic potential due to a charge distribution equals to a Fukui function. In principle, it can be determined straightforward via Eq. 2.22, i.e., as a difference of 'molecular electrostatic potential' or via Eq. 3.9. However, using these equations presents formal difficulties, mainly related to incorporating a CBC in the supercell, for which a correction is needed. In this chapter, we discuss about the corrections methods, alignment, and the corresponding potentials generated. The Fukui potentials are obtained for both electrophilic, $v_f^-(\mathbf{r})$, and nucleophilic Fukui functions, $v_f^+(\mathbf{r})$, for the four titanium surfaces: Ti (0001), TiC (001), anatase TiO_2 (001), and rutile TiO_2 (110). As in the previous chapter, we provide results for four other surfaces: Pt (111), ZrC (001), Mg (001), and rutile SnO_2 (110) in Appendix C. We used three types of correction: ECC, SCPC, and electrodes' methods, which are described in Secs. 3.2, 3.3, and 3.4, respectively, in Chapter 3. Using these correction methods give rise to five calculation methodologies: i) **FD** with $\Delta N = \pm 1$ from VASP calculations, i.e., considering the CBC; ii) **FD-ECC** from Octopus calculations; iii) **SCPC**; iv) **electrodes-FD**; and v) **electrodes-interpolation** with $\delta N = \pm 0.05, \pm 0.10, \pm 0.15$ electrons.

6.1 Alignment

The Fukui potential can be seen as a change in the electrostatic potential due to an electron transfer. If two species A and B approach to each other, A will be under the elec-

trostatic potential of B and vice versa. However, if an amount electrons are transfer between A and B, their electron densities will change and so will do the electrostatic potential. The Fukui functions measures the change in density and the Fukui potentials in electrostatic potentials. An aspect that deserves care is where to set the zero of the electrostatic and Fukui potentials. In the case of the former, it is natural to set it at infinity perpendicular to the surface. As the Fukui potential corresponds to a non-neutral charge distribution, as it moves away from the surface, it will be that of an infinite plane of charge, i.e., it grows or decreases linearly. Note, however, that in the real physical system there is charge neutrality. The charge transferred to or from the surface is balanced by a layer of absorbed or solution molecules. Takes for instance the interface between and electrode and electrolyte. In this, a positive (or negative) charge buildup at the interface of the electrode and electrolyte solution, which is partially neutralized by the gathering of counterions in the solution through the action of the electrostatic potentials, resulting in a structured electric double layer. Then, it seems plausible to establish the zero of Fukui potentials at the same place where the electrostatic zero is established. Namely, we align the Fukui potential fixing its zero in the point where both the electrostatic potential and Fukui function begin to have their asymptotic decay which is when the valence electron density is $\rho(\mathbf{r}) \approx 10^{-4}\, a_0^{-3}$ for all surfaces considered. This criteria is in similar to Bader's suggestion [137] that the contour surface of an small value of density , $\rho(\mathbf{r}) = 0.001\, a_0^{-3}$, reflects the specific features of chemical species, e.g., lone pairs, strained bonds, and so on.

6.2 Correction

The presence of the CBC in the calculation of the electronic structure of surfaces with a net charge makes it imperative to perform a correction to the Fukui potential. As we have previously mentioned, one of the methodologies used to correct the Fukui potential is the *a posteriori correction* of the electrodes' method. Originally Krishnaswamy et al. [54] proposed to fix the limits of the material's dielectric profile by the atomic

positions of the outermost layers of atoms. However, both the electron density and electrostatic potential spill over for some angstroms from that position to the vacuum. For this reason, we modified this boundary condition and optimized it to match, as best as possible, the planar averages of ECC Fukui potentials, since in ECC there is not need to define a dielectric profile as this is implicit in the calculation itself. In contrast, the SCPC method requires a dielectric profile to compute the correction, $v_{cor}(\mathbf{r})$. The best match is achieved when the dielectric step is place around the position where the planar average of the electron density is equal to $\rho(\mathbf{r}) = 0.02\,a_0^{-3}$. As an example, Fig. 6.1 schematically shows the modification in this boundary condition. We also tested our results changing this position in few tenths of angstrom. Computed planar averages of the Fukui potential are stable to this change.

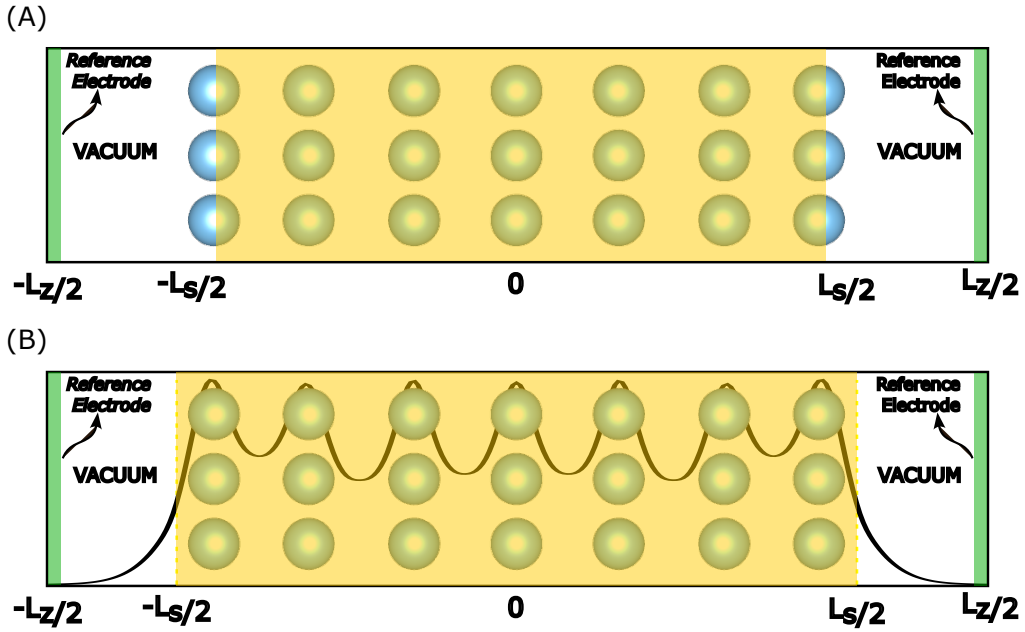

Figure 6.1: Schematic diagram depicting the auxiliary system featuring reference electrodes at the cell edges with the dielectric profile fixed by (a) the atomic positions of the outermost surface layers and by (b) the position where the planar average of the valence electron density is equal to $\rho(\mathbf{r}) = 0.02\,a_0^{-3}$. The black curve corresponds to the planar average of the valence electron density. Adaptation of the original illustration by Krishnaswamy et al. [54]

The planar averages for all titanium surfaces and methodologies used are shown in Fig.

5.2 for both $v_f^-(\mathbf{r})$ and $v_f^+(\mathbf{r})$ Fukui potentials. As one can see, the Fukui potentials with correction schemes are in a good agreement in the main region of chemical interest, which is the transition from the vacuum to the surface (the region between the black and red dashed lines for each plot). These plots suggest that in most cases a simple *a posteriori* correction could be sufficient as it matches the profile of an method free of CBC (ECC) and one in which this self-consistently corrected, SCPC . However, there are several details and differences that are worth discussing. First, the SCPC method presents great differences in the central region of the slabs (bulk), compared to the rest of the correction schemes. Even tough it is a region inaccessible to almost all chemical reagents, it could have consequences in the understanding of the chemistry of hydrogen atoms migrating underneath the surfaces [138]. Second, differences are observed between the resulting Fukui potentials using the electrodes' method with FD and interpolation (see dark-yellow and light-red curves in Fig. 6.2, respectively). Since in both cases the correction performed is the same, the differences arise essentially from the Fukui functions. In the particular case of $v_f^+(\mathbf{r})$ with FD, the CBC locates a large fraction of Fukui function in the vacuum. As consequence, the Fukui function and potential in the slab and the region of chemical interest are underestimated. Third, one can observe that in anatase TiO_2 (001) the decay of the Fukui potentials into the vacuum is asymmetric. This is a direct consequence of the asymmetry of the slab. In this case, the zero of the potential is set in the side of the relaxed layers (the left in each graph).

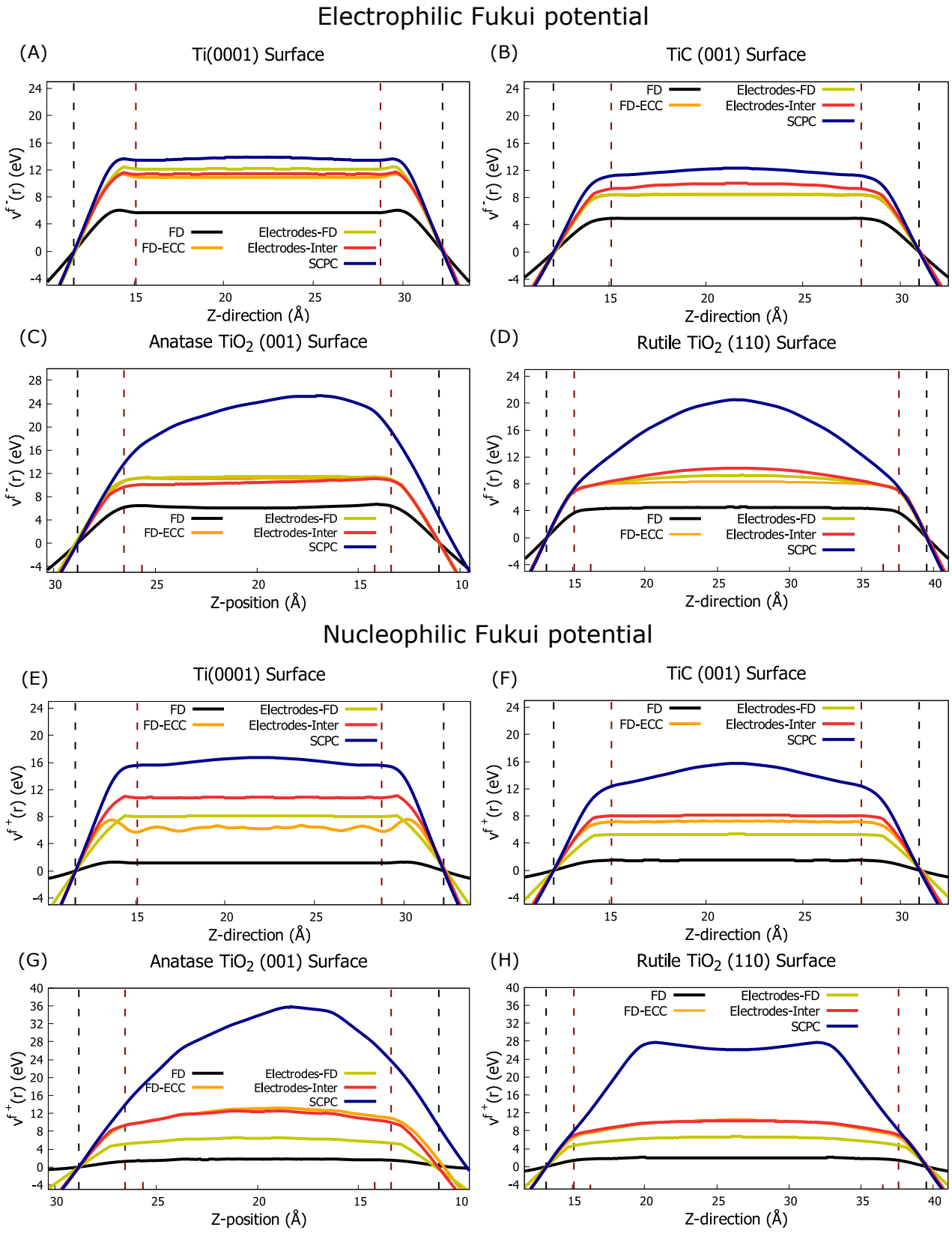

Figure 6.2: Planar average of both electrophilic and nucleophilic Fukui potentials for the titanium surfaces: Ti (0001), TiC (001), anatase TiO_2 (001), and rutile TiO_2 (110). The black dashed vertical lines represent the position where the planar average electron density is equal to $\rho = 10^{-4} a_0^{-3}$ and the red dashed lines represent the position of the surface atoms.

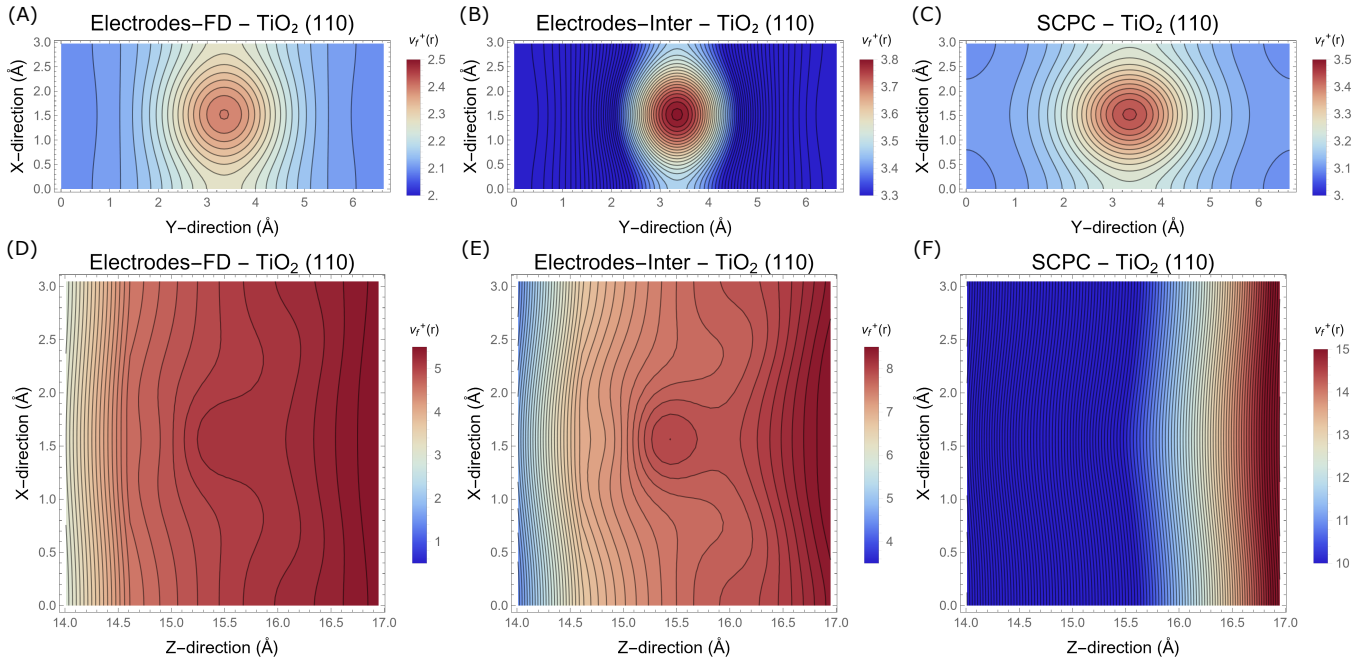

Figure 6.3: Contour maps of the Fukui potential $v_f^+(\mathbf{r})$ for the rutile TiO_2 (110) surface. Panels (a), (b), and (c) show the contour maps in the X-Y plane at the position where the planar average of the electronic density equals $0.001\,a_0^{-3}$, calculated using the Electrodes-FD, Electrodes-Inter, and SCPC methods, respectively. Panels (d), (e), and (f) present the contour maps in the X-Z plane located at the bridging oxygen (O_{2c}), calculated using the Electrodes-FD, Electrodes-Inter, and SCPC methods, respectively.

Although the planar averages of the potential computed with different methods are in fair agreement with each other, they do not capture differences in X-Y planes. As an example, we plotted contour maps of $v_f^+(\mathbf{r})$ for rutile TiO_2 (110) surface, due to the important characteristic and differences observed in the $f^+(\mathbf{r})$ of this system (see Fig. 6.3). One can see that in the X-Y plane representative of the van der Waals surface (where the average of density is $0.001\,a_0^{-3}$), the topology of the potential found with SCPC is more symmetric around the oxygen atom (center of the plot) than the others methods. Potentials by finite differences and interpolation are prolate, with the points of greatest value being strongly located in the twofold-coordinated bridge oxygen atom (see Fig. 4.2 panel D). On the other hand, the contour maps for X-Z plane shows that the Fukui potential from SCPC varies smoothly and it has its largest values into the slab model, whereas the Fukui potential from the another two methodologies have their

largest values more towards the vacuum, that is, to the surface and subsurface layers. These differences in topology could be important when the Fukui potential is used to predict reactivity of different sites of the surfaces, which will be addressed in the next chapter.

Chapter 7

Chemical Model

In this chapter, we present results on the application of the corrected Fukui potential. In Section 7.1, we examine the adsorption of a Na atom on rutile TiO_2 (110) surface using perturbation theory, providing evidence of the utility and scope of the model. Section 7.2 shows another application, presenting results for the adsorption of an Cl atom on the same surface. Finally in Section 7.3 we show the results for a general model, illustrating how electron transfer modulates the regioselectivity of the interactions.

7.1 Perturbative Perspectives: sodium adsorption

The corrected Fukui potential, along with the electrostatic potential, can be used to model and predict the interaction energy of an attacking (perturbing) agent, B, on a given substrate, A. As Ayers et al. [92] has stated, there are two possible effects due to the perturbation of B on A. First, the presence of B changes the external potential "felt" by the electrons in A; that is, the external potential is now due to the nuclei in A, but also to nuclei and electrons in B, $v_A(\mathbf{r}) \rightarrow v_A(\mathbf{r}) + \delta v$. Second, electrons may flow from A to B, or vice-versa. Thus, the number of electrons in A may change from the number in the isolated surface, $N_A \rightarrow N_A + \Delta N$. Considering these changes as perturbations to the isolated surface A, we may use Taylor expansion to characterize the changes (see Eq. 2.2), which after replacing the derivatives for their respective descriptors from CDFT, it

can be rewritten as

$$\Delta U(\mathbf{r}) = \mu^{\pm}\Delta N - \int \left(\sum_{\alpha \in S} \left[Z_\alpha \delta(\mathbf{r}' - \mathbf{R}_\alpha) \right] - \rho(\mathbf{r}') - \Delta N f^{\pm}(\mathbf{r}') \right) \delta v(\mathbf{r})\, d\mathbf{r}' \tag{7.1}$$

where the superscripts "+" and "-" indicate differentiation from above and below, respectively.

As a example of the usefulness of the perturbative scheme and the corrected Fukui potential, we consider the problem of predicting where a surface undergoes nucleophilic attack. In particular, we explore the reactivity of the rutile TiO_2 (110) surface toward an electron donor species, using the interaction energy as a measure of reactivity, that is, to predict the most and least energetically favorable regions. The donor species used as a probe is a sodium atom due its small electronegativity (it readely donates electrons) and because its interaction with rutile TiO_2 (110) has been studied theoretically and experimentally,and the preferential adsorption site is precisely known [136, 139]. Sodium adsorbs on an 'in-between' site where it is bound to two O_{2c} atoms at 2.25 Å and one in-plane oxygen atom (O_{3c}) at 2.40 Å. This site is shown in Fig. 7.1. Apart from a slight change in bond relaxation, sodium does not perturb much the rutile lattice, ensuring minimal disruption to the overall structure [140]. We do not want to miss the opportunity to emphasize that the site at which the sodium atom (or any other) adsorbs to the surface does not have to be the one with the highest value of the Fukui function or potential. The adsorption site will be determined by a balance between electrostatics, electron transfer, Pauli repulsion, van der Waals, etc. Our model only captures the first two.

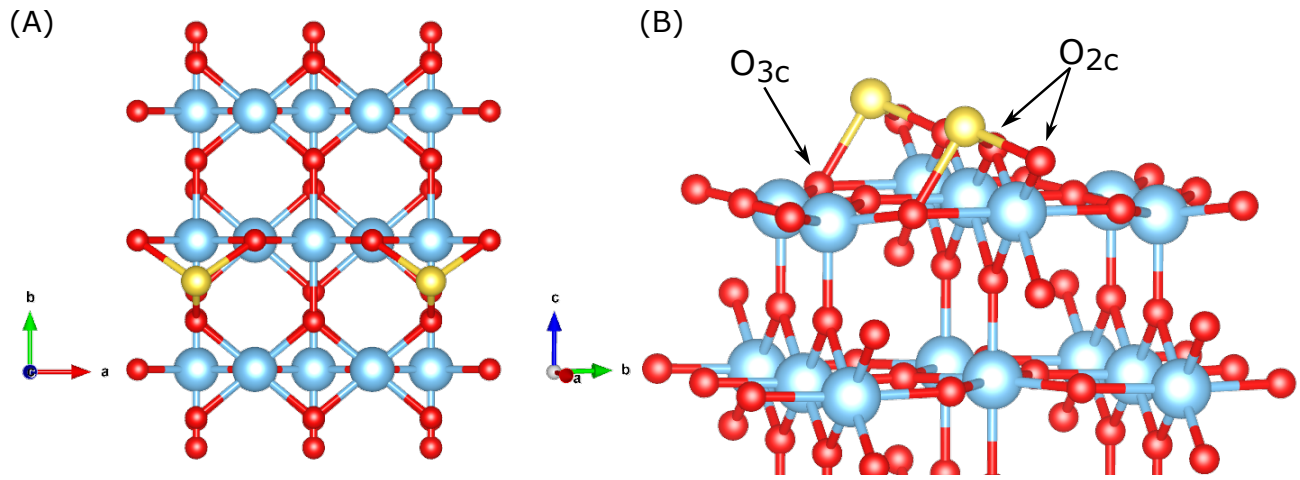

Figure 7.1: Adsorption site of a sodium atom on the rutile TiO_2 (110) surface, indicating the two types of surface oxygen atoms. Panel (A) shows a top view of the adsorption site, while panel (B) presents a side view.

With the aim to obtain a simple, but also useful model to the perturbation, we can approximate the change in the external potential due to the atom by a effective point charge, $-q/|\mathbf{r}-\mathbf{r}'|$, i.e., $\delta v(\mathbf{r}) = -q/|\mathbf{r}-\mathbf{r}'|$. Substituting the latter into the truncated expression of the perturbation expansion,

$$\begin{aligned}\Delta U(\mathbf{r}) &= \mu^{\pm}\Delta N + \underbrace{\sum_{\alpha}\frac{qZ_{\alpha}}{|\mathbf{R}_{\alpha}-\mathbf{r}|} - \int\frac{q\rho(\mathbf{r}')}{|\mathbf{r}-\mathbf{r}'|}d\mathbf{r}'}_{q\Phi(\mathbf{r})} - \Delta N\underbrace{\int\frac{qf^{\pm}(\mathbf{r}')}{|\mathbf{r}-\mathbf{r}'|}d\mathbf{r}'}_{qv^{f^{\pm}}(\mathbf{r})} \\ &= \mu^{\pm}\Delta N + q\Phi(\mathbf{r}) - q\Delta N v_{f^{\pm}}(\mathbf{r})\end{aligned} \tag{7.2}$$

where $\mu^{\pm}$, $\Phi(\mathbf{r})$ and $v_{f^{\pm}}(\mathbf{r})$ are the electronic chemical potential, electrostatic potential and Fukui potential of the surface, respectively, while ΔN is the number of electrons transferred between the atom and the surface or vice versa, and q is the atom effective charge. Because the first term in Eq. 7.2 does not depend on the position of the attacking reagent, the second and third terms control the regioselectivity of the adsorption.
In this equation the two extreme control regimes of a chemical reaction naturally arise. The second term is purely electrostatic, while the third term captures electron transfer effects.

Since the surface-atom system is closed, we will assume that $q = \Delta N$. The change in the

number of electrons, ΔN, can be estimated using the parabolic Parr and Pearson's [141] model for the association reaction $A + B \rightarrow AB$, in which ΔN is given by

$$\Delta N = \frac{\mu_A - \mu_B}{\eta_A + \eta_B} \tag{7.3}$$

where μ and η are the electronic chemical potential and the absolute hardness, respectively. These last two terms can be obtained in terms of ionization potential (I) and the electron affinity (A)

$$\mu_i = -\frac{I_i + A_i}{2} \tag{7.4}$$

and

$$\eta_i = I_i - A_i \tag{7.5}$$

Because the theoretical calculation of the ionization potential and the electron affinity in the supercell requires the shifting of the eigenvalues of the top of valence band, tVB, and the bottom of the conduction band, bCB, with respect to the value of the electrostatic potential in vacuum, and obtaining the latter does is not easy for the case of open shell systems (such as the sodium atom), we decided to use benchmark values proposed from reference data for ionization potentials and electron affinities, which are $\mu = -2.84\,\text{eV}$ and $\eta = 4.59\,\text{eV}$ [142]. For the rutile TiO_2 (110) surface, I was approximated by the negative of the eigenvalue of the tBC and A by the negative of the bCB, $I = 7.35\,\text{eV}$ and $A = 5.50\,\text{eV}$. Introducing these values in Eq. 7.3, we obtain that sodium donates $\Delta N \approx 0.5$ electrons to the surface.

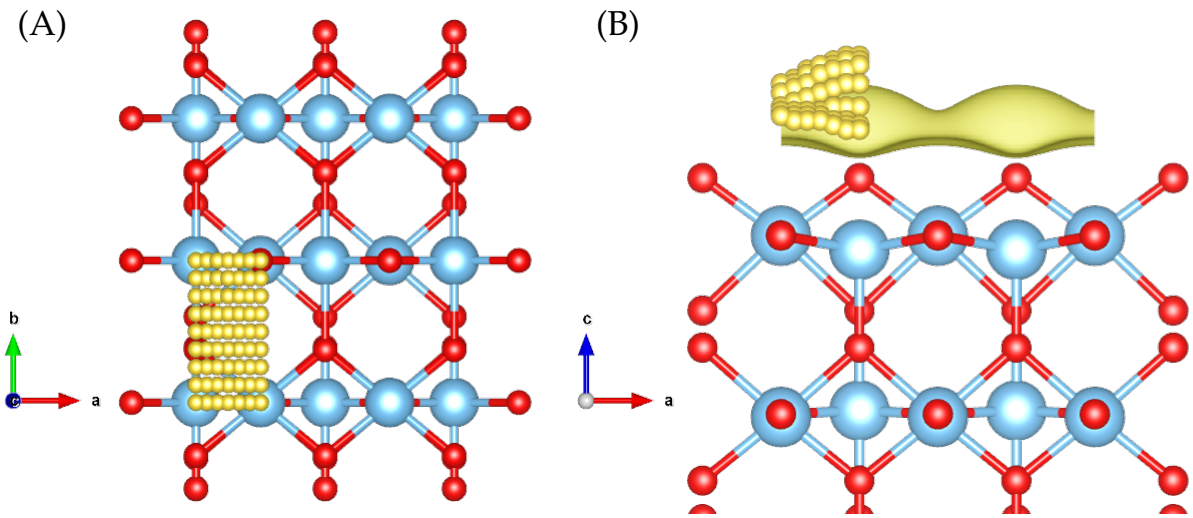

Figure 7.2: Spatial distribution of a 63-point grid of sodium atoms positioned 0.5 Å above the van der Waals surface of rutile TiO_2 (110). Panel (A) displays the points of the grid from top view perspective. Panel (B) is a side view of the same points, accompanied by the isosurface of electron density at an isovalue of $0.001\,a_0^{-3}$. Titanium atoms are depicted with sky blue spheres, oxygen atoms with red spheres, and sodium atoms with yellow spheres.

With the aim of evaluating the interaction energy of the Na probe with all the surface, we constructed a grid with 63 points in a 2×1 supercell surface-model to place the Na atom. The points are separated by an stepsize of 0.25 Å in the $\vec{X}$ direction and 0.42 Å in the $\vec{Y}$ direction. Because in our model the effects of correlation and exchange between the electrons of the two subsystems are neglected, the probes are placed 0.5 Å above the van der Waals surface, thus avoiding a large overlap between their electron densities. Fig. 7.2 shows the arrangement of the grid points on the surface model used.

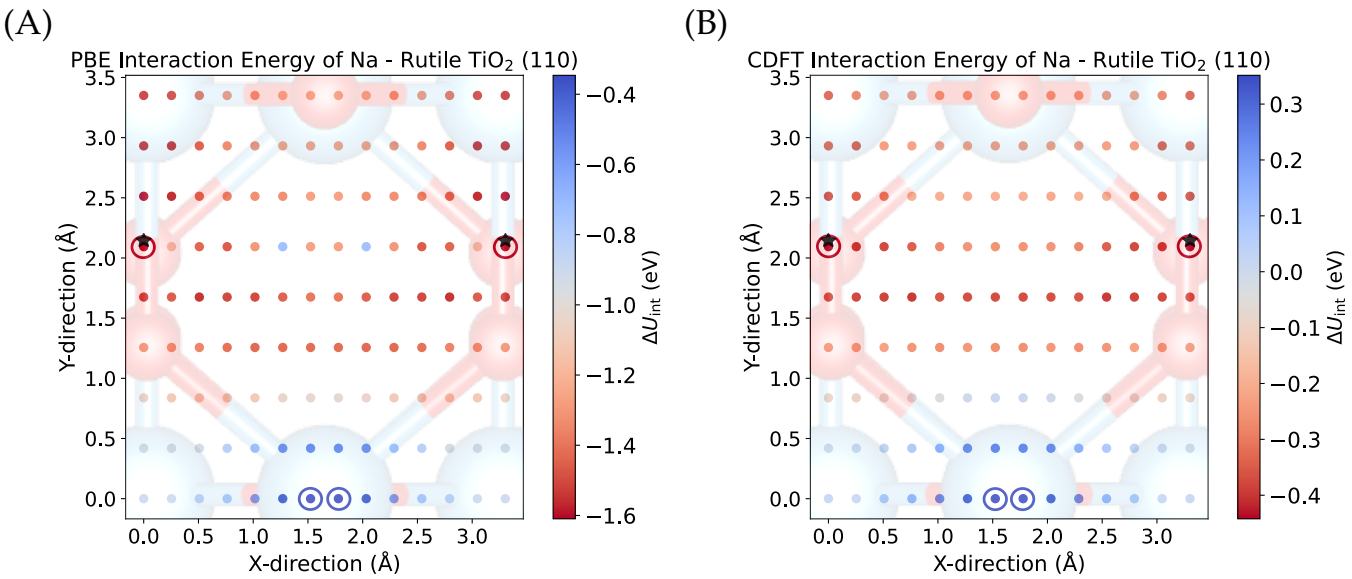

Figure 7.3: Heat maps of the interaction energy, ΔU_{int}, of a sodium atom positioned 0.5 Å above the van der Waals surface of rutile TiO_2 (110) calculated with PBE (panel A) and with the CDFT model (panel B). The maximum and minimum points for both methodologies are shown enclosed by concentric circles. The position reported both theoretically and experimentally for a Na atom adsorbed on rutile TiO_2 (110) is shown with a black star in both panels. $\Delta U_{int} = U[\text{Na} - \text{TiO}_2] - U[\text{Na}] - U[\text{TiO}_2]$ and $\Delta U_{int} = q\Phi(\mathbf{r}) - q\Delta N v_{f^+}(\mathbf{r})$ for PBE and CDFT, respectively.

Heat maps representing the interaction energy between the sodium atom probe and the surface are shown in Fig. 7.3. Panel (A) shows the heat map of the actual interaction energy computed the PBE functional. As Eq.7.2 does not take into account structural relaxation, the interaction energy is computed keeping ions fixed. Panel (B) depicts the heat map of the interaction energy ($U - \mu^{\pm}\Delta N$) estimated from the CDFT model. As Na atoms donates electrons to the surface, one has to use $f^+(\mathbf{r})$ for the latter. Specifically, we used the one computed with the SCPC method. As we can observe from Fig. 7.3, both heat maps exhibit the same trends. The region with the largest (more positive) interaction energy are displayed in shades of blue, extending from 0 to ~ 1 Å in the Y-direction (or $\vec{b}$). This region corresponds to the vicinity of the surface titanium atom Ti_{5c}. The largest interaction energy happens when the Na sits on top of Ti_{5c}, which is indicated with blue circle in Fig. 7.3. Intermediate values of the interaction energy are observed in the vicinity of the oxygen atom O_{2c} (upper central region). The stronger interactions

(red) take place in points between Ti_{6c} atom and the triple-coordinated oxygen (O_{3c}). The point with smallest interaction energy of our model is enclosed with a red circle in Fig. 7.3.

The capability of CDFT model to predict the interaction energy of this particular system is strikingly. It does not only captures the general topology of the actual interaction energy, but it predict with good accuracy the place where Na prefers to adsorb on the surface. X-ray absorption fine structure experiments show that Na adsorbs in the 3-fold hollow site formed by O_{3c} and O_{2c} (see Fig. 7.1). This experimental adsorption site is depicted in Fig. 7.3 with a black star, which is very close to the grid point with the smallest (more negative) interaction energy. We believe that a finer mesh of dots could bring the predicted site closer to the experimental site.

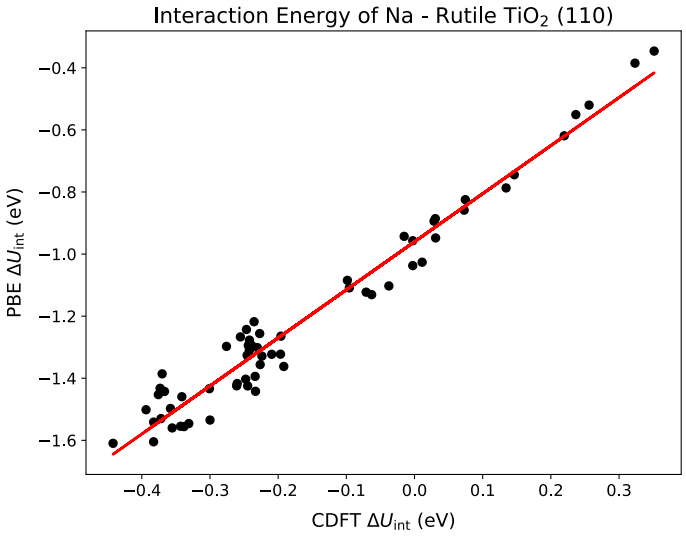

Figure 7.4: Correlation between the interaction energy at the PBE level and the interaction energy predicted by our CDFT model (using only the last two terms of Eq. 7.2). A linear fit yields a slope of 1.39, an intercept of $-0.98\,\mathrm{eV}$, with $r^2 = 0.86$. $\Delta U_{int} = U[\mathrm{Na} - \mathrm{TiO_2}] - U[\mathrm{Na}] - U[\mathrm{TiO_2}]$ and $\Delta U_{int} = q\Phi(\mathbf{r}) - q\Delta N v_{f^+}(\mathbf{r})$ for PBE and CDFT, respectively.

In order to know more details about the usefulness of this model for semiquantitative purposes, that is, to go beyond the trends shown in the heat maps, we made a scatter

plot between the interaction energy at the PBE level and our CDFT model. As we can see from Fig. 7.4, there is a good correlation between both quantities, with the linear fit having $R^2 = 0.86$. This result supports the idea that a truncation to second order in the perturbative expansion (Eq. 2.2) is adequate and could be sufficient for semiquantitative purposes.

7.2 Perturbative Perspectives: chlorine adsorption

As second example of the usefulness of corrected Fukui potential, we considered the adsorption of a chlorine atom on rutile TiO_2 (110) surface. From experiments and calculations, Vogtenhuber et al. have given evidence that in a clean TiO_2 (110) surface, Cl adsorbs preferentially on top of fivefold coordinated Ti atoms, Ti_{5c}, (see Fig. 7.5) [133, 134].

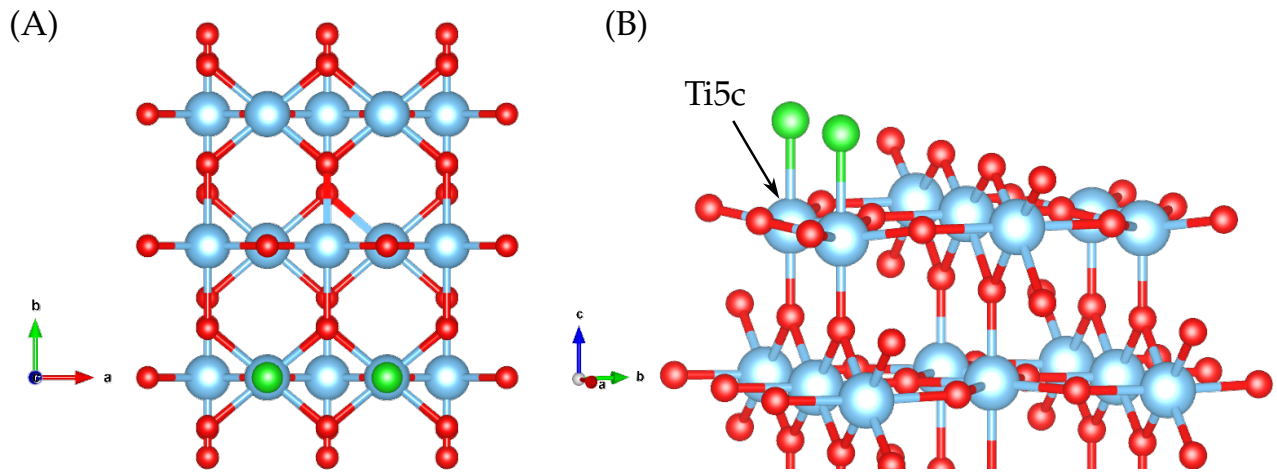

Figure 7.5: Representation of the adsorption site of a chlorine atom on the rutile TiO_2 (110) surface, indicating the fivefold coordinated titanium atom. Panel (A) shows a top view of the adsorption site, while panel (B) presents a side view.

In contrast to sodium atom, chlorine is a strong electron attractor, with a very negative chemical potential (-8.29 eV. Compare with Na, -2.84) [142]. This implies that rutile surface will loose electrons and $v_f^-(\mathrm{r})$ should be used in 7.2. The change in the number of electrons was determined via Parr-Pearson model, Eq. 7.3. For the chlorine atom,

we used the benchmark values proposed from reference data for ionization potentials and electron affinities, which are $\mu = -8.29\,\text{eV}$ and $\eta = 9.35\,\text{eV}$ [142]. For the surface, we considered the same values as before, i.e., $I = 7.35\,\text{eV}$ and $A = 5.50\,\text{eV}$. With these values, the Parr-Pearson model predicts a flux of $\Delta N \approx 0.2\ e$ from the surface to the chlorine atom. With this, we built a heat map of the interaction energy in the same way we did with Na (see Fig. 7.6). As one can see, the stronger interactions (more negative values) are located on fivefold coordinated Ti atoms, Ti_{5c}, in perfect agreement with the experimental and theoretical results [133, 134]. While the weaker interactions (more positive values) correspond to the bridging oxygen atoms O_{2c}. It is worth noting that although there is a considerable electron transfer, the adsorption site matches the site where the electrostatic potential is largest. That is, the adsorption is dominated by electrostatics. Nevertheless, both contributions–electrostatic and electron transfer, have to be taken into account to obtain a good description.

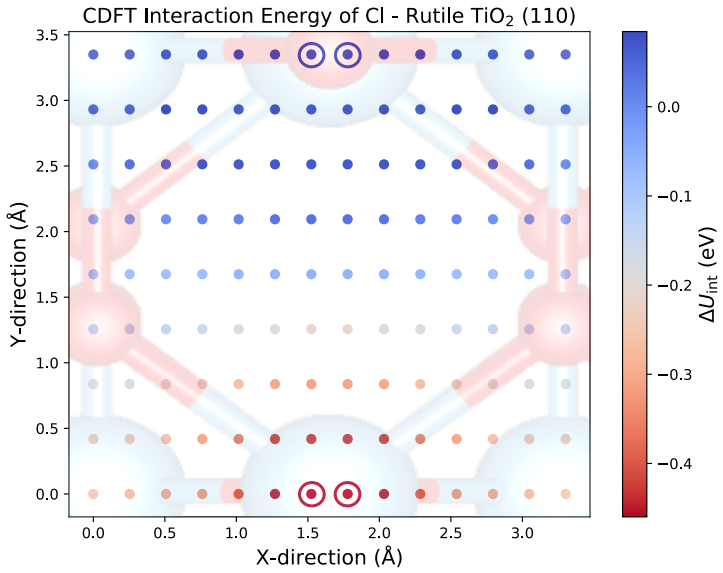

Figure 7.6: Heat map of the interaction energy, ΔU_{int}, of a chlorine atom positioned 0.5 Å above the van der Waals surface of rutile TiO_2 (110) with the CDFT model. The maximum and minimum points are shown enclosed by concentric circles. $\Delta U_{int} = q\Phi(\mathbf{r}) - q\Delta N v_{f^-}(\mathbf{r})$.

7.3 Perturbative Perspectives: a general model

A general model of the interaction between chemical species and surface can be constructed using Eq. 7.2, where ΔN and q enter as parameters that control the relative importance of electron charge and electrostatic effects. Paul Ayers et al. proposed a general-purpose reactivity indicator based on a similar idea, although they a much supplied version of the interaction energy by replacing local quantities by condensed values [82]. Here we consider the case in which the charge of the reactive site is fixed, while the number of electrons transferred is variable. Fig. 7.7 shows the heat maps for the interaction energy of a model species with active site charge $q = -0.25$ and charge transfer in the interval from $\Delta N = [0, 0.5]$. For $\Delta N = 0$ the interaction is determined by the electrostatic potential of the surface, resulting in a more favorable interaction on the bridging oxygen atom O_{2c}. By incorporating the effect of electron donation towards the surface, the Fukui potential "competes" with the electrostatic potential. Thus, for $\Delta N = 0.1, 0.2$ and 0.3, the model predicts that the most favourable interaction is between the model attacking agent and the surface over the Ti_{6c} site, while for $\Delta N = 0.4$ and 0.5, the most favourable interaction moves towards a hollow site of the oxygen, which precisely the site favorable for the sodium adsorption, as it was previously discussed. As we can see, in this model the regioselectivity of the interaction is evidently dependent on the amount of electrons flowing between the species, thus highlighting the importance of an adequate Fukui potential for a general case where both effects, electrostatics and electron transfer are important.

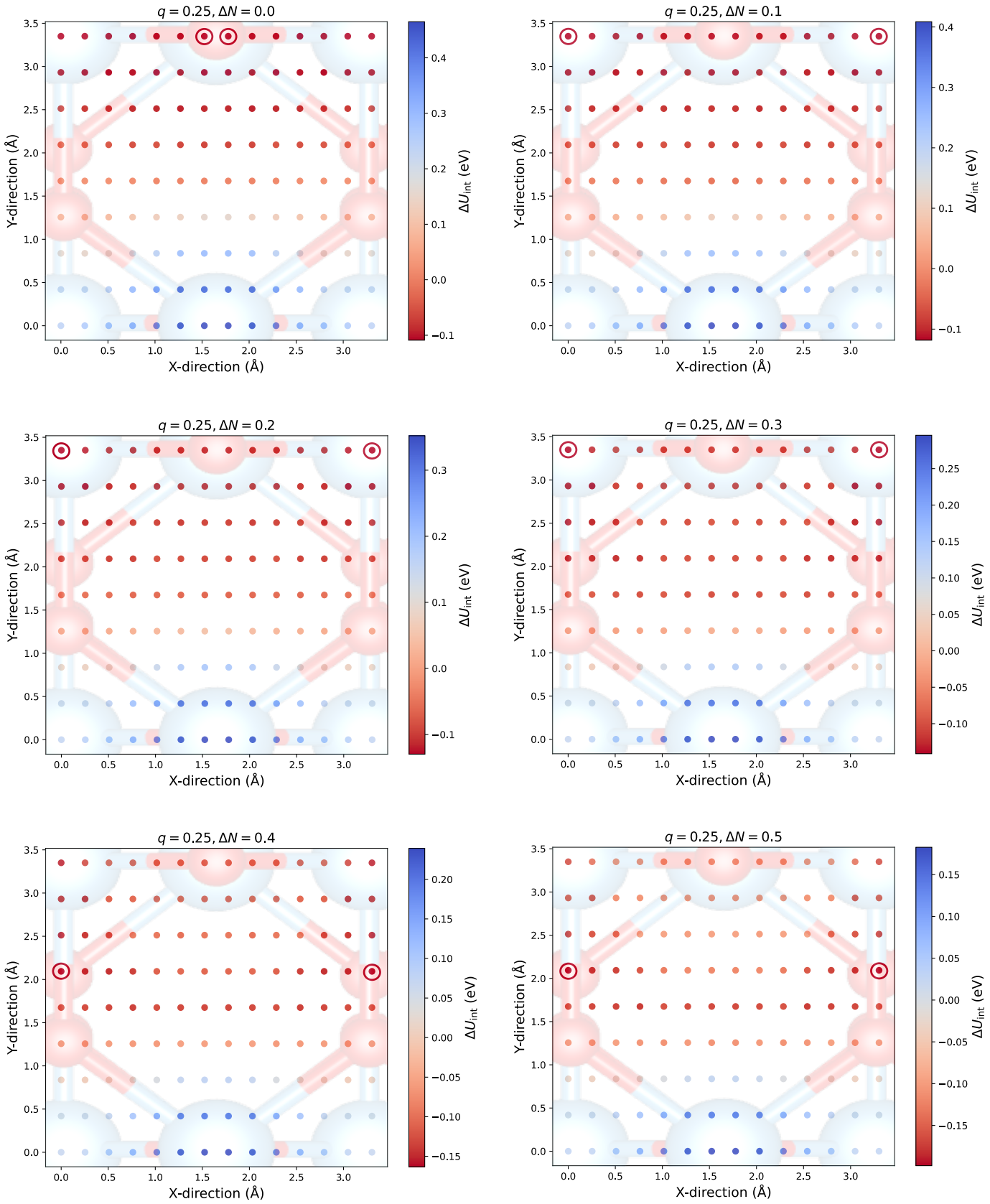

Figure 7.7: Heat maps of interaction energy, ΔU_{int}, for a model with charge $q = -0.25$ varying the change in the number of electrons, ΔN, from 0 to 0.5, for interactions with rutile TiO_2 (110) surface. The maximum are shown enclosed by concentric red circles. $\Delta U_{int} = q\Phi(\mathbf{r}) - q\Delta N v_{f^{\pm}}(\mathbf{r})$.

Chapter 8

Conclusions

In this thesis, we explain how Conceptual Density Functional Theory can be a useful tool in solid-state reactivity. Our research focused on the Fukui function and Fukui potential, specifically on the effects of orbital relaxation and the incorporation of the compensating background charge in the calculation of the electronic structure of net charged systems. We studied four titanium surfaces as models: Ti (0001), TiC (001), anatase TiO_2 (001), and rutile TiO_2 (110).

In Chapter 5, we calculated Fukui functions using five different methodologies, two of which are expected to fully correct or be free of the background charge (SCPC and ECC). Our results show that the use of finite differences without correction should be restricted to the calculation of $f^-(\mathbf{r})$, since for $f^+(\mathbf{r})$, a significant fraction of the anion charge density build up in the vacuum region. Our results also demonstrate that relaxation effects can become so significant that they substantially modify the topology of Fukui functions. Comparison with theoretical and experimental results allows us to conclude that, *a priori*, a self-consistent correction (as provided in SCPC) is necessary, especially for $f^+(\mathbf{r})$, where the largest pathological differences are observed.

In Chapter 6, we calculate the Fukui potentials for the Fukui functions obtained above. We show that an simple *a posteriori* correction is sufficient to correct the potential in the region of main chemical interest, that is, the transition between the vacuum and the sur-

face, but not necessarily within the slab model (bulk).

We leverage the results obtained for the Fukui potentials in the previous chapter to address the chemical-reaction-prediction problem in Chapter 7. We show that a suitable Fukui potential allows predicting the adsorption sites of nucleophiles and electrophiles on a surface. Specifically, by using a perturbation series of Equation (7.2), we predict the adsorption sites of sodium and fluorine atoms on a rutile TiO_2 (110) surface. Moreover, we illustrate how, in general, a reaction is modulated by both electron transfer and electrostatic interactions effects. The former are well captured by the Fukui potential and the latter by the electrostatic potential.

Summarizing, this work provides a methodolgy for predicting adsorption sites and understanding surface interactions. It has potential applications in designing more efficient catalysts and developing advanced materials, thereby contributing to the field of solid-state reactivity.

Part IV

Appendix

Appendix A

Condensed Fukui Functions

A.0.1 Condensed Donor Fukui Function

- Ti (0001) Surface

Table A.1: Condensed Donor Fukui Function, $f^-(\mathbf{r})$, at all sites according to Bader partitioning.

Site	f^- FD	f^- FD-SCPC	f^- Interpolation	f^- LDOS $\delta = 0.1$	f^- FD-ECC
Ti1	0.026414	0.023383	0.025186	0.043980	-0.009687
Ti2	0.030389	0.039305	0.028275	0.061109	-0.000065
Ti3	0.026414	0.023383	0.025186	0.043980	-0.009679
Ti4	0.026414	0.023383	0.025186	0.043980	-0.009690
Ti5	0.030389	0.039305	0.028275	0.061109	-0.000068
Ti6	0.026414	0.023383	0.025186	0.043980	-0.009678
Ti7	0.185159	0.183612	0.185339	0.107528	0.259670
Ti8	0.023223	0.023350	0.025343	0.067937	0.000044
Ti9	0.023224	0.023350	0.025343	0.067937	0.000093
Ti10	0.185159	0.183612	0.185339	0.107528	0.259669
Ti11	0.023223	0.023350	0.025343	0.067937	0.000048
Ti12	0.023224	0.023350	0.025343	0.067937	0.000046
Ti13	0.185177	0.183617	0.185327	0.107528	0.259699
Ti14	0.185177	0.183617	0.185327	0.107528	0.259591

- TiC (001) Surface

Table A.2: Condensed Donor Fukui Function, $f^-(\mathbf{r})$, at all sites according to Bader partitioning.

Site	f^- FD	f^- FD-SCPC	f^- Interpolation	f^- LDOS $\delta = 0.2$	f^- FD-ECC
Ti1	0.008643	0.010056	0.007423	0.027999	-0.000527
Ti2	0.009280	0.016889	0.009329	0.024875	-0.001433
Ti3	0.009280	0.016889	0.009329	0.024875	-0.001433
Ti4	0.008643	0.010056	0.007423	0.027999	-0.000438
Ti5	0.008643	0.010056	0.007423	0.027999	-0.000527
Ti6	0.008643	0.010056	0.007423	0.027999	-0.000438
Ti7	0.006028	0.003726	0.005069	0.023341	-0.003416
Ti8	0.006028	0.003726	0.005069	0.023341	-0.003416
Ti9	0.030741	0.039163	0.028458	0.056163	0.043640
Ti10	0.030741	0.039163	0.028458	0.056163	0.045940
Ti11	0.006028	0.003726	0.005069	0.023341	-0.003416
Ti12	0.006028	0.003726	0.005069	0.023341	-0.003416
Ti13	0.030743	0.039163	0.028459	0.056163	0.043640
Ti14	0.030743	0.039163	0.028459	0.056163	0.045940
C1	0.022199	0.024134	0.022654	0.038629	0.003507
C2	0.016525	0.021464	0.017359	0.026320	0.000579
C3	0.016525	0.021464	0.017359	0.026320	0.000579
C4	0.022199	0.024134	0.022654	0.038629	0.002995
C5	0.016525	0.021464	0.017359	0.026320	0.000579
C6	0.016525	0.021464	0.017359	0.026320	0.000579
C7	0.011676	0.012750	0.013607	0.034669	0.000290
C8	0.011676	0.012750	0.013607	0.034669	0.000457
C9	0.160686	0.142335	0.163156	0.049756	0.207239
C10	0.160590	0.142323	0.161025	0.049756	0.207239

Site	f^- FD	f^- FD-SCPC	f^- Interpolation	f^- LDOS $\delta = 0.2$	f^- FD-ECC
C11	0.011676	0.012750	0.013607	0.034669	0.000290
C12	0.011676	0.012750	0.013607	0.034669	0.000457
C13	0.160702	0.142335	0.163158	0.049756	0.207239
C14	0.160607	0.142322	0.161025	0.049756	0.207239

- Anatase TiO_2 (001) Surface

Table A.3: Condensed Donor Fukui Function, $f^-(\mathbf{r})$, at all sites according to Bader partitioning.

Site	f^- FD	f^- FD-SCPC	f^- Interpolation	f^- LDOS $\delta = 0.3$	f^- FD-ECC
Ti1	0.008155	0.008079	0.019864	0.000598	0.000039
Ti2	0.010383	0.022052	0.012867	0.006299	-0.002785
Ti3	0.010855	0.042274	0.011524	0.014963	0.001374
Ti4	0.007718	0.015155	0.008143	0.000941	0.000250
Ti5	0.028363	0.040913	0.028535	0.010003	0.072694
Ti6	0.027869	0.075420	0.026160	0.005482	0.065263
O1	0.017754	0.033220	0.021561	0.001437	-0.001046
O2	0.024302	0.019885	0.016392	0.006355	-0.002271
O3	0.019080	0.033890	0.012971	0.000114	-0.000172
O4	0.018895	0.050107	0.006728	0.000684	-0.003549
O5	0.082154	0.066197	0.088646	0.097492	0.087269
O6	0.021432	0.042951	0.025876	0.000504	-0.002995
O7	0.027503	0.030391	0.019748	0.010736	-0.016343
O8	0.016892	0.018083	0.004101	0.001257	0.000018
O9	0.288721	0.157301	0.309925	0.429917	0.354102
O10	0.286689	0.154338	0.285825	0.170123	0.356174
O11	0.083891	0.155781	0.088749	0.239254	0.096990
O12	0.019342	0.033962	0.012386	0.003842	-0.005008

- Rutile TiO_2 (110) Surface

Table A.4: Condensed Donor Fukui Function, $f^-(\mathbf{r})$, at all sites according to Bader partitioning.

Site	f^- FD	f^- FD-SCPC	f^- Interpolation	f^- LDOS $\delta = 0.2$	f^- FD-ECC
Ti1	0.005933	0.025319	0.006078	0.001505	-0.000447
Ti2	0.005727	0.018421	0.003796	0.003439	-0.000305
Ti3	0.006299	0.013292	0.005628	0.003074	-0.000060
Ti4	0.005505	0.004494	0.004469	0.004079	-0.001218
Ti5	0.006299	0.013292	0.005628	0.003074	-0.000060
Ti6	0.005727	0.018421	0.003796	0.003439	-0.000305
Ti7	0.006433	0.017614	0.004369	0.000024	-0.001359
Ti8	0.004015	0.004308	-0.000014	0.000106	-0.001489
Ti9	0.021816	0.011471	0.032109	0.000153	0.036360
Ti10	0.005818	0.001228	0.000076	0.000723	0.002257
Ti11	0.006433	0.017614	0.004369	0.000024	-0.001359
Ti12	0.004015	0.004308	-0.000014	0.000106	-0.001489
Ti13	0.021816	0.011471	0.032109	0.000153	0.036360
Ti14	0.005818	0.001228	0.000076	0.000723	0.002257
O1	0.013185	0.026191	0.017516	0.073233	0.000537
O2	0.014070	0.019450	0.015877	0.085099	0.000141
O3	0.014697	0.041936	0.019299	0.089811	0.001017
O4	0.012585	0.032983	0.015940	0.053405	0.000200
O5	0.014623	0.041936	0.019407	0.089813	0.001342
O6	0.012577	0.032786	0.016048	0.053407	0.001030
O7	0.013163	0.026224	0.017516	0.073232	0.000537
O8	0.014070	0.019450	0.015877	0.085099	0.000141
O9	0.012577	0.032786	0.016048	0.053407	0.001030
O10	0.012585	0.032983	0.015940	0.053405	0.000200

Site	f^- FD	f^- FD-SCPC	f^- Interpolation	f^- LDOS $\delta = 0.2$	f^- FD-ECC
O11	0.017793	0.022309	0.026509	0.039411	0.002242
O12	0.009176	0.015478	0.010291	0.027467	0.000580
O13	0.015552	0.032035	0.015383	0.020567	0.001698
O14	0.015675	0.032035	0.015486	0.020567	0.002932
O15	0.007791	0.012026	0.004742	0.004243	0.000380
O16	0.019399	0.021191	0.023102	0.016126	0.001869
O17	0.056796	0.026101	0.053037	0.002904	0.074902
O18	0.057842	0.026140	0.053761	0.002904	0.077995
O19	0.177081	0.078099	0.161812	0.000543	0.299747
O20	0.017793	0.022309	0.026509	0.039411	0.002242
O21	0.009176	0.015478	0.010291	0.027467	0.000580
O22	0.015552	0.032035	0.015383	0.020567	0.001698
O23	0.015675	0.032035	0.015486	0.020567	0.002932
O24	0.007791	0.012026	0.004742	0.004243	0.00038
O25	0.019399	0.021191	0.023102	0.016126	0.001869
O26	0.056796	0.026101	0.053037	0.002904	0.074902
O27	0.057842	0.026140	0.053761	0.002904	0.07799
O28	0.177085	0.078067	0.161621	0.000543	0.299747

- Pt (111) Surface

Table A.5: Condensed Donor Fukui Function, $f^-(\mathbf{r})$, at all sites according to Bader partitioning.

Site	f^- FD	f^- FD-SCPC	f^- Interpolation	f^- LDOS $\delta = 0.3$	f^- FD-ECC
Pt1	0.183745	0.176356	0.182598	0.062650	0.248905
Pt2	0.026648	0.030873	0.025106	0.073953	-0.000996
Pt3	0.027587	0.029703	0.028969	0.076681	0.001524
Pt4	0.026648	0.030873	0.025106	0.073953	-0.001006
Pt5	0.027587	0.029703	0.028969	0.076681	0.001199
Pt6	0.183745	0.176356	0.182598	0.062650	0.250649
Pt7	0.024040	0.026135	0.026654	0.073430	-0.000290
Pt8	0.024040	0.026135	0.026656	0.073430	-0.000250
Pt9	0.026648	0.030873	0.025106	0.073953	-0.001660
Pt10	0.026648	0.030873	0.025106	0.073953	-0.000342
Pt11	0.027587	0.029703	0.028969	0.076681	0.001479
Pt12	0.027587	0.029703	0.028969	0.076681	0.001244
Pt13	0.183745	0.176356	0.182597	0.062650	0.248905
Pt14	0.183745	0.176356	0.182597	0.062650	0.250649

- ZrC (001) Surface

Table A.6: Condensed Donor Fukui Function, $f^-(\mathbf{r})$, at all sites according to Bader partitioning.

Site	f^- FD	f^- FD-SCPC	f^- Interpolation	f^- LDOS $\delta = 0.2$	f^- FD-ECC
Zr1	0.044112	0.065932	0.048364	0.033905	0.057808
Zr2	0.009437	0.010497	0.009326	0.014152	-0.000391
Zr3	0.009437	0.010497	0.009326	0.014152	-0.000363
Zr4	0.003944	-0.000378	0.004712	0.009974	-0.001766

Site	f^- FD	f^- FD-SCPC	f^- Interpolation	f^- LDOS $\delta = 0.2$	f^- FD-ECC
Zr5	0.012944	0.020056	0.014798	0.014287	-0.001822
Zr6	0.003944	-0.000378	0.004712	0.009974	-0.001768
Zr7	0.003944	-0.000378	0.004712	0.009974	-0.001766
Zr8	0.012944	0.020056	0.014798	0.014287	-0.001822
Zr9	0.003944	-0.000378	0.004712	0.009974	-0.001768
Zr10	0.044112	0.065932	0.048364	0.033905	0.057808
Zr11	0.009437	0.010497	0.009326	0.014152	-0.000391
Zr12	0.009437	0.010497	0.009326	0.014152	-0.000363
Zr13	0.044112	0.065931	0.048364	0.033905	0.057809
Zr14	0.044112	0.065931	0.048364	0.033905	0.057809
C1	0.014495	0.013355	0.015374	0.048122	-0.002218
C2	0.021204	0.020866	0.022150	0.048827	0.003093
C3	0.014495	0.013355	0.015374	0.048122	-0.002232
C4	0.142996	0.121021	0.137078	0.078189	0.195230
C5	0.017944	0.019113	0.016672	0.034668	0.000699
C6	0.017944	0.019113	0.016672	0.034668	0.000694
C7	0.142993	0.121021	0.137078	0.078189	0.195230
C8	0.017944	0.019113	0.016672	0.034668	0.000699
C9	0.017944	0.019113	0.016672	0.034668	0.000694
C10	0.014495	0.013355	0.015374	0.048122	-0.002218
C11	0.021204	0.020866	0.022150	0.048827	0.003093
C12	0.014495	0.013355	0.015374	0.048122	-0.002232
C13	0.142996	0.121023	0.137077	0.078189	0.195232
C14	0.142993	0.121023	0.137077	0.078189	0.195232

- MgO (001) Surface

Table A.7: Condensed Donor Fukui Function, $f^-(\mathbf{r})$, at all sites according to Bader partitioning.

Site	f^- FD	f^- FD-SCPC	f^- Interpolation	f^- LDOS $\delta = 0.3$	f^- FD-ECC
Mg1	0.000000	0.000000	-0.000068	0.000000	-0.000113
Mg2	0.000000	0.000000	0.000000	0.000008	-0.000035
Mg3	0.000000	0.000000	0.000000	0.000008	-0.000035
Mg4	0.000000	0.000000	-0.000068	0.000000	-0.000113
Mg5	0.000000	0.000000	-0.000068	0.000000	-0.000113
Mg6	0.000000	0.000000	-0.000068	0.000000	-0.000113
Mg7	-0.000583	0.000037	-0.001361	0.000011	-0.001289
Mg8	-0.000583	0.000037	-0.001361	0.000011	-0.001289
Mg9	0.000317	0.000000	0.000115	0.000000	0.007582
Mg10	0.000317	0.000000	0.000115	0.000000	0.007582
Mg11	-0.000583	0.000037	-0.001361	0.000011	-0.001289
Mg12	-0.000583	0.000037	-0.001361	0.000011	-0.001289
Mg13	0.000320	0.000000	0.000116	0.000000	0.007582
Mg14	0.000320	0.000000	0.000116	0.000000	0.007582
O1	0.021096	0.050827	0.030062	0.047289	0.000861
O2	0.025426	0.056709	0.031708	0.047080	0.002197
O3	0.025426	0.056709	0.031708	0.047080	0.002197
O4	0.021096	0.050827	0.030062	0.047289	0.000860
O5	0.025426	0.056709	0.031705	0.047080	0.002197
O6	0.025426	0.056709	0.031705	0.047080	0.002197
O7	0.031944	0.054516	0.030392	0.053878	0.006563
O8	0.031944	0.054516	0.030392	0.053878	0.006562
O9	0.182345	0.113325	0.174183	0.125382	0.234654
O10	0.182345	0.113324	0.174182	0.125382	0.234654

Site	f^- FD	f^- FD-SCPC	f^- Interpolation	f^- LDOS $\delta = 0.3$	f^- FD-ECC
O11	0.031944	0.054516	0.030392	0.053878	0.006563
O12	0.031944	0.054516	0.030392	0.053878	0.006562
O13	0.182350	0.113325	0.174187	0.125382	0.234654
O14	0.182350	0.113325	0.174185	0.125382	0.234654

- Reduced SnO_2 (110) Rutile Surface

Table A.8: Condensed Donor Fukui Function, $f^-(\mathbf{r})$, at all sites according to Bader partitioning.

Site	f^- FD	f^- FD-SCPC	f^- Interpolation	f^- LDOS $\delta = 0.2$	f^- FD-ECC
Sn1	0.004936	0.007213	0.017564	0.007650	0.000088
Sn2	0.021108	0.016493	0.026960	0.011458	0.000027
Sn3	0.004936	0.007213	0.017564	0.007650	0.000089
Sn4	0.197534	0.169319	0.175173	0.183547	0.300464
Sn5	0.016436	0.015019	0.024803	0.009916	-0.000221
Sn6	0.016437	0.015019	0.024804	0.009916	-0.000240
Sn7	0.085810	0.105165	0.113869	0.076882	0.105160
Sn8	0.011656	0.016102	0.025167	0.009860	0.000117
Sn9	0.011656	0.016102	0.025168	0.009860	0.000116
Sn10	0.004948	0.002291	0.011990	0.002572	-0.000320
Sn11	0.023068	0.016376	0.026831	0.011194	0.000070
Sn12	0.004948	0.002291	0.011990	0.002572	-0.000301
Sn13	0.197535	0.169321	0.175175	0.183547	0.300466
Sn14	0.085810	0.105165	0.113869	0.076882	0.105179
O1	0.010813	0.007152	0.006042	0.004892	-0.000996
O2	0.003796	0.002526	0.003276	0.003343	0.000015
O3	0.010813	0.007152	0.006042	0.004892	-0.000992
O4	0.028302	0.026047	0.023007	0.059083	0.050526
O5	0.006055	0.003107	0.003403	0.002974	-0.000011
O6	0.006055	0.003107	0.003403	0.002974	-0.000010
O7	0.010810	0.007152	0.006042	0.004892	-0.000996
O8	0.003796	0.002526	0.003276	0.003343	0.000016
O9	0.010810	0.007152	0.006042	0.004892	-0.000992
O10	0.028218	0.025983	0.022430	0.059000	0.050526

Site	f^- FD	f^- FD-SCPC	f^- Interpolation	f^- LDOS $\delta = 0.2$	f^- FD-ECC
O11	0.006055	0.003107	0.003403	0.002974	-0.000011
O12	0.006055	0.003107	0.003403	0.002974	-0.000010
O3	0.012605	0.025370	0.007084	0.008321	-0.002793
O14	0.003700	0.004364	0.003355	0.003122	0.000018
O15	0.013037	0.009386	0.003961	0.002415	-0.000366
O16	0.005683	0.002721	0.003756	0.002721	0.000005
O17	0.004317	0.001366	0.003309	0.002785	0.000018
O18	0.023198	0.050173	0.015469	0.041725	-0.001296
O19	0.013037	0.009386	0.003961	0.002415	-0.000355
O20	0.003700	0.004364	0.003355	0.003122	0.000018
O21	0.012605	0.025370	0.007084	0.008321	-0.002789
O22	0.023198	0.050173	0.015469	0.041725	-0.001295
O23	0.004317	0.001366	0.003309	0.002785	0.000018
O24	0.005683	0.002721	0.003756	0.002721	0.000006
O25	0.028305	0.026048	0.023006	0.059083	0.050532
O26	0.028219	0.025986	0.022430	0.059000	0.050532

A.0.2 Condensed Acceptor Fukui Function

- Ti (0001) Surface

Table A.9: Condensed Acceptor Fukui Function, $f^+(\mathbf{r})$, at all sites according to Bader partitioning.

Site	f^+ FD	f^+ FD-SCPC	f^+ Interpolation	f^+ LDOS $\delta = 0.1$	f^+ FD-ECC
Ti1	0.022243	0.017167	0.024696	0.045442	-0.005866
Ti2	0.038050	0.020717	0.034353	0.068537	-0.027928
Ti3	0.022243	0.017167	0.024696	0.045442	-0.005473
Ti4	0.022243	0.017167	0.024696	0.045442	-0.005859
Ti5	0.038050	0.020717	0.034353	0.068537	-0.027918
Ti6	0.022243	0.017167	0.024696	0.045442	-0.005478
Ti7	0.180639	0.182975	0.185985	0.094703	0.246170
Ti8	0.027702	0.039703	0.022145	0.075587	0.023271
Ti9	0.027702	0.039294	0.022145	0.075587	0.023623
Ti10	0.180639	0.182975	0.185985	0.094703	0.246170
Ti11	0.027702	0.039703	0.022145	0.075587	0.023282
Ti12	0.027702	0.039294	0.022145	0.075587	0.023642
Ti13	0.181420	0.182977	0.185980	0.094703	0.246384
Ti14	0.181420	0.182977	0.185980	0.094703	0.246369

- TiC (001) Surface

Table A.10: Condensed Acceptor Fukui Function, $f^+(\mathbf{r})$, at all sites according to Bader partitioning.

Site	f^+ FD	f^+ FD-SCPC	f^+ Interpolation	f^+ LDOS $\delta = 0.2$	f^+ FD-ECC
Ti1	0.009558	0.011090	0.008634	0.033711	0.000327
Ti2	0.010610	0.024750	0.010315	0.040293	-0.000716
Ti3	0.010610	0.024750	0.010315	0.040293	-0.000716
Ti4	0.009558	0.011090	0.008634	0.033711	-0.000250
Ti5	0.009558	0.011090	0.008634	0.033711	0.000327
Ti6	0.009558	0.011090	0.008634	0.033711	-0.000250
Ti7	0.008586	0.006278	0.007613	0.025321	-0.001251
Ti8	0.008586	0.006278	0.007613	0.025321	-0.001251
Ti9	0.041244	0.040036	0.030651	0.050920	0.041486
Ti10	0.041244	0.040036	0.030651	0.050920	0.038228
Ti11	0.008586	0.006278	0.007613	0.025321	-0.001251
Ti12	0.008586	0.006278	0.007613	0.025321	-0.001251
Ti13	0.041753	0.040038	0.030645	0.050920	0.041486
Ti14	0.041753	0.040038	0.030645	0.050920	0.038228
C1	0.018071	0.022623	0.020771	0.036122	0.002907
C2	0.016292	0.024390	0.016872	0.024417	-0.000194
C3	0.016292	0.024390	0.016872	0.024417	-0.000194
C4	0.018071	0.022623	0.020771	0.036122	0.003607
C5	0.016292	0.024390	0.016872	0.024417	-0.000194
C6	0.016292	0.024390	0.016872	0.024417	-0.000194
C7	0.013371	0.010058	0.011385	0.028573	0.000628
C8	0.013371	0.010058	0.011385	0.028573	0.000305
C9	0.180917	0.134462	0.159334	0.048851	0.210011
C10	0.111488	0.134461	0.159323	0.048851	0.210011

Site	f^+ FD	f^+ FD-SCPC	f^+ Interpolation	f^+ LDOS $\delta = 0.2$	f^+ FD-ECC
C11	0.013371	0.010058	0.011385	0.028573	0.000628
C12	0.013371	0.010058	0.011385	0.028573	0.000305
C13	0.181224	0.134460	0.159278	0.048851	0.210011
C14	0.111789	0.134458	0.159291	0.048851	0.210011

- Anatase TiO_2 (001) Surface

Table A.11: Condensed Acceptor Fukui Function, $f^+(\mathbf{r})$, at all sites according to Bader partitioning.

Site	f^+ FD	f^+ FD-SCPC	f^+ Interpolation	f^+ LDOS $\delta = 0.3$	f^+ FD-ECC
Ti1	0.040336	0.042317	0.068126	0.242211	0.038719
Ti2	0.055898	0.100800	0.092746	0.220293	0.042258
Ti3	0.044131	0.151906	0.074531	0.223484	0.028917
Ti4	0.040521	0.074389	0.062036	0.240272	0.034250
Ti5	0.061076	0.118746	0.081587	0.037412	0.144840
Ti6	0.045945	0.106783	0.053525	0.0051806	0.082267
O1	0.012098	0.017406	0.006038	0.003914	-0.005996
O2	0.010998	0.011215	0.011938	0.003325	0.000736
O3	0.009512	0.026814	-0.001577	0.003816	-0.007837
O4	0.004793	0.049926	-0.000262	0.002573	-0.006177
O5	0.030611	0.014172	0.084275	0.001366	0.095779
O6	0.011617	0.057912	0.001778	0.003819	0.002034
O7	0.012925	0.013531	0.011160	0.003285	-0.000185
O8	0.011707	0.013618	0.006041	0.003836	-0.006375
O9	0.280987	0.075610	0.187379	0.000440	0.233297
O10	0.287448	0.046312	0.182985	0.000736	0.250645
O11	0.029145	0.054500	0.075212	0.001500	0.074470
O12	0.010252	0.024042	0.002482	0.002538	-0.001942

- Rutile TiO_2 (110) Surface

Table A.12: Condensed Acceptor Fukui Function, $f^+(\mathbf{r})$, at all sites according to Bader partitioning.

Site	f^+ FD	f^+ FD-SCPC	f^+ Interpolation	f^+ LDOS $\delta = 0.2$	f^+ FD-ECC
Ti1	0.025052	0.022372	0.031090	0.046517	0.047265
Ti2	0.010082	0.000483	0.011296	0.001963	0.002625
Ti3	0.020556	0.030968	0.024708	0.050604	0.020367
Ti4	0.009141	0.005569	0.006776	0.000742	-0.001041
Ti5	0.020556	0.030968	0.024708	0.050604	0.020367
Ti6	0.010082	0.000483	0.011298	0.001963	0.002625
Ti7	0.046627	0.316773	0.079459	0.296705	0.062441
Ti8	0.013784	0.008572	0.014105	0.011842	-0.003127
Ti9	0.048566	0.037667	0.064030	0.090895	0.064303
Ti10	0.008700	-0.005997	0.001488	0.000426	0.001154
Ti11	0.046627	0.316773	0.079459	0.296705	0.062441
Ti12	0.013784	0.008572	0.014105	0.011842	-0.003127
Ti13	0.048566	0.037667	0.064030	0.090895	0.064303
Ti14	0.008700	-0.005997	0.001488	0.000426	0.001154
O1	0.007878	0.003887	0.007468	0.003030	-0.004647
O2	0.006259	0.004716	0.003208	0.000124	-0.008649
O3	0.006899	0.000069	0.007528	0.000025	-0.006675
O4	0.007889	0.005796	0.006779	0.000716	-0.003598
O5	0.006884	0.000069	0.007371	0.000025	-0.005087
O6	0.008046	0.005796	0.006778	0.000754	-0.002225
O7	0.007878	0.003887	0.007468	0.003030	-0.004647
O8	0.006259	0.004716	0.003208	0.000124	-0.008649
O9	0.008046	0.005796	0.006778	0.000754	-0.002225
O10	0.007889	0.005796	0.006778	0.000716	-0.003598

Site	f^+ FD	f^+ FD-SCPC	f^+ Interpolation	f^+ LDOS $\delta = 0.2$	f^+ FD-ECC
O11	0.003711	0.003152	0.002874	0.000137	-0.000983
O12	0.004407	0.004514	0.001415	0.010287	-0.002184
O13	0.006384	0.007912	0.003872	0.000765	-0.006330
O14	0.006384	0.007977	0.003938	0.000765	-0.005902
O15	0.003935	0.000104	-0.000362	0.001471	-0.002585
O16	0.005659	-0.003415	0.008062	0.000089	-0.004255
O17	0.026067	0.005487	0.052565	0.002611	0.071902
O18	0.025944	0.005487	0.052453	0.002611	0.072036
O19	0.214424	0.046082	0.130047	0.000550	0.232163
O20	0.003711	0.003152	0.002874	0.000137	-0.000983
O21	0.004407	0.004514	0.001415	0.010287	-0.002184
O22	0.006384	0.007912	0.003872	0.000765	-0.006330
O23	0.006384	0.007977	0.003938	0.000765	-0.005902
O24	0.003935	0.000104	-0.000362	0.001471	-0.002585
O25	0.005659	-0.003415	0.008062	0.000089	-0.004255
O26	0.026067	0.005487	0.052565	0.002611	0.071902
O27	0.025944	0.005487	0.052453	0.002611	0.072036
O28	0.215847	0.046081	0.128919	0.000550	0.232163

- Pt (111) Surface

Table A.13: Condensed Acceptor Fukui Function, $f^-(\mathbf{r})$, at all sites according to Bader partitioning.

Site	f^+ FD	f^+ FD-SCPC	f^+ Interpolation	f^+ LDOS $\delta = 0.05$
Pt1	0.181982	0.175043	0.180402	0.062650
Pt2	0.026661	0.032362	0.029524	0.073953
Pt3	0.028556	0.029413	0.028626	0.076681
Pt4	0.026661	0.032362	0.029524	0.073953
Pt5	0.028556	0.029413	0.028626	0.076681
Pt6	0.181982	0.175043	0.180416	0.062650
Pt7	0.025532	0.026366	0.022864	0.073430
Pt8	0.025532	0.026366	0.022864	0.073430
Pt9	0.026661	0.032362	0.029524	0.073953
Pt10	0.026661	0.032362	0.029524	0.073953
Pt11	0.028556	0.029413	0.028626	0.076681
Pt12	0.028556	0.029413	0.028626	0.076681
Pt13	0.182051	0.175042	0.180435	0.062650
Pt14	0.182051	0.175043	0.180417	0.062650

- ZrC (001) Surface

Table A.14: Condensed Acceptor Fukui Function, $f^+(\mathbf{r})$, at all sites according to Bader partitioning.

Site	f^+ FD	f^+ FD-SCPC	f^+ Interpolation	f^+ LDOS $\delta = 0.2$
Zr1	0.056369	0.138332	0.051226	0.038869
Zr2	0.012691	0.013525	0.009524	0.024383
Zr3	0.012691	0.013525	0.009524	0.024383
Zr4	0.011893	0.000964	0.005473	0.013484

Site	f^+ FD	f^+ FD-SCPC	f^+ Interpolation	f^+ LDOS $\delta = 0.2$
Zr5	0.013275	0.031991	0.014587	0.024330
Zr6	0.011893	0.000964	0.005473	0.013484
Zr7	0.011893	0.000964	0.005473	0.013484
Zr8	0.013275	0.031991	0.014587	0.024330
Zr9	0.011893	0.000964	0.005473	0.013484
Zr10	0.056369	0.138332	0.051226	0.038869
Zr11	0.012691	0.013525	0.009524	0.024383
Zr12	0.012691	0.013525	0.009524	0.024383
Zr13	0.056156	0.138331	0.051228	0.038869
Zr14	0.056156	0.138331	0.051228	0.038869
C1	0.012870	0.005040	0.015344	0.042215
C2	0.020596	0.023484	0.022579	0.052460
C3	0.012870	0.005040	0.015344	0.042215
C4	0.128798	0.046100	0.133759	0.066188
C5	0.010872	0.018304	0.016085	0.026467
C6	0.010872	0.018304	0.016085	0.026467
C7	0.128798	0.046101	0.133758	0.066188
C8	0.010872	0.018304	0.016085	0.026467
C9	0.010872	0.018304	0.016085	0.026467
C10	0.012870	0.005040	0.015344	0.042215
C11	0.020596	0.023484	0.022579	0.052460
C12	0.012870	0.005040	0.015344	0.042215
C13	0.128156	0.046098	0.133766	0.066188
C14	0.128156	0.046098	0.133767	0.066188

- MgO (001) Surface

Table A.15: Condensed Acceptor Fukui Function, $f^+(\mathbf{r})$, at all sites according to Bader partitioning.

Site	f^+ FD	f^+ FD-SCPC	f^+ Interpolation	f^+ LDOS $\delta = 0.3$
Mg1	0.000000	0.000015	0.000027	0.009181
Mg2	0.000000	0.000000	0.000001	0.003236
Mg3	0.000000	0.000000	0.000001	0.003236
Mg4	0.000000	0.000015	0.000027	0.004407
Mg5	0.000000	0.000015	0.000027	0.009181
Mg6	0.000000	0.000015	0.000027	0.004407
Mg7	-0.000046	-0.000006	0.019082	0.015203
Mg8	-0.000046	-0.000006	0.019082	0.015203
Mg9	0.130960	0.186296	0.123187	0.189929
Mg10	0.130960	0.186296	0.123187	0.178989
Mg111	-0.000046	-0.000006	0.019082	0.015203
Mg12	-0.000046	-0.000006	0.019082	0.015203
Mg13	0.131357	0.100789	0.123187	0.189929
Mg14	0.131425	0.100884	0.123187	0.178989
O1	0.003854	0.002351	0.004535	0.002186
O2	0.020034	0.005343	0.019304	0.003473
O3	0.020034	0.005343	0.019304	0.003473
O4	0.003854	0.002351	0.004535	0.002186
O5	0.020285	0.005324	0.019156	0.003473
O6	0.020285	0.005324	0.019156	0.003473
O7	0.020327	0.011855	0.020777	0.012715
O8	0.020327	0.011855	0.020777	0.009475
O9	0.076609	0.150572	0.244734	0.026265
O10	0.076609	0.150572	0.011476	0.026265

Site	f^+ FD	f^+ FD-SCPC	f^+ Interpolation	f^+ LDOS $\delta = 0.3$
O11	0.020327	0.011855	0.020777	0.012715
O12	0.020327	0.011855	0.020777	0.009475
O13	0.076305	0.025549	0.002754	0.026265
O14	0.076305	0.025549	0.002754	0.026265

- Reduced Rutile SnO_2 (110) Surface

Table A.16: Condensed Acceptor Fukui Function, $f^+(\mathbf{r})$, at all sites according to Bader partitioning.

Site	f^+ FD	f^+ FD-SCPC	f^+ Interpolation	f^+ LDOS $\delta = 0.2$
Sn1	0.019138	0.022198	0.005354	0.022198
Sn2	0.020547	0.015415	0.017198	0.015415
Sn3	0.019138	0.022198	0.005354	0.022198
Sn4	0.084313	0.114813	0.132897	0.114813
Sn5	0.022176	0.018139	0.015490	0.018139
Sn6	0.022176	0.018139	0.015490	0.018139
Sn7	0.068195	0.147498	0.159525	0.147498
Sn8	0.023280	0.023354	0.009640	0.023354
Sn9	0.023280	0.023354	0.009640	0.023354
Sn10	0.016095	0.011746	0.006734	0.011746
Sn11	0.023934	0.016832	0.024943	0.016832
Sn12	0.016095	0.011746	0.006734	0.011746
Sn13	0.084313	0.114803	0.132367	0.114803
Sn14	0.068195	0.147498	0.159525	0.147498
O1	0.006016	0.004783	0.009186	0.004783
O2	0.004920	0.003578	0.004736	0.003578
O3	0.006016	0.004783	0.009186	0.004783
O4	0.170794	0.025222	0.028740	0.025222
O5	0.004964	0.003454	0.007163	0.003454
O6	0.004964	0.003454	0.007163	0.003454
O7	0.006016	0.004783	0.009174	0.004783
O8	0.004920	0.003578	0.004736	0.003578
O9	0.006016	0.004783	0.009174	0.004783
O10	0.013722	0.025061	0.028726	0.025061

Site	f^+ FD	f^+ FD-SCPC	f^+ Interpolation	f^+ LDOS $\delta = 0.2$
O11	0.004964	0.003454	0.007163	0.003454
O12	0.004964	0.003454	0.007163	0.003454
O13	0.006114	0.020796	0.018944	0.020796
O14	0.004587	0.008165	0.004664	0.008165
O15	0.003708	0.010818	0.014308	0.010818
O16	0.003824	0.004551	0.005321	0.004551
O17	0.004005	0.004530	0.002834	0.004530
O18	0.010725	0.026935	0.009534	0.026935
O19	0.003708	0.010818	0.014308	0.010818
O20	0.004588	0.008165	0.004673	0.008165
O21	0.006114	0.020796	0.018944	0.020796
O22	0.010725	0.026935	0.009534	0.026935
O23	0.004005	0.004530	0.002834	0.004530
O24	0.003824	0.004551	0.005321	0.004551
O25	0.171200	0.025231	0.027680	0.025231
O26	0.013722	0.025059	0.027900	0.025059

Appendix B

Additional Fukui Functions

B.1 Electrophilic Fukui Function, $f^{-}(\mathbf{r})$

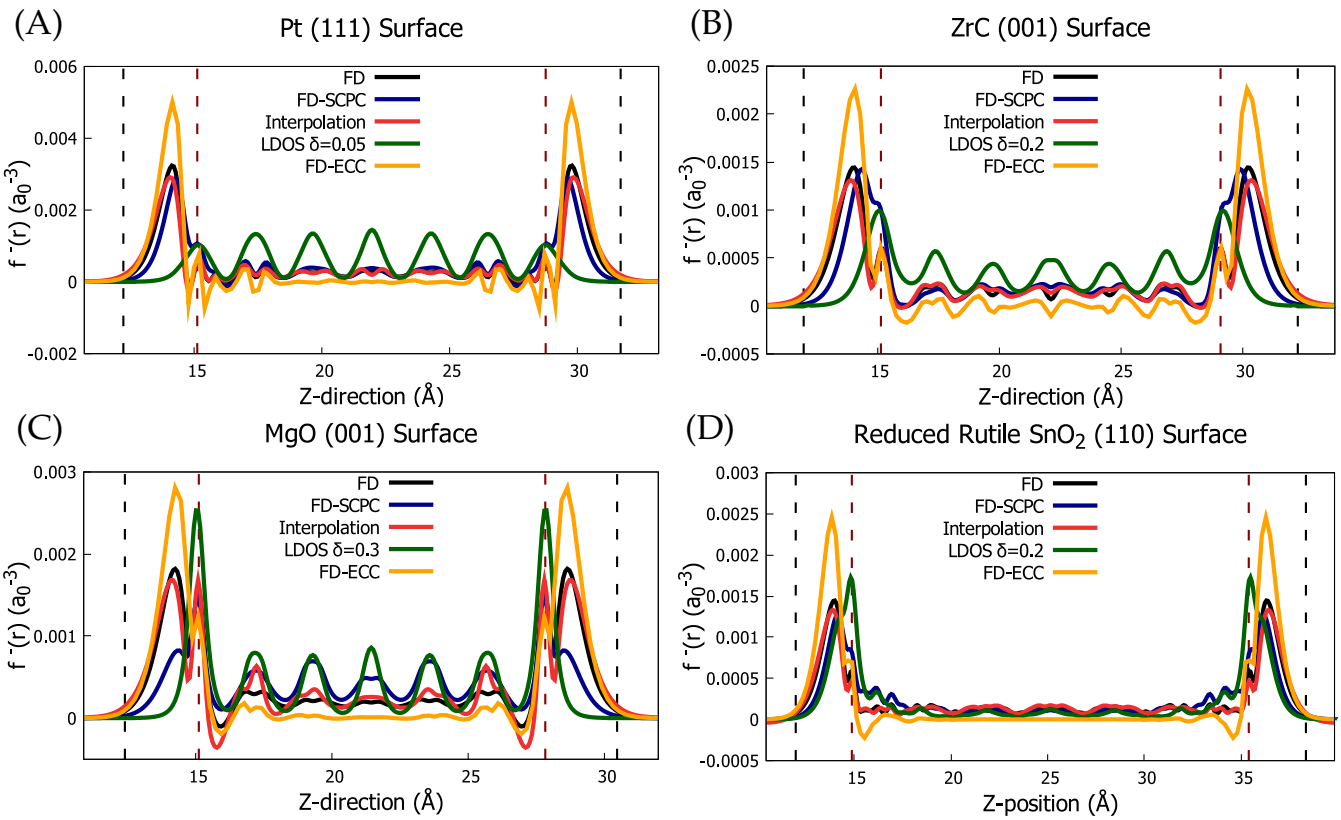

Figure B.1: Planar average of Fukui functions, $f^{-}(\mathbf{r})$, for the surfaces: (A) Pt (111), (B) ZrC (001), (C) MgO (001), and (D) rutile SnO_2 (110). The black dashed lines represent the position where the planar average electron density is equal to $\rho = 10^{-4} a_0^{-3}$ and the red dashed lines represent the position of the surface atoms.

B.2 Nucleophilic Fukui function, $f^+(\mathbf{r})$

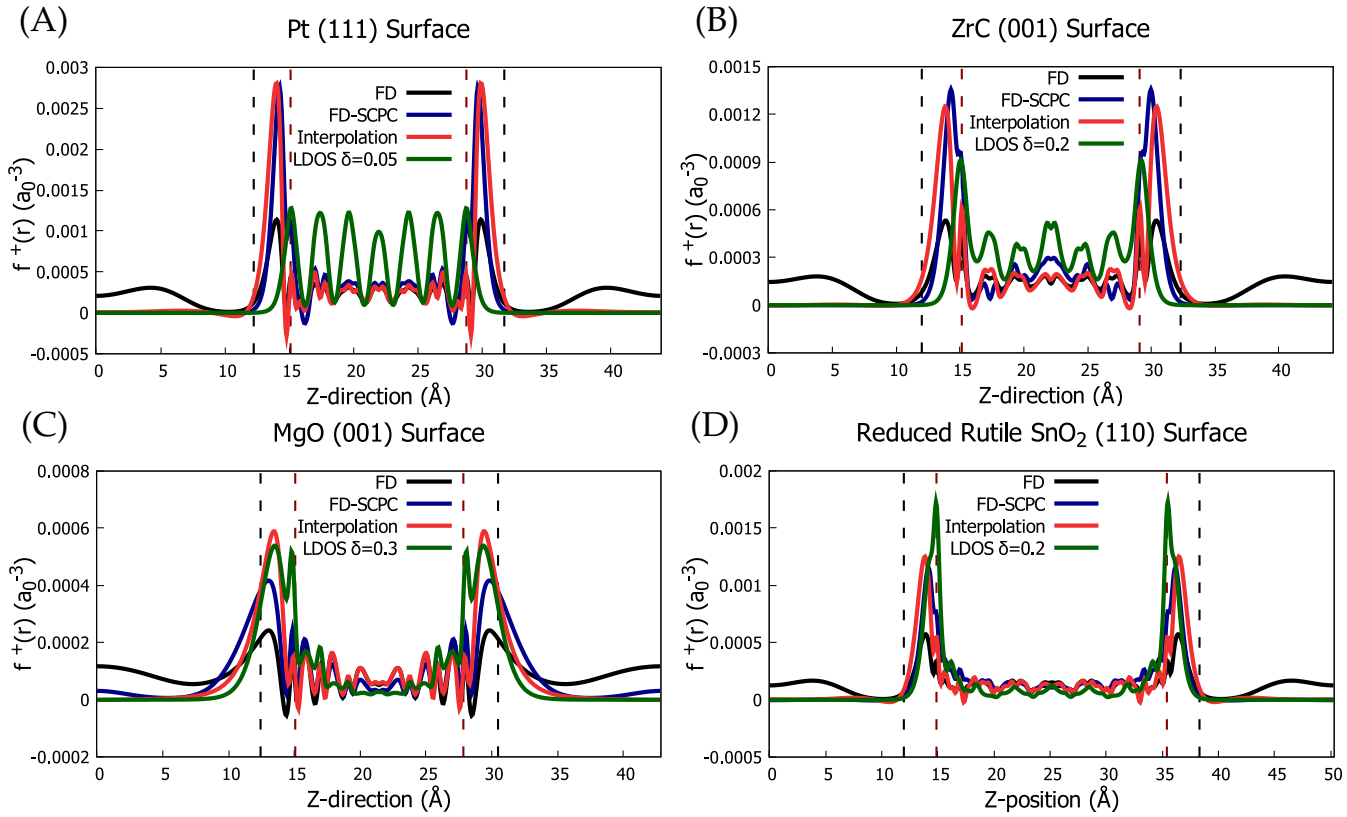

Figure B.2: Planar average of Fukui functions, $f^+(\mathbf{r})$, for the surfaces: (A) Pt (111), (B) ZrC (001), (C) MgO (001), and (D) rutile SnO_2 (110). The black dashed lines represent the position where the planar average electron density is equal to $\rho = 10^{-4} a_0^{-3}$ and the red dashed lines represent the position of the surface atoms.

Appendix C

Additional Fukui Potentials

C.1 Electrophilic Fukui Potential, $v_f^-(\mathbf{r})$

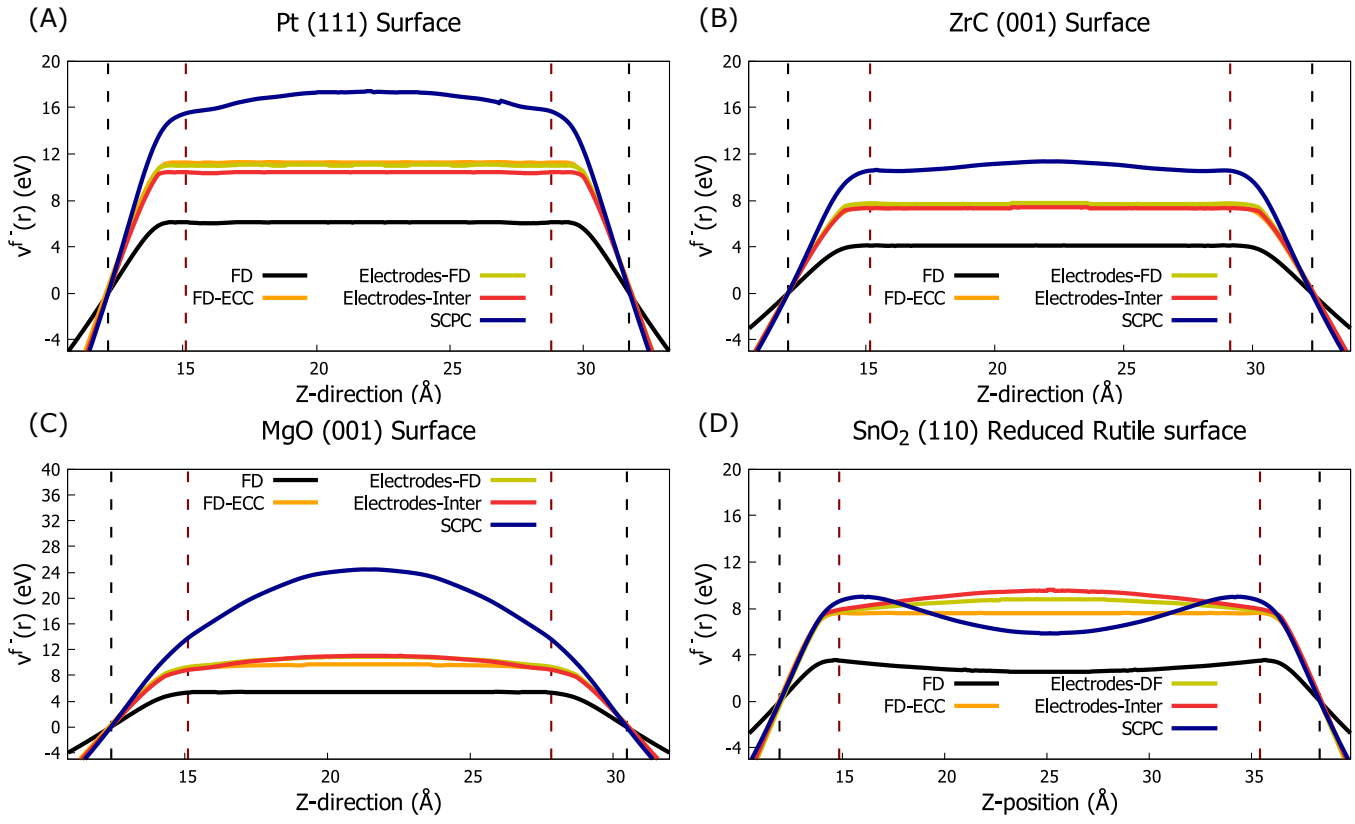

Figure C.1: Planar average of electrophilic Fukui potentials, $v_f^-(\mathbf{r})$, for the surfaces: (A) Pt (111), (B) ZrC (001), (C) MgO (001), and (D) rutile SnO_2 (110). The black dashed lines represent the position where the planar average electron density is equal to $\rho = 10^{-4}\, a_0^{-3}$ and the red dashed lines represent the position of the surface atoms.

C.2 Nucleophilic Fukui Potential, $v_f^+(\mathbf{r})$

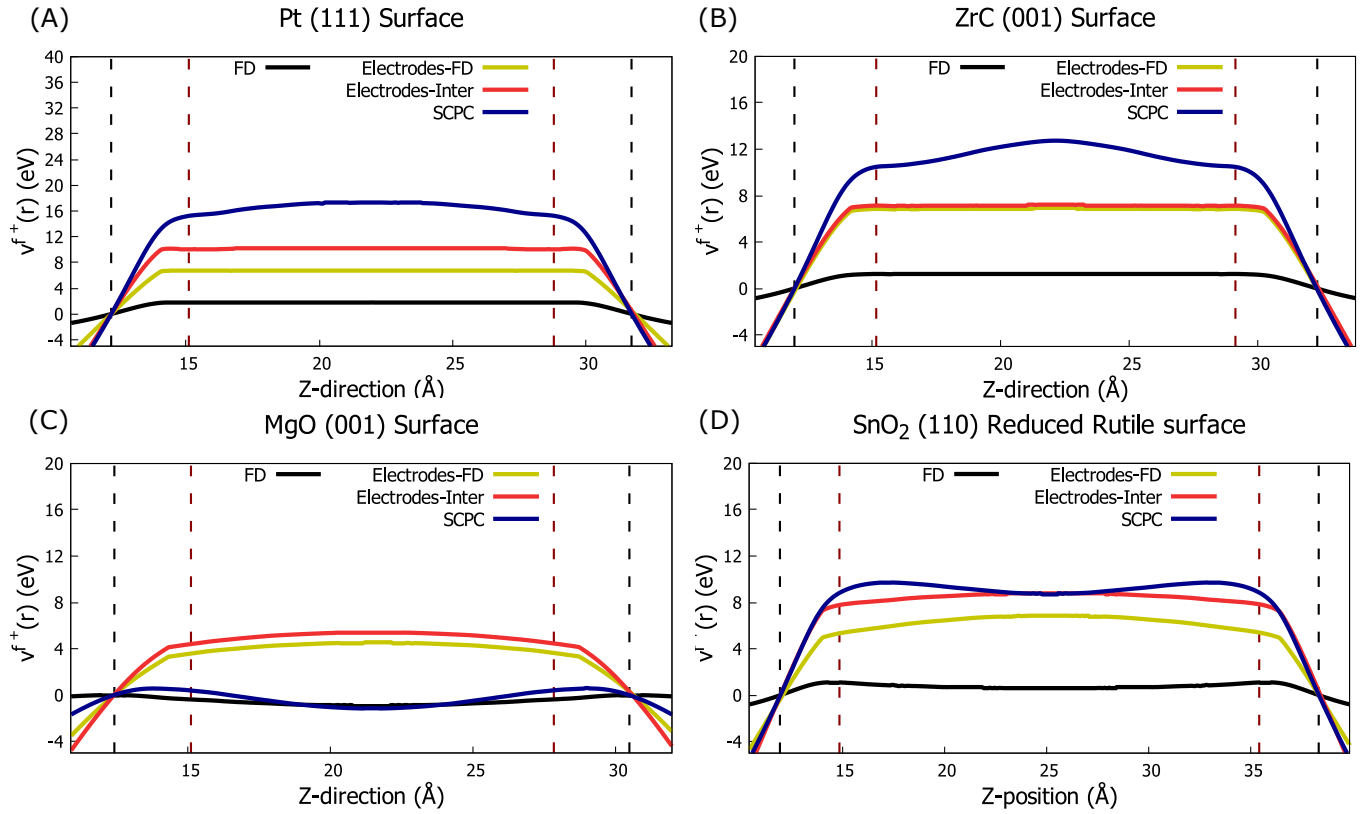

Figure C.2: Planar average of nucleophilic Fukui potentials, $v_f^+(\mathbf{r})$, for the surfaces: (A) Pt (111), (B) ZrC (001), (C) MgO (001), and (D) rutile SnO_2 (110). The black dashed lines represent the position where the planar average electron density is equal to $\rho = 10^{-4}\, a_0^{-3}$ and the red dashed lines represent the position of the surface atoms.

Appendix D

Bader charge analysis

D.1 Bader Charges

- Ti (0001) Surface

Table D.1: Charges at all sites of Ti (0001) surface according to Bader partitioning.

Site	AIM Charge	Site	AIM Charge
Ti1	0.123006	Ti8	-0.028505
Ti2	0.005655	Ti9	-0.028505
Ti3	0.123006	Ti10	-0.097339
Ti4	0.123006	Ti11	-0.028505
Ti5	0.005655	Ti12	-0.028505
Ti6	0.123006	Ti13	-0.097320
Ti7	-0.097339	Ti14	-0.097320

- TiC (001) Surface

Table D.2: Charges at all sites of TiC (001) surface according to Bader partitioning.

Site	AIM Charge	Site	AIM Charge	Site	AIM Charge	Site	AIM Charge
Ti1	1.439252	Ti8	1.428475	C1	-1.457306	C8	-1.452575
Ti2	1.422274	Ti9	1.437220	C2	-1.431081	C9	-1.403785

Site	AIM Charge	Site	AIM Charge	Site	AIM Charge	Site	AIM Charge
Ti3	1.422274	Ti10	1.437220	C3	-1.431081	C10	-1.403781
Ti4	1.439252	Ti11	1.428475	C4	-1.457306	C11	-1.452575
Ti5	1.439252	Ti12	1.428475	C5	-1.431081	C12	-1.452575
Ti6	1.439252	Ti13	1.437220	C6	-1.431081	C13	-1.403769
Ti7	1.428475	Ti14	1.437220	C7	-1.452575	C14	-1.403763

- Anatase TiO_2 (001) Surface

Table D.3: Charges at all sites of TiO_2 (001) anatase surface according to Bader partitioning.

Site	AIM Charge	Site	AIM Charge	Site	AIM Charge
Ti1	2.07086	O1	-1.02763	O7	-1.03308
Ti2	2.0682	O2	-1.03899	O8	-1.02863
Ti3	2.06918	O3	-1.03423	O9	-1.04067
Ti4	2.06262	O4	-1.0076	O10	-1.00307
Ti5	2.04369	O5	-1.04279	O11	-1.03003
Ti6	2.0188	O6	-1.04039	O12	-1.00625

- Rutile TiO_2 (110) Surface

Table D.4: Charges at all sites of TiO_2 (110) rutile surface according to Bader partitioning.

Site	AIM Charge	Site	AIM Charge	Site	AIM Charge	Site	AIM Charge
Ti1	2.059846	Ti12	2.048919	O9	-1.036098	O20	-1.028911
Ti2	2.067652	Ti13	2.046665	O10	-1.037767	O21	-1.015777
Ti3	2.059971	Ti14	2.032251	O11	-1.028911	O22	-1.039956
Ti4	2.065925	O1	-1.020906	O12	-1.015777	O23	-1.038394
Ti5	2.059971	O2	-1.039472	O13	-1.039956	O24	-1.020103
Ti6	2.067652	O3	-1.037458	O14	-1.038394	O25	-1.052384
Ti7	2.069722	O4	-1.037767	O15	-1.020103	O26	-1.048211
Ti8	2.048919	O5	-1.035789	O16	-1.052384	O27	-1.057955
Ti9	2.046665	O6	-1.036098	O17	-1.048211	O28	-0.914613
Ti10	2.032251	O7	-1.022688	O18	-1.057955		
Ti11	2.069722	O8	-1.039472	O19	-0.914639		

- Pt (111) Surface

Table D.5: Charges at all sites of Pt (111) surface surface according to Bader partitioning.

Site	AIM Charge	Site	AIM Charge
Ti1	-0.04804	Ti8	-0.01284
Ti2	0.0101	Ti9	0.0101
Ti3	0.04436	Ti10	0.0101
Ti4	0.0101	Ti11	0.04436
Ti5	0.04436	Ti12	0.04436
Ti6	-0.04804	Ti13	-0.04804
Ti7	-0.01284	Ti14	-0.04804

- ZrC (001) Surface

Table D.6: Charges at all sites of ZrC (001) surface according to Bader partitioning.

Site	AIM Charge	Site	AIM Charge	Site	AIM Charge	Site	AIM Charge
Zr1	1.78493	Zr8	1.80969	C1	-1.83646	C8	-1.81165
Zr2	1.80668	Zr9	1.80916	C2	-1.81076	C9	-1.81165
Zr3	1.80668	Zr10	1.78493	C3	-1.83646	C10	-1.83646
Zr4	1.80916	Zr11	1.80668	C4	-1.75213	C11	-1.81076
Zr5	1.80969	Zr12	1.80668	C5	-1.81165	C12	-1.83646
Zr6	1.80916	Zr13	1.78493	C6	-1.81165	C13	-1.75213
Zr7	1.80916	Zr14	1.78493	C7	-1.75213	C14	-1.75213

- MgO (001) Surface

Table D.7: Charges at all sites of MgO (001) surface surface according to Bader partitioning.

Site	AIM Charge	Site	AIM Charge	Site	AIM Charge	Site	AIM Charge
Mg1	1.64296	Mg8	1.6378	O1	-1.66923	O8	-1.65493
Mg2	1.64335	Mg9	1.64842	O2	-1.61923	O9	-1.64208
Mg3	1.64335	Mg10	1.64842	O3	-1.61923	O10	-1.64208
Mg4	1.64296	Mg11	1.6378	O4	-1.66923	O11	-1.65493
Mg5	1.64296	Mg12	1.6378	O5	-1.61923	O12	-1.65493
Mg6	1.64296	Mg13	1.64842	O6	-1.61923	O13	-1.64208
Mg7	1.6378	Mg14	1.64842	O7	-1.65493	O14	-1.64208

- Reduced Rutile SnO_2 (110) Surface

Table D.8: Charges at all sites of SnO_2 (110) reduced rutile surface according to Bader partitioning.

Site	AIM Charge	Site	AIM Charge	Site	AIM Charge	Site	AIM Charge
Sn1	2.40198	Sn11	2.37376	O7	-1.20078	O17	-1.18731
Sn2	2.34031	Sn12	2.43293	O8	-1.18344	O18	-1.22832
Sn3	2.40198	Sn13	1.46471	O9	-1.20225	O19	-1.19485
Sn4	1.4647	Sn14	2.27083	O10	-1.21536	O20	-1.16646
Sn5	2.35559	O1	-1.20225	O11	-1.188	O21	-1.2356
Sn6	2.35559	O2	-1.18497	O12	-1.1865	O22	-1.22832
Sn7	2.27083	O3	-1.20078	O13	-1.2356	O23	-1.18731
Sn8	2.3588	O4	-1.21719	O14	-1.16808	O24	-1.23426
Sn9	2.3588	O5	-1.1865	O15	-1.19485	O25	-1.21715
Sn10	2.43293	O6	-1.188	O16	-1.23426	O26	-1.21535

Appendix E

Surfaces Structures

In this appendix, we provide the surface structures (in POSCAR format) from our relaxation calculations. Details about the parameters and level of theory used in theses calculations are given in Chapter 4.

E.1 Structures (POSCAR format)

- Ti (0001) Surface

  Ti
  1.00000000000000
  2.9238300323000002 0.0000000000000000 0.0000000000000000
  0.0000000000000000 5.0642223358000003 0.0000000000000000
  0.0000000000000000 0.0000000000000000 43.8761396407999982
  Ti
  14
  Selective dynamics
  Direct
  -0.0000000000000000 0.3333735726520805 0.3930000418216849 T T T
  0.0000000000000000 0.3333333400000029 0.5000000000000000 F F F
  0.0000000000000000 0.3333735726520805 0.6069999581783151 T T T
  0.5000000000000000 0.8333735426520781 0.3930000418216849 T T T

0.5000000000000000	0.8333333100000004	0.5000000000000000	F	F	F
0.5000000000000000	0.8333735426520781	0.6069999581783151	T	T	T
0.0000000000000000	-0.0000053547499946	0.3441944837088804	T	T	T
0.0000000000000000	0.0000000000000000	0.4472904900000003	F	F	F
0.0000000000000000	0.0000000000000000	0.5527095200000005	F	F	F
0.5000000000000000	0.4999946452500055	0.3441944837088804	T	T	T
0.5000000000000000	0.5000000000000000	0.4472904900000003	F	F	F
0.5000000000000000	0.5000000000000000	0.5527095200000005	F	F	F
-0.0000000000000000	-0.0000053547499946	0.6558055162911193	T	T	T
0.5000000000000000	0.4999946452500055	0.6558055162911193	T	T	T

- TiC (001) Surface

TiC
1.00000000000000
4.3832509999999996 0.0000000000000000 0.0000000000000000
0.0000000000000000 4.3832509999999996 0.0000000000000000
0.0000000000000000 0.0000000000000000 43.1497529999999969
Ti C
14 14
Selective dynamics
Direct
0.0000000000000000 0.0000000000000000 0.4492088516999999 F F F
0.0000000000000000 0.5000000000000000 0.5000000000000000 F F F
0.5000000000000000 0.0000000000000000 0.5000000000000000 F F F
0.5000000000000000 0.5000000000000000 0.4492088516999999 F F F
0.0000000000000000 0.0000000000000000 0.5507911481999983 F F F
0.5000000000000000 0.5000000000000000 0.5507911481999983 F F F
-0.0000000000000000 0.5000000000000000 0.6002856372843206 T T T
0.5000000000000000 -0.0000000000000000 0.6002856372843206 T T T
0.0000000000000000 0.0000000000000000 0.6488876704712709 T T T
0.5000000000000000 0.5000000000000000 0.6488876704712709 T T T
0.0000000000000000 0.5000000000000000 0.3997143626156773 T T T
0.5000000000000000 -0.0000000000000000 0.3997143626156773 T T T
0.0000000000000000 0.0000000000000000 0.3511123294287344 T T T
0.5000000000000000 0.5000000000000000 0.3511123294287344 T T T
0.0000000000000000 0.0000000000000000 0.5000000000000000 F F F
0.0000000000000000 0.5000000000000000 0.4492088516999999 F F F
0.5000000000000000 0.0000000000000000 0.4492088516999999 F F F
0.5000000000000000 0.5000000000000000 0.5000000000000000 F F F
0.0000000000000000 0.5000000000000000 0.5507911481999983 F F F

0.5000000000000000	0.0000000000000000	0.5507911481999983	F	F	F
-0.0000000000000000	0.0000000000000000	0.6009261781487875	T	T	T
0.5000000000000000	0.5000000000000000	0.6009261781487875	T	T	T
-0.0000000000000000	0.5000000000000000	0.6514765959633713	T	T	T
0.5000000000000000	0.0000000000000000	0.6514765959633713	T	T	T
-0.0000000000000000	0.0000000000000000	0.3990738217512109	T	T	T
0.5000000000000000	0.5000000000000000	0.3990738217512109	T	T	T
0.0000000000000000	0.5000000000000000	0.3485234039366340	T	T	T
0.5000000000000000	0.0000000000000000	0.3485234039366340	T	T	T

- Anatase TiO_2 (001) Surface

  Ti4 O8

  1.00000000000000

  3.8997984099950789 0.0000000000000000 0.0000000000000000

  0.0000000000000000 3.8997984099950789 0.0000000000000000

  0.0000000000000000 0.0000000000000000 40.0000000000000000

  Ti O

  6 12

  Selective dynamics

  Direct

  0.5000000000000000 0.5004520821715162 0.5299768892345348 T T T

  0.5000000000000000 0.9975525947901642 0.5909213765386289 T T T

  0.0000000000000000 0.0000000000000000 0.4070648750000032 F F F

  0.0000000000000000 0.5000000000000000 0.4690216699999965 F F F

  0.5000000000000000 0.0000000000000000 0.3451081250000030 F F F

  0.0000000000000000 0.0165028272117620 0.6503675967914354 T T T

  0.0000000000000000 0.5006064317361487 0.5194949143839019 T T T

  0.5000000000000000 0.5016058097969492 0.5803864036800952 T T T

  0.5000000000000000 0.0005522675476766 0.5404335170566729 T T T

  -0.0000000000000000 0.0176301103727609 0.6009375133198769 T T T

  0.5000000000000000 0.9719899741409621 0.6410227523805988 T T T

  0.0000000000000000 0.0000000000000000 0.4584028020000019 F F F

  0.0000000000000000 0.5000000000000000 0.4176837429999978 F F F

  0.5000000000000000 0.5000000000000000 0.4796405379999982 F F F

  0.5000000000000000 0.5000000000000000 0.3344891249999975 F F F

  0.0000000000000000 0.4665118565834872 0.6637765970705889 T T T

  0.0000000000000000 0.0000000000000000 0.3557268750000020 F F F

  0.5000000000000000 0.0000000000000000 0.3964461249999971 F F F

- Rutile TiO_2 (110) Surface

Ti2 O4
1.00000000000000
3.0479900836999998 0.0000000000000000 0.0000000000000000
0.0000000000000000 6.7003068924000004 0.0000000000000000
0.0000000000000000 0.0000000000000000 52.7231406800000002
Ti O
14 28
Selective dynamics
Direct
0.0000000000000000 0.0000000000000000 0.5000000000000000 F F F
0.0000000000000000 0.5000000000000000 0.4364576270000029 F F F
0.5000000000000000 0.0000000000000000 0.4364576270000029 F F F
0.5000000000000000 0.5000000000000000 0.5000000000000000 F F F
0.5000000000000000 0.0000000000000000 0.5635423720000006 F F F
0.0000000000000000 0.5000000000000000 0.5635423720000006 F F F
-0.0000000000000000 -0.0000000000000000 0.6255597684685229 T T T
0.5000000000000000 0.5000000000000000 0.6279400784638057 T T T
0.5000000000000000 -0.0000000000000000 0.6871002113867121 T T T
0.0000000000000000 0.5000000000000000 0.6922800290969375 T T T
-0.0000000000000000 -0.0000000000000000 0.3744402305314736 T T T
0.5000000000000000 0.5000000000000000 0.3720599205361907 T T T
0.5000000000000000 -0.0000000000000000 0.3128997876132843 T T T
-0.0000000000000000 0.5000000000000000 0.3077199699030591 T T T
0.5000000000000000 0.0000000000000000 0.5248677789999974 F F F
0.5000000000000000 0.5000000000000000 0.4613254060000003 F F F
0.0000000000000000 0.3043212890000007 0.5000000000000000 F F F
0.0000000000000000 0.8043212890000007 0.4364576270000029 F F F

0.0000000000000000	0.6956787109999993	0.5000000000000000	F	F	F
0.0000000000000000	0.1956787109999993	0.4364576270000029	F	F	F
0.5000000000000000	0.0000000000000000	0.4751322239999993	F	F	F
0.5000000000000000	0.5000000000000000	0.5386745930000032	F	F	F
0.0000000000000000	0.1956787109999993	0.5635423720000006	F	F	F
0.0000000000000000	0.8043212890000007	0.5635423720000006	F	F	F
0.5000000000000000	0.5000000000000000	0.5879879075030647	T	T	T
0.5000000000000000	-0.0000000000000000	0.6021665810665227	T	T	T
-0.0000000000000000	0.3015875812445427	0.6265970448948432	T	T	T
-0.0000000000000000	0.6984124187554573	0.6265970448948432	T	T	T
0.5000000000000000	-0.0000000000000000	0.6511118683604032	T	T	T
0.5000000000000000	0.5000000000000000	0.6647423093602356	T	T	T
0.0000000000000000	0.1858320429929593	0.6923813143563453	T	T	T
0.0000000000000000	0.8141679570070407	0.6923813143563453	T	T	T
0.5000000000000000	0.5000000000000000	0.7135304569653970	T	T	T
0.5000000000000000	0.5000000000000000	0.4120120914969311	T	T	T
0.5000000000000000	-0.0000000000000000	0.3978334219334740	T	T	T
0.0000000000000000	0.3015875812445427	0.3734029541051530	T	T	T
0.0000000000000000	0.6984124187554573	0.3734029541051530	T	T	T
0.5000000000000000	-0.0000000000000000	0.3488881346396006	T	T	T
0.5000000000000000	0.5000000000000000	0.3352576896397681	T	T	T
0.0000000000000000	0.1858320429929593	0.3076186846436513	T	T	T
-0.0000000000000000	0.8141679570070407	0.3076186846436513	T	T	T
0.5000000000000000	0.5000000000000000	0.2864695420346065	T	T	T

- Pt (111) Surface

Pt
1.00000000000000
4.9212403296999998 0.0000000000000000 0.0000000000000000
0.0000000000000000 2.8412795066999998 0.0000000000000000
0.0000000000000000 0.0000000000000000 43.9193599999999975
Pt
14
Selective dynamics
Direct
-0.0002189827899401 -0.0000000000000000 0.3444513368835281 T T T
0.6666666870000029 0.0000000000000000 0.4471783218000027 F F F
0.3332560391848671 0.0000000000000000 0.3962107627903403 T T T
0.1666666719999981 0.5000000000000000 0.4471783218000027 F F F
0.8332560091848646 0.5000000000000000 0.3962107627903403 T T T
0.4997810172100598 0.5000000000000000 0.3444513368835281 T T T
0.0000000000000000 0.0000000000000000 0.5000000000000000 F F F
0.5000000000000000 0.5000000000000000 0.5000000000000000 F F F
0.3333333429999996 0.0000000000000000 0.5528216828000012 F F F
0.8333333129999971 0.5000000000000000 0.5528216828000012 F F F
0.6667439908151354 -0.0000000000000000 0.6037892418096565 T T T
0.1667439758151306 0.5000000000000000 0.6037892418096565 T T T
0.0002189827899401 0.0000000000000000 0.6555486630164702 T T T
0.5002189827899400 0.5000000000000000 0.6555486630164702 T T T

- ZrC (001) Surface

ZrC
1.00000000000000
4.7548799515000004 0.0000000000000000 0.0000000000000000
0.0000000000000000 4.7548799515000004 0.0000000000000000
0.0000000000000000 0.0000000000000000 44.2646398544000022
Zr C
14 14
Selective dynamics
Direct
-0.0000000000000000 -0.0000000000000000 0.3424109990540343 T T T
0.0000000000000000 0.0000000000000000 0.4462903200000028 F F F
0.0000000000000000 0.0000000000000000 0.5537096899999980 F F F
-0.0000000000000000 0.5000000000000000 0.3938179791547299 T T T
0.0000000000000000 0.5000000000000000 0.5000000000000000 F F F
-0.0000000000000000 0.5000000000000000 0.6061820208452702 T T T
0.5000000000000000 0.0000000000000000 0.3938179791547299 T T T
0.5000000000000000 0.0000000000000000 0.5000000000000000 F F F
0.5000000000000000 0.0000000000000000 0.6061820208452702 T T T
0.5000000000000000 0.5000000000000000 0.3424109990540343 T T T
0.5000000000000000 0.5000000000000000 0.4462903200000028 F F F
0.5000000000000000 0.5000000000000000 0.5537096899999980 F F F
0.0000000000000000 -0.0000000000000000 0.6575890009459658 T T T
0.5000000000000000 0.5000000000000000 0.6575890009459658 T T T
0.0000000000000000 0.0000000000000000 0.3929143605743600 T T T
0.0000000000000000 0.0000000000000000 0.5000000000000000 F F F
-0.0000000000000000 0.0000000000000000 0.6070856394256401 T T T
-0.0000000000000000 0.5000000000000000 0.3406949585841665 T T T
0.0000000000000000 0.5000000000000000 0.4462903200000028 F F F

0.0000000000000000	0.5000000000000000	0.5537096899999980	F	F	F
0.5000000000000000	0.0000000000000000	0.3406949585841665	T	T	T
0.5000000000000000	0.0000000000000000	0.4462903200000028	F	F	F
0.5000000000000000	0.0000000000000000	0.5537096899999980	F	F	F
0.5000000000000000	0.5000000000000000	0.3929143605743600	T	T	T
0.5000000000000000	0.5000000000000000	0.5000000000000000	F	F	F
0.5000000000000000	0.5000000000000000	0.6070856394256401	T	T	T
0.0000000000000000	0.5000000000000000	0.6593050414158336	T	T	T
0.5000000000000000	0.0000000000000000	0.6593050414158336	T	T	T

- MgO (001) Surface

MgO
1.00000000000000
4.2889999999999997 0.0000000000000000 0.0000000000000000
0.0000000000000000 4.2889999999999997 0.0000000000000000
0.0000000000000000 0.0000000000000000 42.8699700000000021
Mg O
14 14
Selective dynamics
Direct
0.0000000000000000 0.0000000000000000 0.4499650921000011 F F F
0.0000000000000000 0.5000000000000000 0.5000000000000000 F F F
0.5000000000000000 0.0000000000000000 0.5000000000000000 F F F
0.5000000000000000 0.5000000000000000 0.4499650921000011 F F F
0.0000000000000000 0.0000000000000000 0.5500349077999971 F F F
0.5000000000000000 0.5000000000000000 0.5500349077999971 F F F
-0.0000000000000000 0.5000000000000000 0.5994123546198602 T T T
0.5000000000000000 0.0000000000000000 0.5994123546198602 T T T
0.0000000000000000 -0.0000000000000000 0.6479575645069193 T T T
0.5000000000000000 0.5000000000000000 0.6479575645069193 T T T
0.5000000000000000 0.0000000000000000 0.4005876452801451 T T T
0.0000000000000000 0.5000000000000000 0.4005876452801451 T T T
-0.0000000000000000 -0.0000000000000000 0.3520424353930863 T T T
0.5000000000000000 0.5000000000000000 0.3520424353930863 T T T
0.0000000000000000 0.0000000000000000 0.5000000000000000 F F F
0.0000000000000000 0.5000000000000000 0.4499650921000011 F F F
0.5000000000000000 0.0000000000000000 0.4499650921000011 F F F
0.5000000000000000 0.5000000000000000 0.5000000000000000 F F F
0.5000000000000000 0.0000000000000000 0.5500349077999971 F F F

0.0000000000000000	0.5000000000000000	0.5500349077999971	F	F	F
0.0000000000000000	-0.0000000000000000	0.5992117811849870	T	T	T
0.5000000000000000	0.5000000000000000	0.5992117811849870	T	T	T
0.5000000000000000	0.0000000000000000	0.6491437093919559	T	T	T
-0.0000000000000000	0.5000000000000000	0.6491437093919559	T	T	T
0.0000000000000000	-0.0000000000000000	0.4007882187150182	T	T	T
0.5000000000000000	0.5000000000000000	0.4007882187150182	T	T	T
0.5000000000000000	-0.0000000000000000	0.3508562905080494	T	T	T
0.0000000000000000	0.5000000000000000	0.3508562905080494	T	T	T

- Reduced Rutile SnO_2 (110) Surface

SnO2
1.00000000000000
3.2178599833999999 0.0000000000000000 0.0000000000000000
0.0000000000000000 6.7661209105999998 0.0000000000000000
0.0000000000000000 0.0000000000000000 50.2983627318999993
Sn O
14 26
Selective dynamics
Direct
0.5000000000000000 0.0000000000000000 0.3674659719575288 T T T
0.5000000000000000 0.0000000000000000 0.5000000000000000 F F F
0.5000000000000000 0.0000000000000000 0.6325340280424711 T T T
0.5000000000000000 0.5000000000000000 0.2965132070378025 T T T
0.5000000000000000 0.5000000000000000 0.4327401500000008 F F F
0.5000000000000000 0.5000000000000000 0.5672598600000001 F F F
0.0000000000000000 0.0000000000000000 0.3020936073505889 T T T
0.0000000000000000 0.0000000000000000 0.4327401500000008 F F F
0.0000000000000000 0.0000000000000000 0.5672598600000001 F F F
-0.0000000000000000 0.5000000000000000 0.3654357038583927 T T T
0.0000000000000000 0.5000000000000000 0.5000000000000000 F F F
-0.0000000000000000 0.5000000000000000 0.6345642961416075 T T T
0.5000000000000000 0.5000000000000000 0.7034867929621972 T T T
-0.0000000000000000 0.0000000000000000 0.6979063926494110 T T T
0.5000000000000000 0.3047999312858130 0.3656337795335747 T T T
0.5000000000000000 0.3059722799999989 0.5000000000000000 F F F
0.5000000000000000 0.3047999312858130 0.6343662204664254 T T T
0.5000000000000000 0.8185334601385078 0.2958458144685098 T T T

0.5000000000000000	0.8059722799999989	0.4327401500000008	F	F	F
0.5000000000000000	0.8059722799999989	0.5672598600000001	F	F	F
0.5000000000000000	0.6952000687141872	0.3656337795335747	T	T	T
0.5000000000000000	0.6940277200000011	0.5000000000000000	F	F	F
0.5000000000000000	0.6952000687141872	0.6343662204664254	T	T	T
0.5000000000000000	0.1814665398614917	0.2958458144685098	T	T	T
0.5000000000000000	0.1940277200000011	0.4327401500000008	F	F	F
0.5000000000000000	0.1940277200000011	0.5672598600000001	F	F	F
-0.0000000000000000	0.0000000000000000	0.3414115566427885	T	T	T
0.0000000000000000	0.0000000000000000	0.4738994499999976	F	F	F
-0.0000000000000000	0.0000000000000000	0.6077582772273080	T	T	T
-0.0000000000000000	0.5000000000000000	0.4065599621072626	T	T	T
0.0000000000000000	0.5000000000000000	0.5411592999999968	F	F	F
0.0000000000000000	0.5000000000000000	0.6758400877178491	T	T	T
-0.0000000000000000	0.0000000000000000	0.3922417327726859	T	T	T
0.0000000000000000	0.0000000000000000	0.5261005600000033	F	F	F
-0.0000000000000000	0.0000000000000000	0.6585884533572122	T	T	T
-0.0000000000000000	0.5000000000000000	0.3241599222821449	T	T	T
0.0000000000000000	0.5000000000000000	0.4588407000000032	F	F	F
-0.0000000000000000	0.5000000000000000	0.5934400378927374	T	T	T
0.5000000000000000	0.8185334601385078	0.7041541855314906	T	T	T
0.5000000000000000	0.1814665398614917	0.7041541855314906	T	T	T

Bibliography

(1) Perdew, J. P.; Parr, R. G.; Levy, M.; Balduz Jose L., J. *Phys. Rev. Lett.* **1982**, *49*, 1691–1694.

(2) Yang, W.; Zhang, Y.; Ayers, P. W. *Phys. Rev. Lett.* **2000**, *84*, 5172–5175.

(3) Cohen, M. H.; Wasserman, A. *Isr. J. Chem.* **2003**, *43*, 219–227.

(4) Cohen, M. H.; Wasserman, A. *J. Phys. Chem. A* **2007**, *111*, PMID: 17388293, 2229–2242.

(5) Cárdenas, C.; Chamorro, E.; Galván, M.; Fuentealba, P. *Inter. J. Quantum Chem.* **2007**, *107*, 807–815.

(6) Ayers, P. W. *J. Math. Chem.* **2008**, *43*, 285–303.

(7) Cohen, A. J.; Mori-Sánchez, P.; Yang, W. *Science* **2008**, *321*, 792–794.

(8) Chermette, H. *J. Comput. Chem.* **1999**, *20*, 129–154.

(9) Geerlings, P.; De Proft, F.; Langenaeker, W. *Chem. Rev.* **2003**, *103*, 1793–1874.

(10) Liu, S.-B. *Acta Phys. Chim. Sin.* **2009**, *25*, 590–600.

(11) Fuentealba, P.; Cárdenas, C. In *Chemical Modelling: Volume 11*; The Royal Society of Chemistry: 2014, pp 151–171.

(12) Parr, R. G.; Donnelly, R. A.; Levy, M.; Palke, W. E. *J Chem. Phys.* **1978**, *68*, 3801–3807.

(13) Pearson, R. G. *Journal of the American Chemical society* **1963**, *85*, 3533–3539.

(14) Chattaraj, P. K.; Lee, H.; Parr, R. G. *J. Am. Chem. Soc.* **1991**, *113*, 1855–1856.

(15) Ayers, P. W. *Faraday Discuss.* **2007**, *135*, 161–190.

(16) Sanderson, R. *J. Am. Chem. Soc.* **1952**, *74*, 272–274.

(17) Sanderson, R. *Science* **1955**, *121*, 207–208.

(18) Pearson, R. G. *J. Chem. Educ.* **1987**, *64*, 561.

(19) Pearson, R. G. *Acc. Chem. Res.* **1993**, *26*, 250–255.

(20) Parr, R. G.; Chattaraj, P. K. *J. Am. Chem. Soc.* **1991**, *113*, 1854–1855.

(21) Parr, R. G.; Yang, W. *J. Am. Chem. Soc.* **1984**, *106*, 4049–4050.

(22) Yang, W.; Parr, R. G.; Pucci, R. *J. Chem. Phys.* **1984**, *81*, 2862–2863.

(23) Fuentealba, P. *J. Chem. Phys.* **1995**, *103*, 6571–6575.

(24) Contreras, R. R.; Fuentealba, P.; Galván, M.; Pérez, P. *Chem. Phys. Lett.* **1999**, *304*, 405–413.

(25) Ayers, P. W.; Levy, M. *Theor. Chem. Acc.* **2000**, *103*, 353–360.

(26) Ayers, P. W.; Parr, R. G. *J. Am. Chem. Soc.* **2000**, *122*, 2010–2018.

(27) Fukui, K.; Yonezawa, T.; Shingu, H. *J. Chem. Phys.* **1952**, *20*, 722–725.

(28) Fukui, K.; Yonezawa, T.; Nagata, C.; Shingu, H. *J. Chem. Phys.* **1954**, *22*, 1433–1442.

(29) Fukui, K. In *Orientation and Stereoselection*, Springer Berlin Heidelberg: Berlin, Heidelberg, 1970, pp 1–85.

(30) Fukui, K. *science* **1982**, *218*, 747–754.

(31) Fuentealba, P.; Cárdenas, C. In *Chemical Reactivity*, Kaya, S., von Szentpály, L., Serdaroğlu, G., Guo, L., Eds.; Elsevier: 2023, pp 421–432.

(32) Fuentealba, P.; Cardenas, C.; Pino-Rios, R.; Tiznado, W. *Applications of topological methods in molecular chemistry* **2016**, 227–241.

(33) Cárdenas, C.; Tiznado, W.; Ayers, P. W.; Fuentealba, P. *J. Phys. Chem. A* **2011**, *115*, 2325–2331.

(34) Tiznado, W.; Chamorro, E.; Contreras, R.; Fuentealba, P. *J. Phys. Chem. A* **2005**, *109*, 3220–3224.

(35) Allison, T. C.; Tong, Y. J. *Electrochim. Acta* **2013**, *101*, 334–340.

(36) Wang, B.; Rong, C.; Chattaraj, P. K.; Liu, S. *Theor. Chem. Acc.* **2019**, *138*, 1–9.

(37) Cerón, M. L.; Gomez, T.; Calatayud, M.; Cárdenas, C. *J. Phys. Chem. A* **2020**, *124*, 2826–2833.

(38) Cárdenas, C.; Echeverry, A.; Novoa, T.; Robles-Navarro, A.; Gomez, T.; Fuentealba, P. In *Conceptual Density Functional Theory*; John Wiley I& Sons, Ltd: 2022; Chapter 27, pp 555–571.

(39) Payne, M. C.; Teter, M. P.; Allan, D. C.; Arias, T.; Joannopoulos, a. J. *Rev. Mod. Phys.* **1992**, *64*, 1045.

(40) Pickett, W. E. *Comput. Phys. Rep.* **1989**, *9*, 115–197.

(41) Makov, G.; Payne, M. C. *Phys. Rev. B* **1995**, *51*, 4014.

(42) Frigo, M.; Johnson, S. G. *Proc. IEEE* **2005**, *93*, 216–231.

(43) Heideman, M. T.; Johnson, D. H.; Burrus, C. S. *Arch. Hist. Exact Sci.* **1985**, 265–277.

(44) Jara, C.; Rauch, T.; Botti, S.; Marques, M. A.; Norambuena, A.; Coto, R.; Castellanos-Águila, J.; Maze, J. R.; Munoz, F. *J. Phys. Chem. A* **2021**, *125*, 1325–1335.

(45) Rauch, T.; Munoz, F.; Marques, M. A.; Botti, S. *Phys. Rev. B* **2021**, *104*, 064105.

(46) Hernández-Vázquez, E. E.; López-Moreno, S.; Munoz, F.; Ricardo-Chavez, J. L.; Morán-López, J. L. *RSC adv.* **2021**, *11*, 31073–31083.

(47) Matz, O.; Calatayud, M. *ACS omega* **2018**, *3*, 16063–16073.

(48) Islam, M. M.; Calatayud, M.; Pacchioni, G. *J. Phys. Chem. C* **2011**, *115*, 6809–6814.

(49) Jarvis, M.; White, I.; Godby, R.; Payne, M. C. *Phys. Rev. B* **1997**, *56*, 14972.

(50) Durrant, T. R.; Murphy, S. T.; Watkins, M. B.; Shluger, A. L. *The Journal of Chemical Physics* **2018**, *149*, 024103.

(51) Leslie, M.; Gillan, N. *J. Phys. C: Solid State Phys.* **1985**, *18*, 973.

(52) Castro, A.; Rubio, A.; Stott, M. *Can. J. Phys.* **2003**, *81*, 1151–1164.

(53) Rozzi, C. A.; Varsano, D.; Marini, A.; Gross, E. K.; Rubio, A. *Phys. Rev. B* **2006**, *73*, 205119.

(54) Krishnaswamy, K.; Dreyer, C.; Janotti, A.; Van de Walle, C. G. *Phys. Rev. B* **2015**, *92*, 085420.

(55) Simões, A. *Physics in Perspective* **2002**, *4*, 253–266.

(56) Born, M.; Oppenheimer, R. *Ann. Phys.* **1927**, *389*, 457–484.

(57) Szabo, A.; Ostlund, N. S., *Modern quantum chemistry: introduction to advanced electronic structure theory*; Courier Corporation: 2012.

(58) Mayer, I., *Simple theorems, proofs, and derivations in quantum chemistry*; Springer Science & Business Media: 2013.

(59) Shavitt, I.; Bartlett, R. J., *Many-body methods in chemistry and physics: MBPT and coupled-cluster theory*; Cambridge university press: 2009.

(60) Helgaker, T.; Jorgensen, P.; Olsen, J., *Molecular electronic-structure theory*; John Wiley & Sons: 2013.

(61) Jørgensen, P., *Second quantization-based methods in quantum chemistry*; Elsevier: 2012.

(62) Hohenberg, P.; Kohn, W. *Phys. Rev.* **1964**, *136*, B864.

(63) Levy, M. *Proc. Natl. Acad. Sci* **1979**, *76*, 6062–6065.

(64) Gilbert, T. L. *Phys. Rev. B* **1975**, *12*, 2111.

(65) Dow, J.; Bassani, F.; Fumi, F.; Tosi, M. *Proceedings of the International School of PhysicsEnrico Fermi', Course* **1985**, *89*, 465.

(66) Vignale, G.; Rasolt, M. *Phys. Rev. Lett.* **1987**, *59*, 2360.

(67) Vignale, G.; Rasolt, M. *Phys. Rev. B* **1988**, *37*, 10685.

(68) Kohn, W.; Sham, L. J. *Phys. Rev.* **1965**, *140*, A1133–A1138.

(69) Sahni, V.; Levy, M. *Phys. Rev. B* **1986**, *33*, 3869–3872.

(70) Dirac, P. A. M. *Mathematical Proceedings of the Cambridge Philosophical Society* **1930**, *26*, 376–385.

(71) Wigner, E. *Trans. Faraday Soc.* **1938**, *34*, 678–685.

(72) Vosko, S. H.; Wilk, L.; Nusair, M. *Can. J. Phys.* **1980**, *58*, 1200–1211.

(73) Perdew, J. P.; Schmidt, K. *AIP Conference Proceedings* **2001**, *577*, 1–20.

(74) Mardirossian, N.; Head-Gordon, M. *Molecular Physics* **2017**, *115*, 2315–2372.

(75) "The tragic story of Hans Hellmann" is available at https://pubs.aip.org/physicstoday/.

(76) Hellmann, H. *J. Chem. Phys.* **1935**, *3*, 61–61.

(77) Hellmann, H. *Acta Fizicochem. USSR* **1935**, *913*.

(78) Hellmann, H. *Acta Fizicochem. USSR* **1936**, *225*.

(79) Hellmann, H.; Kassatotschkin, W. *Acta Fizicochem. USSR* **1936**, *23*.

(80) Hamann, D. R.; Schlüter, M.; Chiang, C. *Phys. Rev. Lett.* **1979**, *43*, 1494–1497.

(81) CAS Database is available at https://www.cas.org/.

(82) Anderson, J. S.; Melin, J.; Ayers, P. W. *J. Chem. Theory Comput.* **2007**, *3*, 358–374.

(83) Melin, J.; Ayers, P. W.; Ortiz, J. *J. Chem. Sci.* **2005**, *117*, 387–400.

(84) Geerlings, P.; Fias, S.; Boisdenghien, Z.; De Proft, F. *Chem. Soc. Rev.* **2014**, *43*, 4989–5008.

(85) Chattaraj, P. K., *Chemical reactivity theory: a density functional view*; CRC press: 2009.

(86) Iczkowski, R. P.; Margrave, J. L. *Journal of the American Chemical Society* **1961**, *83*, 3547–3551.

(87) Allen, L. C. *Accounts of Chemical Research* **1990**, *23*, 175–176.

(88) Politzer, P.; Murray, J. S. *J. Mol. Model.* **2018**, *24*, 1–8.

(89) Cohen, M. H.; Ganduglia-Pirovano, M. V.; Kudrnovský, J. *J. Chem. Phys.* **1994**, *101*, 8988–8997.

(90) Cárdenas, C.; De Proft, F.; Chamorro, E.; Fuentealba, P.; Geerlings, P. *J. Chem. Phys.* **2008**, *128*, 034708.

(91) Bryenton, K. R.; Adeleke, A. A.; Dale, S. G.; Johnson, E. R. *WIREs Comput Mol Sci.* **2023**, *13*, e1631.

(92) Ayers, P. W.; Anderson, J. S.; Bartolotti, L. J. *Int. J. Quantum Chem.* **2005**, *101*, 520–534.

(93) Marques, M. A.; Castro, A.; Bertsch, G. F.; Rubio, A. *Comput. Phys. Commun.* **2003**, *151*, 60–78.

(94) Castro, A.; Appel, H.; Oliveira, M.; Rozzi, C. A.; Andrade, X.; Lorenzen, F.; Marques, M. A. L.; Gross, E. K. U.; Rubio, A. *Phys. Stat. Sol. B* **2006**, *243*, 2465–2488.

(95) Andrade, X. et al. *Phys. Chem. Chem. Phys.* **2015**, *17*, 31371–31396.

(96) Tancogne-Dejean, N. et al. *J. Chem. Phys.* **2020**, *152*, 124119.

(97) Da Silva, M. C.; Lorke, M.; Aradi, B.; Tabriz, M. F.; Frauenheim, T.; Rubio, A.; Rocca, D.; Deák, P. *Phys. Rev. Lett.* **2021**, *126*, 076401.

(98) All information about the patch is available at https://github.com/aradi/SCPC-Method.

(99) Lozovoi, A. Y.; Alavi, A.; Kohanoff, J.; Lynden-Bell, R. M. *J. Chem. Phys.* **2001**, *115*, 1661–1669.

(100) Komsa, H.-P.; Pasquarello, A. *Phys. Rev. Lett.* **2013**, *110*, 095505.

(101) Kresse, G.; Hafner, J. *Phys. Rev. B* **1993**, *47*, 558.

(102) Kresse, G.; Furthmüller, J. *Comput. Mater. Sci.* **1996**, *6*, 15–50.

(103) Kresse, G.; Furthmüller, J. *Phys. Rev. B* **1996**, *54*, 11169.

(104) Kresse, G.; Hafner, J. *Phys. Rev. B* **1994**, *49*, 14251–14269.

(105) Blöchl, P. E. *Phys. Rev. B* **1994**, *50*, 17953.

(106) Kresse, G.; Joubert, D. *Phys. Rev. B* **1999**, *59*, 1758.

(107) Perdew, J. P.; Burke, K.; Ernzerhof, M. *Phys. Rev. Lett.* **1996**, *77*, 3865.

(108) Monkhorst, H. J.; Pack, J. D. *Phys. Rev. B* **1976**, *13*, 5188.

(109) Dudarev, S. L.; Botton, G. A.; Savrasov, S. Y.; Humphreys, C.; Sutton, A. P. *Phys. Rev. B* **1998**, *57*, 1505.

(110) Wei, B.; Tielens, F.; Calatayud, M. *Nanomaterials* **2019**, *9*, 1199.

(111) Sopiha, K. V.; Malyi, O. I.; Persson, C.; Wu, P. *ACS Applied Materials & Interfaces* **2021**, *13*, PMID: 34251174, 33664–33676.

(112) Sopiha, K. V.; Malyi, O. I.; Persson, C.; Wu, P. *ACS Applied Materials & Interfaces* **2021**, *13*, 33664–33676.

(113) Hamann, D. *Phys. Rev. B* **2013**, *88*, 085117.

(114) ONCVPSP are available at http://www.pseudo-dojo.org.

(115) Tancogne-Dejean, N.; Oliveira, M. J.; Rubio, A. *Phys. Rev. B* **2017**, *96*, 245133.

(116) Wood, R. M. *Proc. Phys. Soc.* **1962**, *80*, 783.

(117) Zhou, Y.; Sun, Z. *Materials Research Innovations* **2000**, *3*, 286–291.

(118) Kang, W.; Hybertsen, M. S. *Phys. Rev. B* **2010**, *82*, 085203.

(119) Swanson, H. E., *Standard X-ray diffraction powder patterns*; US Department of Commerce, National Bureau of Standards: 1953; Vol. 25.

(120) Mallett, G. R.; Newkirk, J. B.; Henke, B. L., *Advances in X-ray Analysis: Held August 6-8, 1969. Proceedings of the Eighteenth Annual Conference on Applications of X-Ray Analysis*; Plenum Press: 1970.

(121) Calatayud, M.; Ruppert, A. M.; Weckhuysen, B. M. *Chem. Eur. J.* **2009**, *15*, 10864–10870.

(122) Batzill, M.; Diebold, U. *Prog. Surf. Sci.* **2005**, *79*, 47–154.

(123) Fuentealba, P.; Florez, E.; Tiznado, W. *J. Chem. Theory Comput* **2010**, *6*, PMID: 26615684, 1470–1478.

(124) Fuentealba, P.; Cardenas, C.; Pino-Rios, R.; Tiznado, W. In *Applications of Topological Methods in Molecular Chemistry*, Chauvin, R., Lepetit, C., Silvi, B., Alikhani, E., Eds.; Springer International Publishing: Cham, 2016, pp 227–241.

(125) Tang, W.; Sanville, E.; Henkelman, G. *J. Phys.: Condens. Matter* **2009**, *21*, 084204.

(126) Melin, J.; Ayers, P. W.; Ortiz, J. V. *J. Phys. Chem. A* **2007**, *111*, PMID: 17880054, 10017–10019.

(127) Echegaray, E.; Cárdenas, C.; Rabi, S.; Rabi, N.; Lee, S.; Zadeh, F. H.; Toro-Labbe, A.; Anderson, J. S.; Ayers, P. W. *J. Mol. Model.* **2013**, *19*, 2779–2783.

(128) Echegaray, E.; Rabi, S.; Cárdenas, C.; Zadeh, F. H.; Rabi, N.; Lee, S.; Anderson, J. S.; Toro-Labbe, A.; Ayers, P. W. *J. Mol. Model.* **2014**, *20*, 1–7.

(129) Gómez, T.; Florez, E.; Rodriguez, J. A.; Illas, F. *J. Phys. Chem. C* **2010**, *114*, 1622–1626.

(130) Echeverri, A.; Cárdenas, C.; Calatayud, M.; Hadad, C. Z.; Gomez, T. *Surf. Sci.* **2019**, *680*, 95–106.

(131) Wei, B.; Calatayud, M. *Catal. Today* **2022**, *397-399*, SI:CCE-2021, 113–120.

(132) Taudul, B.; Tielens, F.; Calatayud, M. *Nanomaterials* **2023**, *13*, 1856.

(133) Vogtenhuber, D.; Podloucky, R.; Redinger, J. *Surf. Sci.* **2000**, *454-456*, 369–373.

(134) Vogtenhuber, D.; Podloucky, R.; Redinger, J.; Hebenstreit, E. L. D.; Hebenstreit, W.; Diebold, U. *Phys. Rev. B* **2002**, *65*, 125411.

(135) Selcuk, S.; Selloni, A. *Nature Mater.* **2016**, *15*, 1107–1112.

(136) Krüger, P.; Jupille, J.; Bourgeois, S.; Domenichini, B.; Verdini, A.; Floreano, L.; Morgante, A. *Phys. Rev. Lett.* **2012**, *108*, 126803.

(137) Bader, R. F. W.; Carroll, M. T.; Cheeseman, J. R.; Chang, C. *J. Am. Chem. Soc.* **1987**, *109*, 7968–7979.

(138) Wei, B.; Calatayud, M. *Top. Catal.* **2022**, *65*, 270–280.

(139) Lagarde, P.; Flank, A.-M.; Prado, R.; Bourgeois, S.; Jupille, J. *Surf. Sci.* **2004**, *553*, 115–125.

(140) Albaret, T.; Finocchi, F.; Noguera, C.; De Vita, A. *Phys. Rev. B* **2001**, *65*, 035402.

(141) Parr, R. G.; Pearson, R. G. *J. Am. Chem. Soc.* **1983**, *105*, 7512–7516.

(142) Cárdenas, C.; Heidar-Zadeh, F.; Ayers, P. W. *Phys. Chem. Chem. Phys.* **2016**, *18*, 25721–25734.